

Aus dem Deutschen Zentrum für Neurodegenerative Erkrankungen und dem  
Adolf-Butenandt-Institut  
Lehrstuhl: Stoffwechselbiochemie  
im BioMedizinischen Centrum der  
Ludwig-Maximilians-Universität München  
Vorstand: Prof. Dr. rer. nat. Dr. h.c. Christian Haass

# **Analysis of the *C9orf72* Dipeptide-Repeat Proteins and Characterization of a poly-GA Mouse Model**

- Dissertation -

zum Erwerb des Doktorgrades der Naturwissenschaften (Dr. rer. nat.)  
an der Medizinischen Fakultät der Ludwig-Maximilians-Universität München



vorgelegt von  
Martin Haribert Schludi  
aus München

2017

Gedruckt mit Genehmigung der Medizinischen Fakultät der Ludwig-Maximilians-Universität  
München

Betreuer: Prof. Dr. rer. nat. Dr. h.c. Christian Haass

Zweitgutachterin: Dr. Dorothee Dormann

Dekan: Prof. Dr. med. dent. Reinhard Hickel

Tag der mündlichen Prüfung: 11.07.2018

## **Eidesstattliche Versicherung**

Ich erkläre hiermit an Eides statt, dass ich die vorliegende Dissertation mit dem Thema selbständig verfasst, mich außer der angegebenen keiner weiteren Hilfsmittel bedient und alle Erkenntnisse, die aus dem Schrifttum ganz oder annähernd übernommen sind, als solche kenntlich gemacht und nach ihrer Herkunft unter Bezeichnung der Fundstelle einzeln nachgewiesen habe.

Ich erkläre des Weiteren, dass die hier vorgelegte Dissertation nicht in gleicher oder in ähnlicher Form bei einer anderen Stelle zur Erlangung eines akademischen Grades eingereicht wurde.

München, 26.07.2018

---

Martin Haribert Schludi



*„A bissel was geht immer“*

Monaco Franze

## **Publications of the thesis**

### **Distribution of dipeptide repeat proteins in cellular models and *C9orf72* mutation cases suggests link to transcriptional silencing**

Schludi MH, May S, Grässer FA, Rentzsch K, Kremmer E, Küpper C, Klopstock T, German Consortium for Frontotemporal Lobar Degeneration, Bavarian Brain Banking Alliance, Arzberger T, Edbauer D.

Acta Neuropathol. 2015. doi: 10.1007/s00401-015-1450-z

### **Spinal poly-GA inclusions in a *C9orf72* mouse model trigger motor deficits and inflammation without neuron loss**

Schludi MH, Becker L, Garrett L, Gendron TF, Zhou Q, Schreiber F, Popper B, Dimou L, Strom TM, Winkelmann J, von Thaden A, Rentzsch K, May S, Michaelsen M, Schwenk BM, Tan J, Schoser B, Dieterich M, Petrucelli L, Höltter SM, Wurst W, Fuchs H, Gailus-Durner V, Hrabe de Angelis M, Klopstock T, Arzberger T, Edbauer D.

Acta Neuropathol. 2017. doi: 10.1007/s00401-017-1711-0

## Summary

Frontotemporal lobar degeneration (FTLD) and motor neuron disease (MND) are two related fatal neurodegenerative diseases showing major neuropathological, genetic and clinical overlap. The most frequent genetic mutation causing FTLD and MND is a GGGGCC hexanucleotide repeat expansion in the non-coding region of the *C9orf72* gene. Despite the lack of an initiation ATG codon and its intronic location, the repeat is translated into aggregating dipeptide-repeat (DPR) proteins. Translation of the sense strand results in poly-GA, poly-GR, and poly-GP, while translation of the antisense strand leads to poly-PR, poly-PA and additional poly-GP proteins. All DPR proteins predominantly co-aggregate in neuronal cytoplasmic inclusions, that can be labeled with p62 antibodies, a marker of the ubiquitin-proteasome system, but are distinct from the TDP-43 inclusion, another neuropathologic hallmark of FTLD and MND. Since DPR protein deposition precedes the symptoms in *C9orf72* patients, their role for the disease is still under intense debate. For poly-GA and the arginine-rich DPR proteins poly-GR and poly-PR toxicity has been shown in various model systems. In a recent *in vitro* study from our lab Unc119 was identified in poly-GA immunoprecipitates. I confirmed this finding in *C9orf72* patient tissue by showing co-aggregation of Unc119 in DPR aggregates (May&Hornburg&Schludi et al., 2014; not part of this cumulative dissertation).

Based on these initial findings, the overall goal of my studies was to elucidate whether and how DPR proteins contribute to FTLD and MND pathophysiology using a mouse model and patient tissues.

In the first part, I analyzed the distribution pattern of the different DPR species and Unc119 aggregates in *C9orf72* cases subclassified into FTLD, MND or FTLD/MND according to neuropathological criteria. Most inclusions were present in neurons, mainly in the cytoplasm and to a lesser extent in the nucleus and in dystrophic neurites. The majority of intranuclear inclusions was adjacent to the nucleolus and colocalized with heterochromatin and histone 3 dimethylated at lysine 9 (H3K9me2), a marker for transcriptional silencing. Additionally, a small number of aggregates were found in ependymal and subependymal cells. Since the regional distribution of poly-GA aggregates does not correlate with areas of neurodegeneration, I quantitatively analyzed the distribution and correlation of DPR proteins with disease subtypes. This revealed a significant increased number

of poly-PR inclusions in the CA3/4 region of FTLD cases compared to cases with MND, although poly-PR inclusions were very rare in the entire brain of both clinical subtypes. In contrast, poly-GA showed most severe inclusion pathology of all DPR proteins in *C9orf72* cases. Moreover, inclusions of poly-GA, as well as its interacting protein Unc119, were significantly more abundant in the granular cell layer of the cerebellum in FTLD cases compared to MND or FTLD/MND cases. These findings suggest a crucial role of poly-GA to the pathological cascade and a cerebellar involvement in the *C9orf72* disease.

To address the causal role of poly-GA to *C9orf72* disease, I analyzed a new transgenic mouse model expressing (GA)<sub>149</sub>-CFP in the second part of my thesis. These mice developed poly-GA aggregates mainly in neurons of brainstem, spinal cord and deep cerebellar nuclei that increased with age. Remarkably, poly-GA pathology was accompanied by progressive regional activation of microglia in transgenic mice, shown by Iba1 and CD68 expression. At 12 months, poly-GA mice showed no overt neuron loss but mildly increased TDP-43 phosphorylation. Furthermore, I analyzed poly-GA interacting proteins and newly identified co-aggregation of Mif2 with poly-GA in tissues from *C9orf72* patients and transgenic mice. In-depth behavioral phenotyping revealed abnormal gait at four months of age and progressive balance impairment. Thus, poly-GA inclusion pathology likely causes neuronal dysfunction even prior to overt neurodegeneration, which may explain the prodromal behavioral deficits in *C9orf72* patients.

**Taken together, my studies provide the first quantitative analysis of DPR protein aggregates in *C9orf72* patient tissue and show distinct distribution of DPR proteins in FTLD and MND cases, although regional DPR aggregation correlates poorly with neurodegeneration. In addition, colocalization of previously unrecognized para-nucleolar DPR inclusions with heterochromatin suggests a link to transcriptional silencing. Furthermore, I established the first germline transgenic poly-GA mouse and demonstrated that poly-GA triggers motor deficits presumably due to inflammation and sequestration of Mif2 and other proteins leading to neuronal dysfunction prior to cell death.**



## Zusammenfassung

Frontotemporale Lobärdegeneration (FTLD) und Motoneuron Erkrankung (MND) sind zwei tödlich verlaufende Neurodegenerative Erkrankungen mit ähnlichen neuropathologischen, genetischen und klinischen Symptomen. Die häufigste genetische Mutation ist eine Verlängerung der GGGGCC Hexanucleotid-Sequenz im nicht-codierenden Bereich des *C9orf72* Gens. Die Sequenz wird translatiert, obwohl sie in einem Intron lokalisiert ist und kein ATG Startcodon aufweist. Die so entstehenden Proteine bestehen aus einem sich wiederholenden Dipeptid (DPR Proteine). Das Sense-Transkript wird in poly-GA, poly-GR und poly-GP translatiert, das Antisense-Transkript in poly-PR, poly-PA und ebenfalls in poly-GP. Die DPR Proteine aggregieren gemeinsam in neuronalen Einschlüssen, die mit p62, einem Marker für das Ubiquitin-Proteasom System, kolokalisieren. Diese Einschlüsse haben kaum Überlapp mit den TDP-43 positiven Aggregaten, die auch bei anderen Formen von FTLD und MND gefunden werden. Da die DPR Aggregate mehrere Jahre vor den klinischen Symptomen auftreten, wird ihre Rolle zum Krankheitsverlauf kontrovers diskutiert. poly-GA und die Arginin-reichen DPR Proteine poly-GR und poly-PR sind in zahlreichen Modellsystemen toxisch. Unser Labor identifizierte vor kurzem in Zellkultur Unc119 als Interaktor von poly-GA. Ich konnte Unc119 in den DPR Aggregaten von *C9orf72* Patienten nachweisen und so die *in vitro* Daten verifizieren (May&Hornburg&Schludi et al., 2014; nicht Teil der kumulativen Dissertation).

Deshalb wollte ich durch Analyse von Patientengewebe und einem Mausmodell herausfinden ob und wie die DPR Proteine zur Pathogenese von FTLD und MND beitragen.

Im ersten Teil meiner Doktorarbeit verglich ich das Verteilungsmuster von DPR Proteinen und Unc119 in *C9orf72* Patienten mit der neuropathologischen Diagnose FTLD, MND und FTLD/MND. Fast alle Einschlüsse waren in Neuronen, hauptsächlich in Zytoplasma und seltener im Nukleus und in dystrophen Neuriten. Die Mehrheit der intranukleären Einschlüsse grenzt an den Nukleolus und kolokalisiert mit Heterochromatin und dimethyliertem Histon 3 (H3K9me2), einem Marker für inaktive Genesegmente. Einige Aggregate waren auch in Ependym- und Subependymzellen zu finden. Da das Verteilungsmuster von poly-GA Aggregaten schlecht mit Neurodegeneration korreliert, analysierte ich die quantitative Verteilung der DPR Proteine in den verschiedenen Krankheitsgruppen. In dieser Analyse

detektierte ich signifikant mehr poly-PR Einschlüsse in der CA3/4 Region von FTLD Patienten verglichen mit MND Patienten, obwohl im ganzen Gehirn beider Patientengruppen poly-PR Aggregate sehr selten vorkamen. poly-GA zeigte die stärkste Einschlusspathologie. Überdies waren Einschlüsse von poly-GA, und von seinem Interaktor Unc119, in der zerebellaren Körnerzellschicht von FTLD Patienten verglichen mit MND oder FTLD/MND Patienten signifikant erhöht. Diese Entdeckungen legen nahe, dass poly-GA den Krankheitsverlauf beeinflusst und das Zerebellum mit involviert ist.

Um die kausale Rolle von poly-GA zur *C9orf72* Erkrankung zu untersuchen, fokussierte ich mich im zweiten Teil meiner Doktorarbeit auf ein neues transgenes Mausmodell, welches (GA)<sub>149</sub>-CFP exprimiert. Die transgenen Mäuse entwickelten zunehmend poly-GA Aggregate in den tiefen Kleinhirnkernen, im Hirnstamm und im Rückenmark. Parallel dazu kommt es zu einer zunehmenden lokalen Mikroglia-Aktivierung mit Expression von Iba1 und CD68. Obwohl pathologisches TDP-43 leicht zunahm, zeigten die poly-GA Mäuse keinen offensichtlichen Verlust an Neuronen. Ich identifizierte Mlf2 als ein neues mit poly-GA interagierendes Protein, indem ich dessen Ko-Aggregation im Mausmodell und in *C9orf72* Patienten nachweisen konnte. Mit Verhaltensanalysen konnte ich in den transgenen Mäusen eine progressive Gang- und Gleichgewichtsstörung nachweisen. poly-GA Ablagerungen stören also wahrscheinlich schon vor einer offensichtlichen Neurodegeneration die neuronalen Funktionen, was die prodromalen Symptome von *C9orf72* Patienten erklären könnte.

**Zusammengefasst habe ich die erste quantitative Analyse von DPR Proteinen in *C9orf72* Patienten durchgeführt, in der ich eine unterschiedliche Verteilung von DPR Proteinen zwischen FTLD und MND Patienten detektierte, obwohl DPR Aggregate nicht mit Neurodegeneration korrelieren. Die Kolokalisierung von bisher nicht beschriebenen para-nukleolaren DPR Aggregaten mit Heterochromatin lässt auf eine Verbindung mit Gen-Inaktivierung schließen. Außerdem etablierte ich das erste keimbahngängige transgene poly-GA Mausmodell, in dem ich zeigen konnte, dass poly-GA motorische Störungen verursacht. Diese motorischen Störungen entstehen vermutlich durch fehlfunktionierende Neuronen, ausgelöst durch Mikroglia-Aktivierung und Sequestrierung von Mlf2 und anderen Proteinen.**

## Table of Contents

Eidesstattliche Versicherung .....	2
Publications of the thesis .....	5
Summary .....	6
Zusammenfassung .....	8
List of Abbreviations .....	12
I. Introduction .....	14
1 Terminology of FTD/FTLD and ALS/MND .....	14
1.1 Clinical characterization .....	14
1.1.1 The clinical syndrome FTD .....	14
1.1.2 The clinical syndrome ALS .....	15
1.1.3 The clinical syndrome FTD/ALS .....	15
1.2 Genetics of FTD and ALS .....	16
2 FTD/ALS with <i>C9orf72</i> mutation.....	17
2.1 <i>C9orf72</i> function and mutation .....	17
2.2 Clinical presentation of <i>C9orf72</i> cases .....	19
2.3 <i>C9orf72</i> pathomechanisms and pathology .....	20
2.3.1 <i>C9orf72</i> loss-of-function.....	22
2.3.2 RNA toxicity .....	23
2.3.3 DPR protein toxicity.....	24
3 Mammalian models for the <i>C9orf72</i> disease .....	26
3.1 <i>C9orf72</i> gene knock-out models .....	26
3.2 Transgenic <i>C9orf72</i> models.....	27
II. Aim of the study.....	30
III. References .....	31
IV. Results .....	41
1.1 Publication 1: Distribution of the dipeptide repeat proteins in cellular models and <i>C9orf72</i> mutation cases suggests link to transcriptional silencing.....	41
1.2 Contribution to the publication.....	75
2.1 Publication 2: Spinal poly-GA inclusions in a <i>C9orf72</i> mouse model trigger motor deficits and inflammation without neuron loss .....	76
2.2 Contribution to the publication.....	99
V. Acknowledgements.....	100

VI. Curriculum Vitae.....	102
VII. List of Publications .....	103

## List of Abbreviations

3110043O21RIK	RIKEN cDNA 3110043O21
AAV	adeno-associated virus
ADARB2	adenosine deaminase RNA specific B2
ALS	amyotrophic lateral sclerosis
ALYREF	Aly/REF export factor
ATG	adenine, thymine, guanine
ATG101	autophagy-related protein 101
BAC	bacterial-artificial-chromosome
bvFTD	behavioral-variant frontotemporal dementia
C9orf72	chromosome 9 open reading frame 72
CA3/4	Cornu Ammonis 3/4
CCCCGG	4x cytosine, 2x guanine
CFP	cyan fluorescent protein
CHCHD10	coiled-coil-helix-coiled-coil-helix domain 10
CHMP2B	charged multivesicular body protein 2b
CpG	5'-cytosine-phosphate-guanine-3'
CT	computed tomography
DNA	deoxyribonucleic acid
DPR protein	dipeptide-repeat protein
FTD	frontotemporal dementia
FTLD	frontotemporal lobar degeneration
FUS	fused in sarcoma
G3BP1	Ras GTPase-activating protein-binding protein 1
GA	glycine (Gly), alanine (Ala)
GDP	guanosine diphosphate
GEF	guanine nucleotide exchange factor
GGGGCC	4x guanine, 2x cytosine
GP	glycine (Gly), proline (Pro)
GR	glycine (Gly), arginine (Arg)
GRN	progranulin
GTP	guanosine triphosphate
H3K9me2	histone 3 dimethylated at lysine 9
hnRNP-A1	heterogenous nuclear ribonucleoprotein A1
hnRNP-A2	heterogenous nuclear ribonucleoprotein A2
hnRNP-A3	heterogenous nuclear ribonucleoprotein A3
hnRNP-H1	heterogenous nuclear ribonucleoprotein H1
MAPT	microtubule-associated protein Tau
Mif2	myeloid leukemia factor 2
MND	motor neuron disease
MRI	magnetic resonance imaging
mRNA	messenger ribonucleic acid
NCL	nucleolin

NF-kappa-B	nuclear factor kappa B
NPM1	nucleophosmin
OPTN	optineurin
p62	nucleoporin 62
PA	proline (Pro), alanine (Ala)
PLS	primary lateral sclerosis
PMA	progressive muscular atrophy
PNFA	progressive non-fluent aphasia
Pom121	nuclear pore membrane protein 121 kDa
PPA	primary progressive aphasia
PR	proline (Pro), arginine (Arg)
Pur- $\alpha$	purine-rich element binding protein A
Rab39b	Ras-related in brain protein 39b
Rab8a	Ras-related in brain protein 8a
Rad23	radiation 23 homolog A
RAN translation	repeat-associated non-ATG translation
RanGAP1	Ran GTPase-activating protein 1
RNA	ribonucleic acid
SD	semantic dementia
SF3a	splicing factor 3a
SMCR8	smith-magenis syndrome chromosome region, candidate 8
snRNP	small nuclear ribonucleo protein
SNRPB2	U2 small nuclear ribonucleoprotein B
SOD1	superoxide dismutase 1
SQSTM1	sequestome 1
SRSF1	serine/arginine rich splicing factor 1
TAA	thymine, adenine, adenine
TANK	TRAF family member-associated NF-kappa-B activator
TAR	transactive response
TBK1	TANK-binding kinase 1
TDP-43	TAR DNA-binding protein 43
TIA1	T-cell-restricted intracellular antigen-1
TNF	tumor necrosis factor
TRAF	TNF receptor-associated factor
TREM2	triggering receptor expressed on myeloid cells 2
UBQLN2	ubiquilin 2
ULK1	Unc-51-like kinase 1
Unc119	uncoordinated 119
VPC	valosin-containing protein
WDR41	WD repeat-containing protein 41
Zfp106	zinc finger protein 106

## **I. Introduction**

### **1 Terminology of FTD/FTLD and ALS/MND**

Frontotemporal lobar degeneration (FTLD) and motor neuron disease (MND) are two devastating neurodegenerative disorders with overlapping clinical, neuropathological and genetic features. The neuropathological diagnosis FTLD is typically associated with the clinical diagnosis frontotemporal dementia (FTD). FTD is one of the leading causes of presenile dementia (Vieira et al., 2013) and, the third most common form of dementia at all age groups after Alzheimer's disease and dementia with Lewy bodies, (Bang et al., 2015).

MND has an average prevalence of 5.4 per 100,000 people in European countries (Chio et al., 2013) and the distinction between clinical syndrome and the pathological process is somewhat inconsistent (Al-Chalabi et al., 2016). The term MND is often used to cover a spectrum of neurodegenerative disorders including the most common form, amyotrophic lateral sclerosis (ALS), also known as Lou Gehrig's disease. In the United States, the term ALS is used as an umbrella term for all forms of the MND disease. In the following, the term ALS denotes the clinical diagnosis and MND denotes the neuropathological diagnosis.

#### **1.1 Clinical characterization**

##### **1.1.1 The clinical syndrome FTD**

In 1892, Arnold Pick, a Czech neurologist, gave the first description of FTD. The patient, a 71-year-old man, suffered from rapidly progressive mental retardation with apathy and aphasia, but his motor system was not impaired (Pick A. 1892). These exclusively cognitive deficits without motor symptoms represent the key characteristics of FTD.

With continuing advances in clinical diagnostics and imaging techniques, FTD now encompasses three main clinical variants: The behavioral-variant frontotemporal dementia (bvFTD) and the primary progressive aphasia (PPA), whereby the latter comprises progressive non-fluent aphasia (PNFA) and semantic dementia (SD) (Bang et al., 2015). The different clinical symptoms of the three subtypes manifest as a result of a different regional pattern of brain atrophy in the frontal and temporal lobe, measured by structural imaging using MRI and CT (Rosen et al., 2002).

bvFTD is the most frequent variant affecting more than half of all FTD patients (Hogan et al., 2016). The main diagnostic criteria are progressive deterioration of behavior and cognition with behavioral disinhibition, apathy and loss of sympathy or empathy resulting from degeneration of the frontal lobe (Rascovsky et al., 2011). PPA is characterized by a progressive decline in language skills, but while patients with PNFA suffer from

agrammatism and apraxia of speech caused by atrophy in the left posterior frontal and insular region, SD features fluent speech with impaired single-word comprehension and confrontation naming due to anterior temporal lobe degeneration (Gorno-Tempini et al., 2011). The average age of disease onset is 59 years (Kansal et al., 2016). With progression of disease the symptoms of the three clinical variants often converge and the patients develop globally impaired cognition (Bang et al., 2015). Death due to pneumonia or other secondary infections typically occurs about 8 years after symptom onset (Rascovsky et al., 2011).

### **1.1.2 The clinical syndrome ALS**

The first clinical description of ALS reaches back to the early 19<sup>th</sup> century, but it was Jean-Martin Charcot who deduced in 1874 that muscle atrophy was caused by sclerosis in the spinal cord, and the disease was henceforth termed amyotrophic lateral sclerosis (Rowland, 2001).

The clinical syndrome ALS presents as a combination of signs involving the upper and lower motor neurons of the brainstem and/or the spinal cord leading to progressive paralysis. It is distinct from primary lateral sclerosis (PLS) and progressive muscular atrophy (PMA), which affect either only the upper or only the lower motor neurons. The clinical hallmark of PMA is the presence of weakness, muscle atrophy and fasciculation, whereas PLS typically results in a pathologic spread of reflexes like rhythmic muscular contractions and relaxations (Brooks et al., 2000; Kiernan et al., 2011). Nevertheless, most PLS patients subsequently develop symptoms of lower motor neuron degeneration. Thus, ALS appears to be a disease continuum with the two extreme subtypes PMA and PLS (Al-Chalabi et al., 2016). The mean age of ALS disease onset is 61.8 years (Chio et al., 2013) and most patients die within 2-4 years after symptom onset as a consequence of respiratory failure (Haverkamp et al., 1995).

### **1.1.3 The clinical syndrome FTD/ALS**

As mentioned earlier, the shared clinical symptoms of FTD and ALS support the view that both diseases are two extreme ends of a disease continuum with predominantly cognitive symptoms at the one end, and predominantly motor dysfunction at the other. With disease progression 5-15% of the FTD patients develop ALS that meets clinical diagnosis criteria and a greater proportion develop some clinical symptoms (Burrell et al., 2011; Hogan et al., 2016). Conversely, up to half of the ALS patients develop cognitive or behavioral symptoms at some stage of the disease course with about 8-15% meeting the diagnostic criteria of FTD



(Murphy et al., 2016). Notably, the course of disease in the mixed FTD/ALS cases is more severe.

## 1.2 Genetics of FTD and ALS

Both, FTD and ALS are mainly sporadic diseases with unknown genetic predisposition. About 10-27% of all FTD cases (Pottier et al., 2016) and 5-10% of the ALS cases have an autosomal dominant inheritance (Kiernan et al., 2011). Beside the clinical evidence for a link between FTD and ALS, genetic analyses clearly show a connection of both diseases. The identification of a GGGGCC hexanucleotide repeat expansion at chromosome 9 open reading frame 72 (*C9orf72*) as the most frequent genetic cause for inherited FTD and ALS was a breakthrough discovery (DeJesus-Hernandez et al., 2011; Renton et al., 2011). Additionally, rare mutations leading to FTD and ALS were identified in the coiled-coil-helix-coiled-coil-helix domain 10 (*CHCHD10*), optineurin (*OPTN*), sequestome 1 (*SQSTM1*), TANK-binding kinase 1 (*TBK1*), ubiquilin 2 (*UBQLN2*) and the valosin-containing protein (*VCP*) genes (Bannwarth et al., 2014; Cirulli et al., 2015; Deng et al., 2011; Fecto et al., 2011; Johnson et al., 2010; Maruyama et al., 2010; Pottier et al., 2015; Rubino et al., 2012; Watts et al., 2004). Of note, almost all gene mutations that cause both FTD and ALS are functionally involved in protein degradation, namely in the ubiquitin-proteasome system or in autophagy, underlying the importance of this pathway to the disease cascade. Known genetic mutations causing pure FTD include the microtubule-associated protein Tau (*MAPT*), progranulin (*GRN*) (Baker et al., 2006; Cruts et al., 2006; Hutton et al., 1998), and less frequently also mutations in the charged multivesicular body protein 2b (*CHMP2B*) (Skibinski et al., 2005) or heterozygous loss of function mutations in the triggering receptor expressed on myeloid cells 2 (*TREM2*) (Borrioni et al., 2014). The most common genetic cause leading to ALS are mutations in the superoxide dismutase 1 (*SOD1*) (Rosen et al., 1993), followed by mutations in the TAR DNA-binding protein 43 (*TDP-43*) (Sreedharan et al., 2008) and fused in sarcoma (*FUS*) genes (Kwiatkowski et al., 2009; Vance et al., 2009). An overview of the most common genes linked to familial FTD and ALS are illustrated in Figure 1.

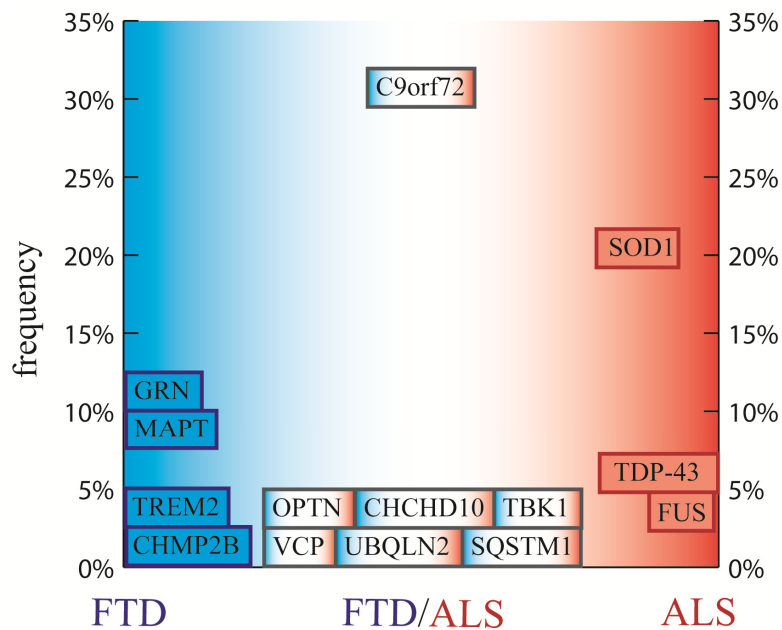


**Figure 1: Genetics of familial FTD and ALS cases.**

FTD and ALS represent the two ends of a disease spectrum. Mutations leading to pure FTD include gene mutations in *GRN*, *MAPT*, *TREM2* and *CHMP2B* (blue). Mutations mainly leading to pure ALS are mutations in the *SOD1*, *TDP-43* and *FUS* genes (red). The largest genetic cause for both FTD and ALS is a mutation in the *C9orf72* gene, followed by less frequent mutations in *OPTN*, *CHCHD10*, *TBK1*, *VCP*, *UBQLN* and *SQSTM1*.

## 2 FTD/ALS with *C9orf72* mutation

In 2006 two groups identified a candidate locus for FTD and ALS on chromosome 9p21-p13 using linkage analysis in large kindreds with hereditary FTD and ALS (Morita et al., 2006; Vance et al., 2006). In 2011, this locus was mapped to a GGGGCC hexanucleotide repeat expansion within the non-coding region of chromosome 9 open reading frame 72 (*C9orf72*). This mutation is the most common genetic cause of frontotemporal dementia and amyotrophic lateral sclerosis (DeJesus-Hernandez et al., 2011; Renton et al., 2011) with a prevalence of 25% of familial FTD, 34% of familial ALS and about 5% of sporadic FTD and ALS in people of European decent (Ng et al., 2015; Zou et al., 2017).

### 2.1 *C9orf72* function and mutation

Bioinformatic analyses have predicted the *C9orf72* protein to function as a guanine nucleotide exchange factor (GEF) (Levine et al., 2013; Zhang et al., 2012). Recent studies confirmed that *C9orf72* is a component of a multiprotein complex with *SMCR8*, *WDR41* and *ATG101*, which acts as a GDP-GTP exchange factor for small GTPases regulating vesicle trafficking in

the autophagy pathway, namely Rab8a and Rab39b. Furthermore, the C9orf72 complex gets phosphorylated by the autophagy related TANK-binding kinase 1 (TBK1) and interacts with the autophagy initiation complex Unc-51-like kinase 1 (ULK1), implicating C9orf72 in the regulation of autophagy (Sellier et al., 2016; Sullivan et al., 2016; Webster et al., 2016; Yang et al., 2016).

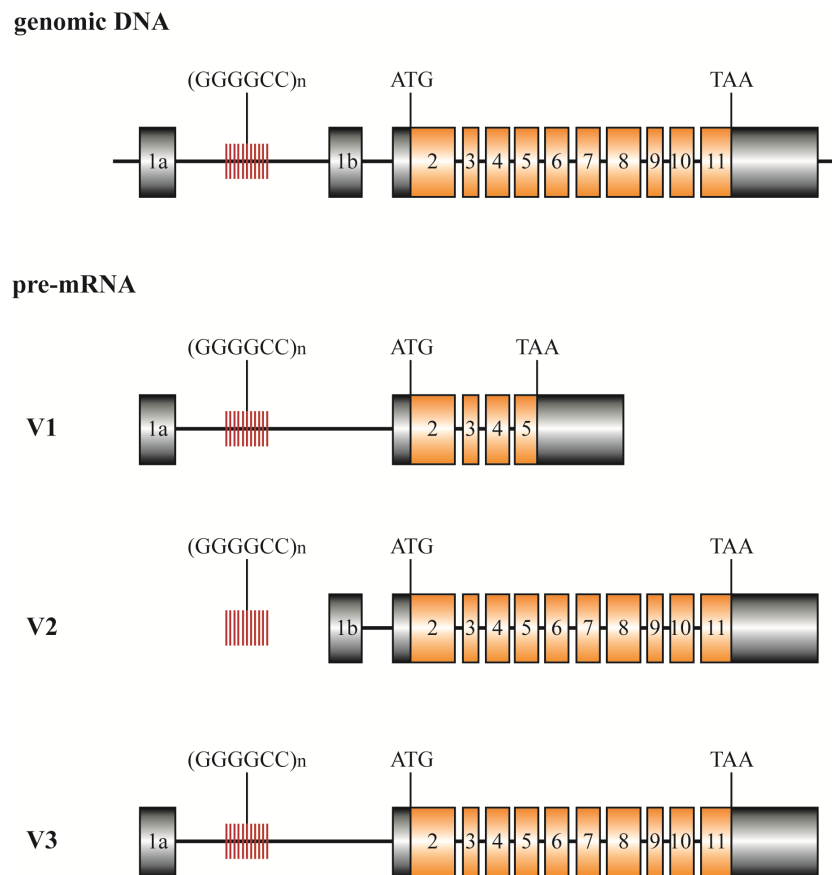


**Figure 2: Overview of genomic structure of the *C9orf72* locus and pre-mRNA splicing products.**

Schematic sequence of the genomic *C9orf72* locus and the pre-mRNA transcript variants. Transcript variant 1 (V1) encodes for the short *C9orf72* isoform, transcript variant 2 and 3 (V2 and V3) encode for the long *C9orf72* isoform. Boxes represent noncoding (black) and coding (orange) exons. The positions of the GGGGCC repeat sequence (red), the start codon (ATG) and stop codon (TAA) are indicated.

According to the latest information in the NCBI database (September 2017), alternative splicing of *C9orf72* yields three transcript variants that code for two protein isoforms (Figure 2). Transcript variant 2 (NCBI: NM\_018325.4) and 3 (NCBI: NM\_001256054.2) lead to a long *C9orf72* protein isoform involved in the autophagy pathway, variant 1 (NCBI:

NM\_145005.6) to a short isoform with a yet unknown function (Sellier et al., 2016; Sullivan et al., 2016) (take note, some of the publications cited in this dissertation refer to nomenclature from an older version of the NCBI database). Depending on the transcript, the expanded GGGGCC repeat is located in either the promoter region of transcript variant 2 or the first intron of transcript variants 1 and 3 of chromosome 9 open reading frame 72. In patients, the GGGGCC repeat is expanded up to several thousands of times, in contrast to healthy individuals who harbor less than 24 repeats (van der Zee et al., 2013). However, the exact threshold for a pathogenic expanded repeat is unclear, because most people have only 2 repeats (Gami et al., 2015; Gomez-Tortosa et al., 2013). Due to the germline and somatic instability of the GGGGCC sequence, the repeats expand or shrink between generations and show even variability between tissues (Beck et al., 2013; Dols-Icardo et al., 2014; van Blitterswijk et al., 2013).

## **2.2 Clinical presentation of *C9orf72* cases**

FTD and ALS patients carrying a *C9orf72* mutation show a considerable heterogeneity of clinical features and differ from non-mutation carriers by a significant higher co-morbidity of FTD and ALS (Byrne et al., 2012; Stewart et al., 2012). According to the literature, both syndromes converge during disease progression in approximately half of the *C9orf72* carriers (Boeve et al., 2012; Chio et al., 2012). *C9orf72* FTD patients progress faster in motor symptoms, and *C9orf72* patients diagnosed with ALS have a higher decline of cognitive and behavior functions compared to patients without the *C9orf72* mutation. FTD symptoms mainly manifest in bvFTD with apathy, disinhibition and impaired executive dysfunction, as well as delusions and hallucinations accompanied by predominantly anterior temporal cerebral atrophy (Hsiung et al., 2012; Simon-Sanchez et al., 2012). ALS patients present with a combination of both upper and lower motor neuron deficits with mainly spinal onset and bulbar involvement. Consequently, patients show motor symptoms like muscle atrophy, weakness, hyperreflexia and spasticity. Additionally, signs of Parkinsonism such as symmetric akinetic-rigid syndrome are rarely seen (Boeve et al., 2012; Byrne et al., 2012). Besides, the severity of the *C9orf72* disease precipitates with increasing repeat size (Gijssels et al., 2016). The gender of the parents transmitting the mutant allele does not influence phenotype or age at onset of the affected child, but children develop the disease ~7 years earlier than their affected parent (Byrne et al., 2012; Stewart et al., 2012). In all *C9orf72* cases an autosomal dominant inheritance pattern is apparent and patients show heterozygosity for the expanded allele with the exception of a few reported homozygous cases (Cooper-

Knock et al., 2013; Fratta et al., 2013). The age at disease onset varies from 27 to 82 years with an average of 57 years, and survival ranges from 9 months to 22 years (Boeve et al., 2012; Byrne et al., 2012; Majounie et al., 2012; Simon-Sanchez et al., 2012; Stewart et al., 2012).

### **2.3 *C9orf72* pathomechanisms and pathology**

Insoluble protein aggregates in the brain are pathognomonic hallmarks of FTLN, MND and other neurodegenerative diseases. For example, FTLN and MND disease-causing gene mutations in TDP-43, FUS and MAPT promote aggregation of the mutated protein. If aggregated proteins or their soluble oligomers are the toxic species is under intense debate. For Huntingtin and Tau intracellular inclusions seem to be less toxic than soluble oligomers (Arrasate et al., 2004; de Calignon et al., 2010). In contrast TDP-43 deposits highly correlate with areas of neurodegeneration (Van Deerlin et al., 2008). In *C9orf72* FTLN and MND patients is one pathognomonic hallmark neuronal cytoplasmic inclusions containing phosphorylated TDP-43, which are detectable in both brain and spinal cord tissues of affected individuals (DeJesus-Hernandez et al., 2011). The function of TDP-43 includes mRNA processing, alternative splicing and transcriptional repression (Buratti and Baralle, 2008). TDP-43 is located in the nuclei of healthy individuals and in unaffected neurons of FTLN and MND patients, but is absent in the nuclei of neurons with cytoplasmic phospho-TDP-43 inclusions, suggesting that TDP-43 redistributes from the nucleus to the cytoplasm with disease progression (Neumann et al., 2006). Like most of the other inclusions, phospho-TDP-43 aggregates can be labeled with antibodies against p62, a marker of the ubiquitin-proteasome system. The phospho-TDP-43 pathology is closely correlated with neurodegeneration in *C9orf72* patients. FTLN cases show more abundant phospho-TDP-43 pathology in the degenerated areas of the frontal and temporal lobe compared to MND patients. In contrast, MND cases with spinal cord degeneration have significant more phospho-TDP-43 in the spinal cord than FTLN patients (Mackenzie et al., 2013).

The precise mechanism underlying the TDP-43 redistribution and neurodegeneration in the *C9orf72* disease has remained unknown. Three potential pathomechanisms are under intense debate (Figure 3). First, loss-of-function due to silencing of the mutated *C9orf72* gene may leads to haploinsufficiency. Second, a toxic gain-of-function mechanism might be triggered by the transcribed repeat containing RNA, which sequesters RNA-binding proteins. Third, the expanded GGGGCC repeat is translated by an unconventional mechanism resulting in the

production of potentially toxic dipeptide-repeat proteins. In the following paragraph, the three postulated pathomechanisms and their resulting pathologies are discussed in more detail.

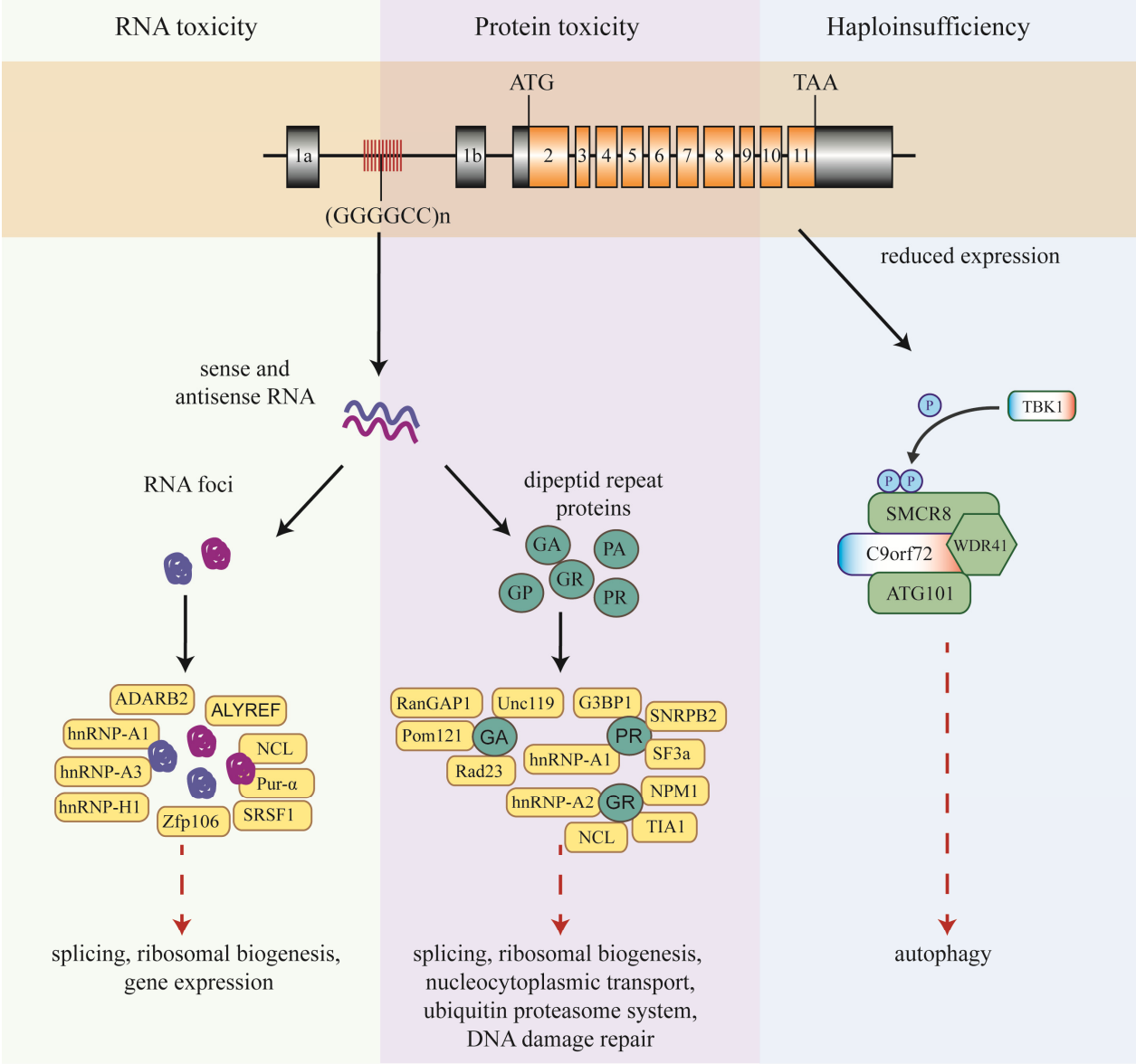


**Figure 3: Pathomechanisms of the *C9orf72* disease.**

Schematic overview of the three postulated mechanisms underlying *C9orf72* FTL/MND. Left column (green): Sense and antisense transcripts derived from the repeat expansion accumulate into RNA foci, that sequester RNA binding proteins (ADARB2, ALYREF, hnRNP-A1, hnRNP-A3, hnRNP-H1, NCL, Pur- $\alpha$ , SRSF1 and Zfp106) resulting in an impairment of RNA processing. Middle column (red): Repeat RNA is unconventionally translated into five dipeptide-repeat proteins that bind to different proteins (G3BP1, hnRNP-A1, hnRNP-A2, NCL, NPM1, Pom121, Rad23, RanGAP1, SF3a, SNRNPB2, TIA1, and Unc119) and impair the cell homeostasis and function. Right column (blue): The *C9orf72* protein forms a complex with ATG101, SMCR8 and WDR41 that gets phosphorylated (P) by TBK1. Reduced *C9orf72* expression levels, caused by the repeat expansion, are associated with impaired autophagy.

### 2.3.1 *C9orf72* loss-of-function

Patients with GGGGCC repeat mutation in the *C9orf72* gene typically carry hundreds, or even thousands of repeats. This immense length could interfere with functions of the transcribed product, leads to splicing deficits or results in epigenetic silencing. Gene silencing has already been described for other repeat-associated neurodegenerative diseases (Colak et al., 2014; Verkerk et al., 1991). Therefore, haploinsufficiency of *C9orf72* is proposed as one mechanism underlying the disease pathogenesis. Indeed, a single patient has been reported with a loss-of-function mutation in the *C9orf72* gene and clinical ALS symptoms, although other mutations were not excluded in this case (Liu et al., 2016a).

Evidence for epigenetic silencing has emerged from the finding that the mutated allele in *C9orf72* patients is bound to histones that are trimethylated at lysine residues indicative of gene expression repression (Belzil et al., 2013). Moreover, the 5' CpG island promoter upstream of the *C9orf72* gene of affected alleles is hypermethylated, consequently inhibiting the expression of mutant RNA (Xi et al., 2014; Xi et al., 2013). Both, histone methylation and promoter hypermethylation have also been shown in transgenic *C9orf72* mice (Esanov et al., 2017). In patients, the extent of the repeat length correlates with the degree of promoter methylation (Gijssels et al., 2016). However, most studies revealed no effect of CpG island hypermethylation and reduced mRNA levels on disease progression and pathology (Lagier-Tourenne et al., 2013; Liu et al., 2014; Russ et al., 2015). Therefore, promoter hypermethylation of the mutated allele is thought to be a partial protective mechanism by reducing the abnormal expression of the GGGGCC repeat RNA (Esanov et al., 2017; Liu et al., 2014; Russ et al., 2015).

Potential defects in mutated *C9orf72* also do not appear related to disease outcomes. Of the three annotated *C9orf72* mRNAs, patients with GGGGCC repeat expansion solely show a 50% reduction of *C9orf72* transcript variant 2, whereas most studies found no change in transcription of total *C9orf72* mRNA (DeJesus-Hernandez et al., 2011; Liu et al., 2014; Sareen et al., 2013; van Blitterswijk et al., 2015). Moreover, the expression of the *C9orf72* protein is only slightly changed up to 25% in the frontal cortex (Waite et al., 2014). In addition, a patient homozygous for the *C9orf72* hexanucleotide repeat expansion, and with 80% loss of transcript 2 and 30% reduction of transcript 1 and 3, had no exacerbation of the disease and his clinical symptoms fell within the typical range of the disease (Fratta et al., 2013). Correspondingly, ablation of *3110043O21RIK*, the mouse ortholog of *C9orf72*, does not lead to neurodegeneration (Koppers et al., 2015; Lagier-Tourenne et al., 2013) (discussed in more detail in paragraph 3.1. *C9orf72* gene knock-out models). Together, these data

strongly suggest that *C9orf72* gene silencing is not the driving cause of degeneration in the nervous system of *C9orf72* patients. However, *C9orf72* loss of function may promote DPR protein toxicity by inhibiting autophagy (see paragraph 2.1 *C9orf72* function and mutation) (Sellier et al., 2016; Webster et al., 2016; Yang et al., 2016).

### **2.3.2 RNA toxicity**

In *C9orf72* patients, both the sense strand including the intronic GGGGCC expansion and the antisense strand with the CCCCGG sequence, are transcribed into repeat RNAs. These repeat RNAs form highly stable inter- and intramolecular structures (e.g. G-quadruplexes, R-loops and hairpins) and accumulate into predominantly nuclear, and occasionally cytoplasmic, RNA foci (DeJesus-Hernandez et al., 2011; Fratta et al., 2012; Gendron et al., 2013; Mori et al., 2013c; Reddy et al., 2013). Abundant RNA foci pathology is seen in neurons of *C9orf72* mutation carriers but also to a lesser extent in astrocytes, microglia and oligodendrocytes (Lagier-Tourenne et al., 2013; Mizielinska et al., 2013). Thus, sense and antisense repeat RNA may cause toxicity by sequestering essential RNA-binding proteins, potentially altering RNA processing and gene transcription. Among the RNA-binding proteins trapped by the GGGGCC and CCCCGG repeat, there are regulators of alternative splicing factors, namely ALYREF (Aly/REF export factor), SRSF1 (serine/arginine rich splicing factor 1), Zfp106 (zinc finger protein 106), members of heterogeneous nuclear ribonucleoprotein (hnRNP) family hnRNP-A1, hnRNP-A3, hnRNP-H1, the transcriptional regulator Pur- $\alpha$  (purine-rich element binding protein A), the mRNA nuclear export adapter ADARB2 (adenosine deaminase RNA specific B2), and the ribosome associated protein NCL (nucleolin) (Celona et al., 2017; Cooper-Knock et al., 2014; Donnelly et al., 2013; Haeusler et al., 2014; Lee et al., 2013; Mori et al., 2013b; Reddy et al., 2013; Sareen et al., 2013; Xu et al., 2013). Most repeat-binding proteins are involved in alternative splicing, and widespread splicing dysregulation has consequently been reported in the frontal cortex and cerebellum of *C9orf72* patients when compared to sporadic ALS patients and healthy controls (Prudencio et al., 2015). The transcriptome profile of *C9orf72* patients reveals a high number of differentially expressed genes through exon-skipping and alternative polyadenylation events. A substantial number of the differentially expressed genes are targets of the splicing regulators hnRNP-H1 and SRSF1, and are involved in inflammatory and defense response, unfolded protein response, neuron development, and protein localization (Conlon et al., 2016; Prudencio et al., 2015). Although misregulation in gene expression is striking, the expression levels of the RNA-binding proteins in the brains of *C9orf72* patients are not affected (Cooper-Knock et al.,



2015; Donnelly et al., 2013). Of note, some studies revealed a toxic effect of RNA foci, or discovered a correlation between disease phenotype and hnRNA-H1 inclusions or antisense RNA foci (Conlon et al., 2016; Cooper-Knock et al., 2015; DeJesus-Hernandez et al., 2017; Xu et al., 2013). In contrast, other studies failed to substantiate RNA toxicity and showed that RNA foci pathology does not correlate with neurodegeneration. Moreover, *C9orf72* cases with a higher burden of RNA foci do not have a more severe disease course (DeJesus-Hernandez et al., 2017; Mizielinska et al., 2014; Mizielinska et al., 2013; Tran et al., 2015). Taken together, further disease modulating factors might play an essential role in the *C9orf72* disease and the role of repeat RNA induced toxicity to disease cascade and progression is still unclear.

### **2.3.3 DPR protein toxicity**

It is becoming increasingly clear that many hairpin-forming microsatellite repeat expansions, such as the GGGGCC repeat in the *C9orf72* disease, can undergo repeat-associated non-ATG (RAN) translation. This unconventional mode of translation occurs in non-coding regions and in the absence of an initiating ATG codon (Zu et al., 2011). RAN translation of the sense strand GGGGCC repeat results in the three dipeptide-repeat (DPR) proteins poly-GA (Gly-Ala), poly-GP (Gly-Pro) and poly-GR (Gly-Arg), while the translation of the antisense strand CCGGCC repeat leads to poly-PR (Pro-Arg), poly-PA (Pro-Ala) and also poly-GP (Ash et al., 2013; Gendron et al., 2013; Mori et al., 2013a; Mori et al., 2013c). With increasing repeat length, RAN translation becomes more efficient and the DPR proteins subsequently aggregate in the brains of *C9orf72* mutation carriers. poly-GA is the most abundant DPR protein in *C9orf72* cases followed by poly-GP and poly-GR. The antisense proteins poly-PR and poly-PA are very sparse in post mortem tissues (Mori et al., 2013a; Mori et al., 2013c). The DPR protein inclusions colocalize with p62 in characteristic star-shaped or dot-like neuronal cytoplasmic inclusions, neuronal nuclear inclusions or dystrophic neurites, and colocalize only rarely with phosphorylated TDP-43 inclusions (Mori et al., 2013c). No glial DPR protein inclusions have been detected so far. In semi-quantitative analysis, the pattern of poly-GA protein pathology is highly consistent among *C9orf72* cases regardless of their clinical phenotype and DPR proteins do not correlate with areas of neurodegeneration (Mackenzie et al., 2013). The highest load of poly-GA proteins is found in the cerebellum, hippocampus, thalamus and in neocortical regions including the frontal, motor and occipital cortex. Moderate pathology is detected in subcortical areas and pathology is rarely found in the lower

motor neurons of the spinal cord (Ash et al., 2013; Mackenzie et al., 2013; Mann et al., 2013; Mori et al., 2013a).

The relative contribution of the different DPR species is still a matter of debate. Recent studies indicate that poly-GR, poly-PR and poly-GA disturb cell homeostasis in various ways. The arginine-rich DPR proteins poly-GR and poly-PR interact with low complexity domains of intermediate filaments such as the heavy, medium, and light chain neurofilaments and vimentin leading to altered cell morphology (Lin et al., 2016). Furthermore, poly-GR and poly-PR bind to components of the nucleoli and other membrane-less organelles such as G3BP1 (Ras GTPase-activating protein-binding protein 1), hnRNP-A1, hnRNP-A2 (heterogenous nuclear ribonucleoprotein A1 and A2), NCL (nucleolin), NPM1 (nucleophosmin), TIA1 (T-cell-restricted intracellular antigen-1), and the U2 snRNP complex namely SF3a (splicing factor 3a), and SNRPB2 (U2 small nuclear ribonucleoprotein B) (Boeynaems et al., 2017; Kanekura et al., 2016; Kwon et al., 2014; Lee et al., 2016; Wen et al., 2014; Yin et al., 2017). As a result of protein sequestration pre-mRNA splicing and ribosomal biogenesis is impaired, and the nucleocytoplasmic transport is inhibited, ultimately leading to cell death (Boeynaems et al., 2016; Jovicic et al., 2015; Kwon et al., 2014; Lopez-Gonzalez et al., 2016). However, due to the relative paucity of poly-GR and especially poly-PR, the contribution of the arginine-rich DPR proteins to the *C9orf72* disease remains unclear. poly-GA, the most abundant DPR protein, is highly aggregation-prone *in vitro* and, in contrast to the other DPR proteins, forms  $\beta$ -sheet containing amyloid fibrils (Chang et al., 2016). The aggregation of the poly-GA proteins is essential to its toxicity, impairing neurite outgrowth and the ubiquitin-proteasome system (May et al., 2014; Zhang et al., 2016; Zhang et al., 2014). poly-GA aggregates sequester essential proteins into the inclusions namely the cargo protein Unc119 (uncoordinated 119) and proteins involved in the assembly of the nuclear pore, Pom121 (nuclear pore membrane protein 121 kDa) and RanGAP1 (Ran GTPase-activating protein 1). Moreover Rad23 (radiation 23 homolog A), a protein related to the ubiquitin-proteasome system, is recruited into the poly-GA inclusions.

In conclusion, most studies attribute toxicity to either the arginine-rich DPR proteins or to poly-GA, although both hypotheses require further investigations and are not mutually exclusive. Since in semi-quantitative studies poly-GA aggregates do not correlate with brain atrophy, one critical remaining question is the correlation of the arginine-rich poly-GR/PR with neurodegeneration. Furthermore, quantitative in-depth analyses of all DPR proteins are missing as well. Nonetheless pathological and clinical examinations of asymptomatic or mildly cognitively impaired *C9orf72* mutation carriers with extensive DPR protein pathology

suggest, that DPR protein formation and deposition precedes phospho-TDP-43 accumulation, and causes prodromal symptoms in patients (Baborie et al., 2015; Gami et al., 2015; Lehmer et al., 2017; Proudfoot et al., 2014).

### **3 Mammalian models for the *C9orf72* disease**

Recently, several mouse models have been generated to gain more insight into the pathomechanism of the *C9orf72* disease. Reportedly, both *C9orf72* gene knockout mice mimicking haploinsufficiency and mice overexpressing diverse repeat-constructs for RNA and protein gain-of-function toxicity have been generated. The following section provides a detailed overview of all mammalian *C9orf72* disease models published until September 2017.

#### **3.1 *C9orf72* gene knock-out models**

Several knockout mice lacking *3110043O21RIK*, the mouse ortholog of *C9orf72* (henceforth referred as *C9orf72*), have been generated to elucidate the possible loss-of-*C9orf72* function mechanism due to haploinsufficiency. The *C9orf72* protein is expressed in both neuron and glial cells in the central nervous system of human and mouse (Suzuki et al., 2013; Uhlen et al., 2015). Heterozygous knockout mice have a 50% reduced expression of the *C9orf72* protein resembling the haploinsufficiency in *C9orf72* mutation carriers, though the mice neither develop a motor phenotype nor pathological hallmarks of *C9orf72* patients. However, some mice develop a slight reduction in body weight, phagocytic deficits or a slightly increased mortality (Burberry et al., 2016; Koppers et al., 2015; O'Rourke et al., 2016). Remarkably, full ablation of *C9orf72* in mice results in a fatal autoimmune disease. These mice suffer from splenomegaly, enlarged lymph nodes and increased cytokine levels (Atanasio et al., 2016; Burberry et al., 2016; Jiang et al., 2016; O'Rourke et al., 2016; Sudria-Lopez et al., 2016). Homozygous knockout mice show a massive inflammation with infiltration of macrophages and lymphocytes into multiple organs including the central nervous system, but no sign of neurodegeneration. The immune system related pathology decreases the mice's survival and some develop a mild motor phenotype (Atanasio et al., 2016; Burberry et al., 2016; Jiang et al., 2016; Sudria-Lopez et al., 2016). However, partial and full ablation of *C9orf72* in mice does not result in FTD or ALS like symptoms. This finding is consistent with the report of a patient with homozygosity for the expanded repeat allele who showed symptoms and disease progression comparable to heterozygous *C9orf72* cases. The findings in mice corroborate the observations made in *C9orf72* patients and suggest that haploinsufficiency is not the driver for FTD or ALS symptoms, but contributes to

the disease by an impaired autophagy system (Fratta et al., 2013; Sellier et al., 2016; Webster et al., 2016; Yang et al., 2016).

### **3.2 Transgenic *C9orf72* models**

A total of seven different mammalian gain-of-function models have been developed and published in parallel to my study so far (Figure 4). While some of these mouse models express a patient-derived bacterial-artificial-chromosome (BAC) construct containing parts of the human *C9orf72* gene including the GGGGCC expansion (Jiang et al., 2016; Liu et al., 2016b; O'Rourke et al., 2015; Peters et al., 2015), others express a GGGGCC repeat from a AAV-injected promoter-driven synthetic construct (Chew et al., 2015; Herranz-Martin et al., 2017; Zhang et al., 2016). In AAV-injected mice, the construct is inserted into somatic cells and shows variable expression levels. In contrast, BAC transgenic mice have a germline insertion and the expression constantly passes through generations.

In the different mouse lines, divergent outcomes are reported regarding pathological features as well as behavior and motor phenotypes. All the transgenic mice show RNA and protein pathology regardless of the GGGGCC repeat length and their expression system. RNA foci formation occurs at a variable frequency throughout the central nervous system. Moreover, the sense strand DPR proteins poly-GA, poly-GR and poly-GP are detected in neurons and glial cells throughout the entire brain with the highest prevalence in either neocortical regions and hippocampus (Chew et al., 2015; Jiang et al., 2016; Liu et al., 2016b; Zhang et al., 2016) or cerebellum (Herranz-Martin et al., 2017; O'Rourke et al., 2015; Peters et al., 2015).

Due to the DPR protein toxicity cellular functions are disturbed in the majority of the mouse models. Here, the DPR proteins co-aggregate with p62 and inhibit the ubiquitin-proteasome system, as observed in patients. Furthermore, proteins involved in the synthesis of ribosomes (NCL), the nuclear pore complex (RanGAP1, Pom121), and DNA damage repair (Rad23) are found to be mislocalized in some animal models (Chew et al., 2015; O'Rourke et al., 2015; Zhang et al., 2016). TDP-43 aggregates, the pathological hallmark of *C9orf72* patients, are also observed, as well as activated microglia or astrocytes in some mouse lines (Chew et al., 2015; Herranz-Martin et al., 2017; Liu et al., 2016b; Zhang et al., 2016). In brains of patients, reactive gliosis and TDP-43 mislocalization are often accompanied by neurodegeneration. However, only some mouse lines show a loss of neurons (Chew et al., 2015; Jiang et al., 2016; Liu et al., 2016b; Zhang et al., 2016) or a loss of axons at neuromuscular junctions (Herranz-Martin et al., 2017; Liu et al., 2016b). The different transgenic mouse models show very different phenotypes. While some mice show no behavioral or cognitive abnormalities

(O'Rourke et al., 2015; Peters et al., 2015), others develop an anxiety-like behavior, social abnormalities, cognitive deficits or an impairment of the motor system (Chew et al., 2015; Herranz-Martin et al., 2017; Jiang et al., 2016; Liu et al., 2016b; Zhang et al., 2016).

	expression system	repeat length	RNA foci	reported DPR proteins	reported protein mislocalizations	glial activation	TDP-43 pathology	neuro-degeneration	phenotype
O'Rourke et al.	BAC	(GGGGCC) <sub>100-1000</sub>	sense, antisense	GP	NCL	-	-	-	-
Peters et al.	BAC	(GGGGCC) <sub>300-500</sub>	sense, antisense	GP	-	-	-	-	-
Liu et al.	BAC	(GGGGCC) <sub>500</sub>	sense, antisense	GA, GP	p62/ubiquitin	astrocytes, microglia	phospho-TDP-43 aggregates	neuron and axon loss	motor impairment
Jiang et al.	BAC	(GGGGCC) <sub>110-450</sub>	sense, antisense	GA, GP, GR	p62/ubiquitin	-	TDP-43 phosphorylation	neuron loss	behavior and cognitive impairment
Chew et al.	AAV	(GGGGCC) <sub>66</sub>	sense	GA, GP, GR	Rad23*, p62/ubiquitin	astrocytes	pTDP-43 aggregates	neuron loss	behavior and motor impairment
Herranz-Martin et al.	AAV	(GGGGCC) <sub>102</sub>	sense	GA	p62/ubiquitin	-	TDP-43 mislocalization	axon loss	behavior, motor and cognitive impairment
Zhang et al.	AAV	(GA) <sub>50</sub>	-	GA	Rad23, Pom121, RanGAP1, p62/ubiquitin	astrocytes	phospho-TDP-43 aggregates	neuron loss	behavior, motor and cognitive impairment

\*reported in Zhang et al.

#### Figure 4: Gain-of-function *C9orf72* disease models.

Overview of published *C9orf72* gain-of-function models with combined RNA and DPR protein toxicity (green) and DPR protein toxicity only (red). On the top are bacterial-artificial-chromosome (BAC) transgenic and on the bottom AAV-injected transgenic mouse models listed. Respective repeat lengths, detected RNA foci, DPR proteins, changes in expression and localization of proteins, neurodegeneration and phenotypes are listed.

A major disadvantage of most mouse models is that toxicity mediated by RNA or by the different DPR proteins cannot be distinguished, which is crucial for future drug target approaches. Only in a single mouse model the effect of poly-GA was exclusively studied. Here they used a synthetic DNA sequence without any extensive GGGGCC repeats avoiding confounding effects of RNA toxicity (Zhang et al., 2016). These AAV-injected poly-GA mice developed mislocalization of Rad23 suggesting an impaired DNA damage repair in the cells. Furthermore, the nuclear pore complex was disrupted, shown by altered RanGAP1 and Pom121 distribution. These findings of this singular mammalian poly-GA toxicity model suggest a crucial role of poly-GA to disease pathology. However, the expression of poly-GA at unphysiological high levels in cortical regions and the very low expression of poly-GA in the motor system limit the significance of this model with respect to the consequences of DPR

protein pathology, particularly in *C9orf72* ALS patients (Zhang et al., 2016). For pure neuromuscular studies, no mouse model with exclusive expression of DPR proteins in the upper and lower motor neurons is available so far. In conclusion, more mouse models with physiological expression levels of the DPR proteins, especially poly-GA/GR/PR, have to be generated and analyzed to get a better understanding of the pathological features of the diseases and to develop therapeutic approaches in future.

## II. Aim of the study

Despite enormous progress on many aspects of *C9orf72* disease, it is still unknown how the GGGGCC repeat expansion actually triggers FTD and/or ALS. Especially the relative contribution of the individual DPR species is still unclear. One major challenge is to mimic the pathognomonic hallmarks of *C9orf72* patients in *in vitro* and *in vivo* models. In *C9orf72* patients, all DPR proteins are aggregating into p62-positive cytoplasmic and nuclear inclusions, whereas in cell culture only poly-GA expression resembles the pattern observed in patients (May et al., 2014; Zhang et al., 2014). In contrast, when poly-GR and poly-PR are expressed in different cell culture models or in *Drosophila*, they show a diffuse cytoplasmic and nuclear pattern and a dense accumulation in the nucleolus. Poly-GP and poly-PA are diffusely distributed throughout the cells *in vitro* (May et al., 2014; Tao et al., 2015; Yamakawa et al., 2015; Yang et al., 2015; Zhang et al., 2014). Based on these findings, the aim of my study was to elucidate the contribution of the DPR proteins to the *C9orf72* disease. Therefore, my first goal was to dissect the regional and subcellular distributions of the DPR proteins in *C9orf72* mutation carriers and primary neuron models. Furthermore, I aimed to correlate the distribution of DPR protein pathology with areas of neurodegeneration and disease subtypes FTLD, MND and FTLD/MND.

Transgenic mouse models are crucial for elucidating the physiological processes occurring in human diseases. When I started my dissertation in the Edbauer lab, no *C9orf72* disease mouse model was available. Therefore, my second aim was to generate and analyze a transgenic poly-GA mouse model. In parallel to my work, several other groups reported various *C9orf72* animal models. However, in these models, the specific contribution of DPR proteins to the clinical and pathological symptoms remained unclear (Chew et al., 2015; Herranz-Martin et al., 2017; Jiang et al., 2016; Liu et al., 2016b; O'Rourke et al., 2015; Peters et al., 2015; Zhang et al., 2016) and none of these mouse models showed significant pathology in the ALS related upper and lower motor neurons. Thus, I focused on neuropathological effects of poly-GA in the brainstem and spinal cord and analyzed behavioral and motor deficits.

Together, these new pathological insights and *in vivo* analyses provide a better understanding of the mechanism underlying the *C9orf72* disease, and may assist future development of efficient treatments and therapies.

### III. References

- Al-Chalabi, A., Hardiman, O., Kiernan, M.C., Chio, A., Rix-Brooks, B., and van den Berg, L.H. (2016). Amyotrophic lateral sclerosis: moving towards a new classification system. *Lancet Neurol* 15, 1182-1194.
- Arrasate, M., Mitra, S., Schweitzer, E.S., Segal, M.R., and Finkbeiner, S. (2004). Inclusion body formation reduces levels of mutant huntingtin and the risk of neuronal death. *Nature* 431, 805-810.
- Ash, P.E., Bieniek, K.F., Gendron, T.F., Caulfield, T., Lin, W.L., DeJesus-Hernandez, M., van Blitterswijk, M.M., Jansen-West, K., Paul, J.W., 3rd, Rademakers, R., *et al.* (2013). Unconventional translation of C9ORF72 GGGGCC expansion generates insoluble polypeptides specific to c9FTD/ALS. *Neuron* 77, 639-646.
- Atanasio, A., Decman, V., White, D., Ramos, M., Ikiz, B., Lee, H.C., Siao, C.J., Brydges, S., LaRosa, E., Bai, Y., *et al.* (2016). C9orf72 ablation causes immune dysregulation characterized by leukocyte expansion, autoantibody production, and glomerulonephropathy in mice. *Sci Rep* 6, 23204.
- Baborie, A., Griffiths, T.D., Jaros, E., Perry, R., McKeith, I.G., Burn, D.J., Masuda-Suzukake, M., Hasegawa, M., Rollinson, S., Pickering-Brown, S., *et al.* (2015). Accumulation of dipeptide repeat proteins predates that of TDP-43 in frontotemporal lobar degeneration associated with hexanucleotide repeat expansions in C9ORF72 gene. *Neuropathol Appl Neurobiol* 41, 601-612.
- Baker, M., Mackenzie, I.R., Pickering-Brown, S.M., Gass, J., Rademakers, R., Lindholm, C., Snowden, J., Adamson, J., Sadovnick, A.D., Rollinson, S., *et al.* (2006). Mutations in progranulin cause tau-negative frontotemporal dementia linked to chromosome 17. *Nature* 442, 916-919.
- Bang, J., Spina, S., and Miller, B.L. (2015). Frontotemporal dementia. *Lancet* 386, 1672-1682.
- Bannwarth, S., Ait-El-Mkadem, S., Chausse, A., Genin, E.C., Lacas-Gervais, S., Fragaki, K., Berg-Alonso, L., Kageyama, Y., Serre, V., Moore, D.G., *et al.* (2014). A mitochondrial origin for frontotemporal dementia and amyotrophic lateral sclerosis through CHCHD10 involvement. *Brain* 137, 2329-2345.
- Beck, J., Poulter, M., Hensman, D., Rohrer, J.D., Mahoney, C.J., Adamson, G., Campbell, T., Uphill, J., Borg, A., Fratta, P., *et al.* (2013). Large C9orf72 hexanucleotide repeat expansions are seen in multiple neurodegenerative syndromes and are more frequent than expected in the UK population. *Am J Hum Genet* 92, 345-353.
- Belzil, V.V., Bauer, P.O., Prudencio, M., Gendron, T.F., Stetler, C.T., Yan, I.K., Prent, L., Daugherty, L., Baker, M.C., Rademakers, R., *et al.* (2013). Reduced C9orf72 gene expression in c9FTD/ALS is caused by histone trimethylation, an epigenetic event detectable in blood. *Acta Neuropathol* 126, 895-905.
- Boeve, B.F., Boylan, K.B., Graff-Radford, N.R., DeJesus-Hernandez, M., Knopman, D.S., Pedraza, O., Vemuri, P., Jones, D., Lowe, V., Murray, M.E., *et al.* (2012). Characterization of frontotemporal dementia and/or amyotrophic lateral sclerosis associated with the GGGGCC repeat expansion in C9ORF72. *Brain* 135, 765-783.
- Boeynaems, S., Bogaert, E., Kovacs, D., Konijnenberg, A., Timmerman, E., Volkov, A., Guharoy, M., De Decker, M., Jaspers, T., Ryan, V.H., *et al.* (2017). Phase Separation of C9orf72 Dipeptide Repeats Perturbs Stress Granule Dynamics. *Mol Cell* 65, 1044-1055 e1045.
- Boeynaems, S., Bogaert, E., Michiels, E., Gijssels, I., Sieben, A., Jovicic, A., De Baets, G., Scheveneels, W., Steyaert, J., Cuijt, I., *et al.* (2016). Drosophila screen connects nuclear transport genes to DPR pathology in c9ALS/FTD. *Sci Rep* 6, 20877.



Borroni, B., Ferrari, F., Galimberti, D., Nacmias, B., Barone, C., Bagnoli, S., Fenoglio, C., Piaceri, I., Archetti, S., Bonvicini, C., *et al.* (2014). Heterozygous TREM2 mutations in frontotemporal dementia. *Neurobiol Aging* 35, 934 e937-910.

Brooks, B.R., Miller, R.G., Swash, M., Munsat, T.L., and World Federation of Neurology Research Group on Motor Neuron, D. (2000). El Escorial revisited: revised criteria for the diagnosis of amyotrophic lateral sclerosis. *Amyotroph Lateral Scler Other Motor Neuron Disord* 1, 293-299.

Buratti, E., and Baralle, F.E. (2008). Multiple roles of TDP-43 in gene expression, splicing regulation, and human disease. *Frontiers in bioscience : a journal and virtual library* 13, 867-878.

Burberry, A., Suzuki, N., Wang, J.Y., Moccia, R., Mordes, D.A., Stewart, M.H., Suzuki-Uematsu, S., Ghosh, S., Singh, A., Merkle, F.T., *et al.* (2016). Loss-of-function mutations in the C9ORF72 mouse ortholog cause fatal autoimmune disease. *Sci Transl Med* 8, 347ra393.

Burrell, J.R., Kiernan, M.C., Vucic, S., and Hodges, J.R. (2011). Motor neuron dysfunction in frontotemporal dementia. *Brain* 134, 2582-2594.

Byrne, S., Elamin, M., Bede, P., Shatunov, A., Walsh, C., Corr, B., Heverin, M., Jordan, N., Kenna, K., Lynch, C., *et al.* (2012). Cognitive and clinical characteristics of patients with amyotrophic lateral sclerosis carrying a C9orf72 repeat expansion: a population-based cohort study. *Lancet Neurol* 11, 232-240.

Celona, B., Dollen, J.V., Vatsavayai, S.C., Kashima, R., Johnson, J.R., Tang, A.A., Hata, A., Miller, B.L., Huang, E.J., Krogan, N.J., *et al.* (2017). Suppression of C9orf72 RNA repeat-induced neurotoxicity by the ALS-associated RNA-binding protein Zfp106. *Elife* 6.

Chang, Y.J., Jeng, U.S., Chiang, Y.L., Hwang, I.S., and Chen, Y.R. (2016). The Glycine-Alanine Dipeptide Repeat from C9orf72 Hexanucleotide Expansions Forms Toxic Amyloids Possessing Cell-to-Cell Transmission Properties. *J Biol Chem* 291, 4903-4911.

Chew, J., Gendron, T.F., Prudencio, M., Sasaguri, H., Zhang, Y.J., Castanedes-Casey, M., Lee, C.W., Jansen-West, K., Kurti, A., Murray, M.E., *et al.* (2015). Neurodegeneration. C9ORF72 repeat expansions in mice cause TDP-43 pathology, neuronal loss, and behavioral deficits. *Science* 348, 1151-1154.

Chio, A., Borghero, G., Restagno, G., Mora, G., Drepper, C., Traynor, B.J., Sendtner, M., Brunetti, M., Ossola, I., Calvo, A., *et al.* (2012). Clinical characteristics of patients with familial amyotrophic lateral sclerosis carrying the pathogenic GGGGCC hexanucleotide repeat expansion of C9ORF72. *Brain* 135, 784-793.

Chio, A., Logroscino, G., Traynor, B.J., Collins, J., Simeone, J.C., Goldstein, L.A., and White, L.A. (2013). Global epidemiology of amyotrophic lateral sclerosis: a systematic review of the published literature. *Neuroepidemiology* 41, 118-130.

Cirulli, E.T., Lasseigne, B.N., Petrovski, S., Sapp, P.C., Dion, P.A., Leblond, C.S., Couthouis, J., Lu, Y.F., Wang, Q., Krueger, B.J., *et al.* (2015). Exome sequencing in amyotrophic lateral sclerosis identifies risk genes and pathways. *Science* 347, 1436-1441.

Colak, D., Zaninovic, N., Cohen, M.S., Rosenwaks, Z., Yang, W.Y., Gerhardt, J., Disney, M.D., and Jaffrey, S.R. (2014). Promoter-bound trinucleotide repeat mRNA drives epigenetic silencing in fragile X syndrome. *Science* 343, 1002-1005.

Conlon, E.G., Lu, L., Sharma, A., Yamazaki, T., Tang, T., Shneider, N.A., and Manley, J.L. (2016). The C9ORF72 GGGGCC expansion forms RNA G-quadruplex inclusions and sequesters hnRNP H to disrupt splicing in ALS brains. *Elife* 5.

Cooper-Knock, J., Higginbottom, A., Connor-Robson, N., Bayatti, N., Bury, J.J., Kirby, J., Ninkina, N., Buchman, V.L., and Shaw, P.J. (2013). C9ORF72 transcription in a frontotemporal dementia case with two expanded alleles. *Neurology* 81, 1719-1721.

Cooper-Knock, J., Higginbottom, A., Stopford, M.J., Highley, J.R., Ince, P.G., Wharton, S.B., Pickering-Brown, S., Kirby, J., Hautbergue, G.M., and Shaw, P.J. (2015). Antisense RNA

foci in the motor neurons of C9ORF72-ALS patients are associated with TDP-43 proteinopathy. *Acta Neuropathol* 130, 63-75.

Cooper-Knock, J., Walsh, M.J., Higginbottom, A., Robin Highley, J., Dickman, M.J., Edbauer, D., Ince, P.G., Wharton, S.B., Wilson, S.A., Kirby, J., *et al.* (2014). Sequestration of multiple RNA recognition motif-containing proteins by C9orf72 repeat expansions. *Brain* 137, 2040-2051.

Cruts, M., Gijselinck, I., van der Zee, J., Engelborghs, S., Wils, H., Pirici, D., Rademakers, R., Vandenberghe, R., Dermaut, B., Martin, J.J., *et al.* (2006). Null mutations in progranulin cause ubiquitin-positive frontotemporal dementia linked to chromosome 17q21. *Nature* 442, 920-924.

de Calignon, A., Fox, L.M., Pitstick, R., Carlson, G.A., Bacskai, B.J., Spires-Jones, T.L., and Hyman, B.T. (2010). Caspase activation precedes and leads to tangles. *Nature* 464, 1201-1204.

DeJesus-Hernandez, M., Finch, N.A., Wang, X., Gendron, T.F., Bieniek, K.F., Heckman, M.G., Vasilevich, A., Murray, M.E., Rousseau, L., Weesner, R., *et al.* (2017). In-depth clinico-pathological examination of RNA foci in a large cohort of C9ORF72 expansion carriers. *Acta Neuropathol*.

DeJesus-Hernandez, M., Mackenzie, I.R., Boeve, B.F., Boxer, A.L., Baker, M., Rutherford, N.J., Nicholson, A.M., Finch, N.A., Flynn, H., Adamson, J., *et al.* (2011). Expanded GGGGCC hexanucleotide repeat in noncoding region of C9ORF72 causes chromosome 9p-linked FTD and ALS. *Neuron* 72, 245-256.

Deng, H.X., Chen, W., Hong, S.T., Boycott, K.M., Gorrie, G.H., Siddique, N., Yang, Y., Fecto, F., Shi, Y., Zhai, H., *et al.* (2011). Mutations in UBQLN2 cause dominant X-linked juvenile and adult-onset ALS and ALS/dementia. *Nature* 477, 211-215.

Dols-Icardo, O., Garcia-Redondo, A., Rojas-Garcia, R., Sanchez-Valle, R., Noguera, A., Gomez-Tortosa, E., Pastor, P., Hernandez, I., Esteban-Perez, J., Suarez-Calvet, M., *et al.* (2014). Characterization of the repeat expansion size in C9orf72 in amyotrophic lateral sclerosis and frontotemporal dementia. *Hum Mol Genet* 23, 749-754.

Donnelly, C.J., Zhang, P.W., Pham, J.T., Haeusler, A.R., Mistry, N.A., Vidensky, S., Daley, E.L., Poth, E.M., Hoover, B., Fines, D.M., *et al.* (2013). RNA toxicity from the ALS/FTD C9ORF72 expansion is mitigated by antisense intervention. *Neuron* 80, 415-428.

Esanov, R., Cabrera, G.T., Andrade, N.S., Gendron, T.F., Brown, R.H., Jr., Benatar, M., Wahlestedt, C., Mueller, C., and Zeier, Z. (2017). A C9ORF72 BAC mouse model recapitulates key epigenetic perturbations of ALS/FTD. *Molecular neurodegeneration* 12, 46.

Fecto, F., Yan, J., Vemula, S.P., Liu, E., Yang, Y., Chen, W., Zheng, J.G., Shi, Y., Siddique, N., Arrat, H., *et al.* (2011). SQSTM1 mutations in familial and sporadic amyotrophic lateral sclerosis. *Arch Neurol* 68, 1440-1446.

Fratta, P., Mizielinska, S., Nicoll, A.J., Zloh, M., Fisher, E.M., Parkinson, G., and Isaacs, A.M. (2012). C9orf72 hexanucleotide repeat associated with amyotrophic lateral sclerosis and frontotemporal dementia forms RNA G-quadruplexes. *Sci Rep* 2, 1016.

Fratta, P., Poulter, M., Lashley, T., Rohrer, J.D., Polke, J.M., Beck, J., Ryan, N., Hensman, D., Mizielinska, S., Waite, A.J., *et al.* (2013). Homozygosity for the C9orf72 GGGGCC repeat expansion in frontotemporal dementia. *Acta Neuropathol* 126, 401-409.

Gami, P., Murray, C., Schottlaender, L., Bettencourt, C., De Pablo Fernandez, E., Mudanohwo, E., Mizielinska, S., Polke, J.M., Holton, J.L., Isaacs, A.M., *et al.* (2015). A 30-unit hexanucleotide repeat expansion in C9orf72 induces pathological lesions with dipeptide-repeat proteins and RNA foci, but not TDP-43 inclusions and clinical disease. *Acta Neuropathol* 130, 599-601.

Gendron, T.F., Bieniek, K.F., Zhang, Y.J., Jansen-West, K., Ash, P.E., Caulfield, T., Daugherty, L., Dunmore, J.H., Castanedes-Casey, M., Chew, J., *et al.* (2013). Antisense transcripts of the expanded C9ORF72 hexanucleotide repeat form nuclear RNA foci and

undergo repeat-associated non-ATG translation in c9FTD/ALS. *Acta Neuropathol* 126, 829-844.

Gijssels, I., Van Mossevelde, S., van der Zee, J., Sieben, A., Engelborghs, S., De Bleecker, J., Ivanoiu, A., Deryck, O., Edbauer, D., Zhang, M., *et al.* (2016). The C9orf72 repeat size correlates with onset age of disease, DNA methylation and transcriptional downregulation of the promoter. *Mol Psychiatry* 21, 1112-1124.

Gomez-Tortosa, E., Gallego, J., Guerrero-Lopez, R., Marcos, A., Gil-Neciga, E., Sainz, M.J., Diaz, A., Franco-Macias, E., Trujillo-Tiebas, M.J., Ayuso, C., *et al.* (2013). C9ORF72 hexanucleotide expansions of 20-22 repeats are associated with frontotemporal deterioration. *Neurology* 80, 366-370.

Gorno-Tempini, M.L., Hillis, A.E., Weintraub, S., Kertesz, A., Mendez, M., Cappa, S.F., Ogar, J.M., Rohrer, J.D., Black, S., Boeve, B.F., *et al.* (2011). Classification of primary progressive aphasia and its variants. *Neurology* 76, 1006-1014.

Haeusler, A.R., Donnelly, C.J., Periz, G., Simko, E.A., Shaw, P.G., Kim, M.S., Maragakis, N.J., Troncoso, J.C., Pandey, A., Sattler, R., *et al.* (2014). C9orf72 nucleotide repeat structures initiate molecular cascades of disease. *Nature* 507, 195-200.

Haverkamp, L.J., Appel, V., and Appel, S.H. (1995). Natural history of amyotrophic lateral sclerosis in a database population. Validation of a scoring system and a model for survival prediction. *Brain* 118 (Pt 3), 707-719.

Herranz-Martin, S., Chandran, J., Lewis, K., Mulcahy, P., Higginbottom, A., Walker, C., Valenzuela, I.M.Y., Jones, R.A., Coldicott, I., Iannitti, T., *et al.* (2017). Viral delivery of C9ORF72 hexanucleotide repeat expansions in mice lead to repeat length dependent neuropathology and behavioral deficits. *Dis Model Mech*.

Hogan, D.B., Jette, N., Fiest, K.M., Roberts, J.I., Pearson, D., Smith, E.E., Roach, P., Kirk, A., Pringsheim, T., and Maxwell, C.J. (2016). The Prevalence and Incidence of Frontotemporal Dementia: a Systematic Review. *Can J Neurol Sci* 43 Suppl 1, S96-S109.

Hsiung, G.Y., DeJesus-Hernandez, M., Feldman, H.H., Sengdy, P., Bouchard-Kerr, P., Dwosh, E., Butler, R., Leung, B., Fok, A., Rutherford, N.J., *et al.* (2012). Clinical and pathological features of familial frontotemporal dementia caused by C9ORF72 mutation on chromosome 9p. *Brain* 135, 709-722.

Hutton, M., Lendon, C.L., Rizzu, P., Baker, M., Froelich, S., Houlden, H., Pickering-Brown, S., Chakraverty, S., Isaacs, A., Grover, A., *et al.* (1998). Association of missense and 5'-splice-site mutations in tau with the inherited dementia FTDP-17. *Nature* 393, 702-705.

Jiang, J., Zhu, Q., Gendron, T.F., Saberi, S., McAlonis-Downes, M., Seelman, A., Stauffer, J.E., Jafar-Nejad, P., Drenner, K., Schulte, D., *et al.* (2016). Gain of Toxicity from ALS/FTD-Linked Repeat Expansions in C9ORF72 Is Alleviated by Antisense Oligonucleotides Targeting GGGGCC-Containing RNAs. *Neuron* 90, 535-550.

Johnson, J.O., Mandrioli, J., Benatar, M., Abramzon, Y., Van Deerlin, V.M., Trojanowski, J.Q., Gibbs, J.R., Brunetti, M., Gronka, S., Wu, J., *et al.* (2010). Exome sequencing reveals VCP mutations as a cause of familial ALS. *Neuron* 68, 857-864.

Jovicic, A., Mertens, J., Boeynaems, S., Bogaert, E., Chai, N., Yamada, S.B., Paul, J.W., 3rd, Sun, S., Herdy, J.R., Bieri, G., *et al.* (2015). Modifiers of C9orf72 dipeptide repeat toxicity connect nucleocytoplasmic transport defects to FTD/ALS. *Nat Neurosci* 18, 1226-1229.

Kanekura, K., Yagi, T., Cammack, A.J., Mahadevan, J., Kuroda, M., Harms, M.B., Miller, T.M., and Urano, F. (2016). Poly-dipeptides encoded by the C9ORF72 repeats block global protein translation. *Hum Mol Genet* 25, 1803-1813.

Kansal, K., Mareddy, M., Sloane, K.L., Minc, A.A., Rabins, P.V., McGready, J.B., and Onyike, C.U. (2016). Survival in Frontotemporal Dementia Phenotypes: A Meta-Analysis. *Dement Geriatr Cogn Disord* 41, 109-122.

Kiernan, M.C., Vucic, S., Cheah, B.C., Turner, M.R., Eisen, A., Hardiman, O., Burrell, J.R., and Zoing, M.C. (2011). Amyotrophic lateral sclerosis. *Lancet* 377, 942-955.

Koppers, M., Blokhuis, A.M., Westeneng, H.J., Terpstra, M.L., Zundel, C.A., Vieira de Sa, R., Schellevis, R.D., Waite, A.J., Blake, D.J., Veldink, J.H., *et al.* (2015). C9orf72 ablation in mice does not cause motor neuron degeneration or motor deficits. *Ann Neurol* 78, 426-438.

Kwiatkowski, T.J., Jr., Bosco, D.A., Leclerc, A.L., Tamrazian, E., Vanderburg, C.R., Russ, C., Davis, A., Gilchrist, J., Kasarskis, E.J., Munsat, T., *et al.* (2009). Mutations in the FUS/TLS gene on chromosome 16 cause familial amyotrophic lateral sclerosis. *Science* 323, 1205-1208.

Kwon, I., Xiang, S., Kato, M., Wu, L., Theodoropoulos, P., Wang, T., Kim, J., Yun, J., Xie, Y., and McKnight, S.L. (2014). Poly-dipeptides encoded by the C9orf72 repeats bind nucleoli, impede RNA biogenesis, and kill cells. *Science* 345, 1139-1145.

Lagier-Tourenne, C., Baughn, M., Rigo, F., Sun, S., Liu, P., Li, H.R., Jiang, J., Watt, A.T., Chun, S., Katz, M., *et al.* (2013). Targeted degradation of sense and antisense C9orf72 RNA foci as therapy for ALS and frontotemporal degeneration. *Proc Natl Acad Sci U S A* 110, E4530-4539.

Lee, K.H., Zhang, P., Kim, H.J., Mitrea, D.M., Sarkar, M., Freibaum, B.D., Cika, J., Coughlin, M., Messing, J., Molliex, A., *et al.* (2016). C9orf72 Dipeptide Repeats Impair the Assembly, Dynamics, and Function of Membrane-Less Organelles. *Cell* 167, 774-788 e717.

Lee, Y.B., Chen, H.J., Peres, J.N., Gomez-Deza, J., Attig, J., Stalekar, M., Troakes, C., Nishimura, A.L., Scotter, E.L., Vance, C., *et al.* (2013). Hexanucleotide repeats in ALS/FTD form length-dependent RNA foci, sequester RNA binding proteins, and are neurotoxic. *Cell Rep* 5, 1178-1186.

Lehmer, C., Oeckl, P., Weishaupt, J.H., Volk, A.E., Diehl-Schmid, J., Schroeter, M.L., Lauer, M., Kornhuber, J., Levin, J., Fassbender, K., *et al.* (2017). Poly-GP in cerebrospinal fluid links C9orf72-associated dipeptide repeat expression to the asymptomatic phase of ALS/FTD. *EMBO Mol Med*.

Levine, T.P., Daniels, R.D., Gatta, A.T., Wong, L.H., and Hayes, M.J. (2013). The product of C9orf72, a gene strongly implicated in neurodegeneration, is structurally related to DENN Rab-GEFs. *Bioinformatics* 29, 499-503.

Lin, Y., Mori, E., Kato, M., Xiang, S., Wu, L., Kwon, I., and McKnight, S.L. (2016). Toxic PR Poly-Dipeptides Encoded by the C9orf72 Repeat Expansion Target LC Domain Polymers. *Cell* 167, 789-802 e712.

Liu, E.Y., Russ, J., Wu, K., Neal, D., Suh, E., McNally, A.G., Irwin, D.J., Van Deerlin, V.M., and Lee, E.B. (2014). C9orf72 hypermethylation protects against repeat expansion-associated pathology in ALS/FTD. *Acta Neuropathol* 128, 525-541.

Liu, F., Liu, Q., Lu, C.X., Cui, B., Guo, X.N., Wang, R.R., Liu, M.S., Li, X.G., Cui, L.Y., and Zhang, X. (2016a). Identification of a novel loss-of-function C9orf72 splice site mutation in a patient with amyotrophic lateral sclerosis. *Neurobiol Aging* 47, 219 e211-219 e215.

Liu, Y., Pattamatta, A., Zu, T., Reid, T., Bardhi, O., Borchelt, D.R., Yachnis, A.T., and Ranum, L.P. (2016b). C9orf72 BAC Mouse Model with Motor Deficits and Neurodegenerative Features of ALS/FTD. *Neuron* 90, 521-534.

Lopez-Gonzalez, R., Lu, Y., Gendron, T.F., Karydas, A., Tran, H., Yang, D., Petrucelli, L., Miller, B.L., Almeida, S., and Gao, F.B. (2016). Poly(GR) in C9ORF72-Related ALS/FTD Compromises Mitochondrial Function and Increases Oxidative Stress and DNA Damage in iPSC-Derived Motor Neurons. *Neuron* 92, 383-391.

Mackenzie, I.R., Arzberger, T., Kremmer, E., Troost, D., Lorenzl, S., Mori, K., Weng, S.M., Haass, C., Kretschmar, H.A., Edbauer, D., *et al.* (2013). Dipeptide repeat protein pathology in C9ORF72 mutation cases: clinico-pathological correlations. *Acta Neuropathol* 126, 859-879.

Majounie, E., Renton, A.E., Mok, K., Dopper, E.G., Waite, A., Rollinson, S., Chio, A., Restagno, G., Nicolaou, N., Simon-Sanchez, J., *et al.* (2012). Frequency of the C9orf72

hexanucleotide repeat expansion in patients with amyotrophic lateral sclerosis and frontotemporal dementia: a cross-sectional study. *Lancet Neurol* *11*, 323-330.

Mann, D.M., Rollinson, S., Robinson, A., Bennion Callister, J., Thompson, J.C., Snowden, J.S., Gendron, T., Petrucelli, L., Masuda-Suzukake, M., Hasegawa, M., *et al.* (2013). Dipeptide repeat proteins are present in the p62 positive inclusions in patients with frontotemporal lobar degeneration and motor neurone disease associated with expansions in C9ORF72. *Acta Neuropathol Commun* *1*, 68.

Maruyama, H., Morino, H., Ito, H., Izumi, Y., Kato, H., Watanabe, Y., Kinoshita, Y., Kamada, M., Nodera, H., Suzuki, H., *et al.* (2010). Mutations of optineurin in amyotrophic lateral sclerosis. *Nature* *465*, 223-226.

May, S., Hornburg, D., Schludi, M.H., Arzberger, T., Rentzsch, K., Schwenk, B.M., Grasser, F.A., Mori, K., Kremmer, E., Banzhaf-Strathmann, J., *et al.* (2014). C9orf72 FTLD/ALS-associated Gly-Ala dipeptide repeat proteins cause neuronal toxicity and Unc119 sequestration. *Acta Neuropathol* *128*, 485-503.

Mizielinska, S., Gronke, S., Niccoli, T., Ridler, C.E., Clayton, E.L., Devoy, A., Moens, T., Norona, F.E., Woollacott, I.O., Pietrzyk, J., *et al.* (2014). C9orf72 repeat expansions cause neurodegeneration in *Drosophila* through arginine-rich proteins. *Science* *345*, 1192-1194.

Mizielinska, S., Lashley, T., Norona, F.E., Clayton, E.L., Ridler, C.E., Fratta, P., and Isaacs, A.M. (2013). C9orf72 frontotemporal lobar degeneration is characterised by frequent neuronal sense and antisense RNA foci. *Acta Neuropathol* *126*, 845-857.

Mori, K., Arzberger, T., Grasser, F.A., Gijssels, I., May, S., Rentzsch, K., Weng, S.M., Schludi, M.H., van der Zee, J., Cruts, M., *et al.* (2013a). Bidirectional transcripts of the expanded C9orf72 hexanucleotide repeat are translated into aggregating dipeptide repeat proteins. *Acta Neuropathol* *126*, 881-893.

Mori, K., Lammich, S., Mackenzie, I.R., Forne, I., Zilow, S., Kretschmar, H., Edbauer, D., Janssens, J., Kleinberger, G., Cruts, M., *et al.* (2013b). hnRNP A3 binds to GGGGCC repeats and is a constituent of p62-positive/TDP43-negative inclusions in the hippocampus of patients with C9orf72 mutations. *Acta Neuropathol* *125*, 413-423.

Mori, K., Weng, S.M., Arzberger, T., May, S., Rentzsch, K., Kremmer, E., Schmid, B., Kretschmar, H.A., Cruts, M., Van Broeckhoven, C., *et al.* (2013c). The C9orf72 GGGGCC repeat is translated into aggregating dipeptide-repeat proteins in FTLD/ALS. *Science* *339*, 1335-1338.

Morita, M., Al-Chalabi, A., Andersen, P.M., Hosler, B., Sapp, P., Englund, E., Mitchell, J.E., Habgood, J.J., de Belleruche, J., Xi, J., *et al.* (2006). A locus on chromosome 9p confers susceptibility to ALS and frontotemporal dementia. *Neurology* *66*, 839-844.

Murphy, J., Factor-Litvak, P., Goetz, R., Lomen-Hoerth, C., Nagy, P.L., Hupf, J., Singleton, J., Woolley, S., Andrews, H., Heitzman, D., *et al.* (2016). Cognitive-behavioral screening reveals prevalent impairment in a large multicenter ALS cohort. *Neurology* *86*, 813-820.

Neumann, M., Sampathu, D.M., Kwong, L.K., Truax, A.C., Micsenyi, M.C., Chou, T.T., Bruce, J., Schuck, T., Grossman, M., Clark, C.M., *et al.* (2006). Ubiquitinated TDP-43 in frontotemporal lobar degeneration and amyotrophic lateral sclerosis. *Science* *314*, 130-133.

Ng, A.S., Rademakers, R., and Miller, B.L. (2015). Frontotemporal dementia: a bridge between dementia and neuromuscular disease. *Ann NY Acad Sci* *1338*, 71-93.

O'Rourke, J.G., Bogdanik, L., Muhammad, A.K., Gendron, T.F., Kim, K.J., Austin, A., Cady, J., Liu, E.Y., Zarrow, J., Grant, S., *et al.* (2015). C9orf72 BAC Transgenic Mice Display Typical Pathologic Features of ALS/FTD. *Neuron* *88*, 892-901.

O'Rourke, J.G., Bogdanik, L., Yanez, A., Lall, D., Wolf, A.J., Muhammad, A.K., Ho, R., Carmona, S., Vit, J.P., Zarrow, J., *et al.* (2016). C9orf72 is required for proper macrophage and microglial function in mice. *Science* *351*, 1324-1329.

Peters, O.M., Cabrera, G.T., Tran, H., Gendron, T.F., McKeon, J.E., Metterville, J., Weiss, A., Wightman, N., Salameh, J., Kim, J., *et al.* (2015). Human C9ORF72 Hexanucleotide

Expansion Reproduces RNA Foci and Dipeptide Repeat Proteins but Not Neurodegeneration in BAC Transgenic Mice. *Neuron* 88, 902-909.

Pick, A. (1892). Über die Beziehungen der senilen Hirnatrophie zur Aphasie. *Prager Medicinische Wochenschrift* 17, 165-167.

Pottier, C., Bieniek, K.F., Finch, N., van de Vorst, M., Baker, M., Perkersen, R., Brown, P., Ravenscroft, T., van Blitterswijk, M., Nicholson, A.M., *et al.* (2015). Whole-genome sequencing reveals important role for TBK1 and OPTN mutations in frontotemporal lobar degeneration without motor neuron disease. *Acta Neuropathol* 130, 77-92.

Pottier, C., Ravenscroft, T.A., Sanchez-Contreras, M., and Rademakers, R. (2016). Genetics of FTL: overview and what else we can expect from genetic studies. *J Neurochem* 138 Suppl 1, 32-53.

Proudfoot, M., Gutowski, N.J., Edbauer, D., Hilton, D.A., Stephens, M., Rankin, J., and Mackenzie, I.R. (2014). Early dipeptide repeat pathology in a frontotemporal dementia kindred with C9ORF72 mutation and intellectual disability. *Acta Neuropathol* 127, 451-458.

Prudencio, M., Belzil, V.V., Batra, R., Ross, C.A., Gendron, T.F., Pregent, L.J., Murray, M.E., Overstreet, K.K., Piazza-Johnston, A.E., Desaro, P., *et al.* (2015). Distinct brain transcriptome profiles in C9orf72-associated and sporadic ALS. *Nat Neurosci* 18, 1175-1182.

Rascovsky, K., Hodges, J.R., Knopman, D., Mendez, M.F., Kramer, J.H., Neuhaus, J., van Swieten, J.C., Seelaar, H., Dopper, E.G., Onyike, C.U., *et al.* (2011). Sensitivity of revised diagnostic criteria for the behavioural variant of frontotemporal dementia. *Brain* 134, 2456-2477.

Reddy, K., Zamiri, B., Stanley, S.Y., Macgregor, R.B., Jr., and Pearson, C.E. (2013). The disease-associated r(GGGGCC)<sub>n</sub> repeat from the C9orf72 gene forms tract length-dependent uni- and multimolecular RNA G-quadruplex structures. *J Biol Chem* 288, 9860-9866.

Renton, A.E., Majounie, E., Waite, A., Simon-Sanchez, J., Rollinson, S., Gibbs, J.R., Schymick, J.C., Laaksovirta, H., van Swieten, J.C., Myllykangas, L., *et al.* (2011). A hexanucleotide repeat expansion in C9ORF72 is the cause of chromosome 9p21-linked ALS-FTD. *Neuron* 72, 257-268.

Rosen, D.R., Siddique, T., Patterson, D., Figlewicz, D.A., Sapp, P., Hentati, A., Donaldson, D., Goto, J., O'Regan, J.P., Deng, H.X., *et al.* (1993). Mutations in Cu/Zn superoxide dismutase gene are associated with familial amyotrophic lateral sclerosis. *Nature* 362, 59-62.

Rosen, H.J., Gorno-Tempini, M.L., Goldman, W.P., Perry, R.J., Schuff, N., Weiner, M., Feiwell, R., Kramer, J.H., and Miller, B.L. (2002). Patterns of brain atrophy in frontotemporal dementia and semantic dementia. *Neurology* 58, 198-208.

Rowland, L.P. (2001). How amyotrophic lateral sclerosis got its name: the clinical-pathologic genius of Jean-Martin Charcot. *Arch Neurol* 58, 512-515.

Rubino, E., Rainero, I., Chio, A., Rogaeva, E., Galimberti, D., Fenoglio, P., Grinberg, Y., Isaia, G., Calvo, A., Gentile, S., *et al.* (2012). SQSTM1 mutations in frontotemporal lobar degeneration and amyotrophic lateral sclerosis. *Neurology* 79, 1556-1562.

Russ, J., Liu, E.Y., Wu, K., Neal, D., Suh, E., Irwin, D.J., McMillan, C.T., Harms, M.B., Cairns, N.J., Wood, E.M., *et al.* (2015). Hypermethylation of repeat expanded C9orf72 is a clinical and molecular disease modifier. *Acta Neuropathol* 129, 39-52.

Sareen, D., O'Rourke, J.G., Meera, P., Muhammad, A.K., Grant, S., Simpkinson, M., Bell, S., Carmona, S., Ornelas, L., Sahabian, A., *et al.* (2013). Targeting RNA foci in iPSC-derived motor neurons from ALS patients with a C9ORF72 repeat expansion. *Sci Transl Med* 5, 208ra149.

Sellier, C., Campanari, M.L., Julie Corbier, C., Gaucherot, A., Kolb-Cheynel, I., Oulad-Abdelghani, M., Ruffenach, F., Page, A., Ciura, S., Kabashi, E., *et al.* (2016). Loss of C9ORF72 impairs autophagy and synergizes with polyQ Ataxin-2 to induce motor neuron dysfunction and cell death. *EMBO J* 35, 1276-1297.

Simon-Sanchez, J., Dopper, E.G., Cohn-Hokke, P.E., Hukema, R.K., Nicolaou, N., Seelaar, H., de Graaf, J.R., de Koning, I., van Schoor, N.M., Deeg, D.J., *et al.* (2012). The clinical and pathological phenotype of C9ORF72 hexanucleotide repeat expansions. *Brain* *135*, 723-735.

Skibinski, G., Parkinson, N.J., Brown, J.M., Chakrabarti, L., Lloyd, S.L., Hummerich, H., Nielsen, J.E., Hodges, J.R., Spillantini, M.G., Thusgaard, T., *et al.* (2005). Mutations in the endosomal ESCRTIII-complex subunit CHMP2B in frontotemporal dementia. *Nat Genet* *37*, 806-808.

Sreedharan, J., Blair, I.P., Tripathi, V.B., Hu, X., Vance, C., Rogelj, B., Ackerley, S., Durnall, J.C., Williams, K.L., Buratti, E., *et al.* (2008). TDP-43 mutations in familial and sporadic amyotrophic lateral sclerosis. *Science* *319*, 1668-1672.

Stewart, H., Rutherford, N.J., Briemberg, H., Krieger, C., Cashman, N., Fabros, M., Baker, M., Fok, A., DeJesus-Hernandez, M., Eisen, A., *et al.* (2012). Clinical and pathological features of amyotrophic lateral sclerosis caused by mutation in the C9ORF72 gene on chromosome 9p. *Acta Neuropathol* *123*, 409-417.

Sudria-Lopez, E., Koppers, M., de Wit, M., van der Meer, C., Westeneng, H.J., Zundel, C.A., Youssef, S.A., Harkema, L., de Bruin, A., Veldink, J.H., *et al.* (2016). Full ablation of C9orf72 in mice causes immune system-related pathology and neoplastic events but no motor neuron defects. *Acta Neuropathol* *132*, 145-147.

Sullivan, P.M., Zhou, X., Robins, A.M., Paushter, D.H., Kim, D., Smolka, M.B., and Hu, F. (2016). The ALS/FTLD associated protein C9orf72 associates with SMCR8 and WDR41 to regulate the autophagy-lysosome pathway. *Acta Neuropathol Commun* *4*, 51.

Suzuki, N., Maroof, A.M., Merkle, F.T., Koszka, K., Intoh, A., Armstrong, I., Moccia, R., Davis-Dusenbery, B.N., and Eggan, K. (2013). The mouse C9ORF72 ortholog is enriched in neurons known to degenerate in ALS and FTD. *Nat Neurosci* *16*, 1725-1727.

Tao, Z., Wang, H., Xia, Q., Li, K., Li, K., Jiang, X., Xu, G., Wang, G., and Ying, Z. (2015). Nucleolar stress and impaired stress granule formation contribute to C9orf72 RAN translation-induced cytotoxicity. *Hum Mol Genet* *24*, 2426-2441.

Tran, H., Almeida, S., Moore, J., Gendron, T.F., Chalasani, U., Lu, Y., Du, X., Nickerson, J.A., Petrucelli, L., Weng, Z., *et al.* (2015). Differential Toxicity of Nuclear RNA Foci versus Dipeptide Repeat Proteins in a Drosophila Model of C9ORF72 FTD/ALS. *Neuron* *87*, 1207-1214.

Uhlen, M., Fagerberg, L., Hallstrom, B.M., Lindskog, C., Oksvold, P., Mardinoglu, A., Sivertsson, A., Kampf, C., Sjostedt, E., Asplund, A., *et al.* (2015). Proteomics. Tissue-based map of the human proteome. *Science* *347*, 1260419.

van Blitterswijk, M., DeJesus-Hernandez, M., Niemantsverdriet, E., Murray, M.E., Heckman, M.G., Diehl, N.N., Brown, P.H., Baker, M.C., Finch, N.A., Bauer, P.O., *et al.* (2013). Association between repeat sizes and clinical and pathological characteristics in carriers of C9ORF72 repeat expansions (Xpansize-72): a cross-sectional cohort study. *Lancet Neurol* *12*, 978-988.

van Blitterswijk, M., Gendron, T.F., Baker, M.C., DeJesus-Hernandez, M., Finch, N.A., Brown, P.H., Daugherty, L.M., Murray, M.E., Heckman, M.G., Jiang, J., *et al.* (2015). Novel clinical associations with specific C9ORF72 transcripts in patients with repeat expansions in C9ORF72. *Acta Neuropathol* *130*, 863-876.

Van Deerlin, V.M., Leverenz, J.B., Bekris, L.M., Bird, T.D., Yuan, W., Elman, L.B., Clay, D., Wood, E.M., Chen-Plotkin, A.S., Martinez-Lage, M., *et al.* (2008). TARDBP mutations in amyotrophic lateral sclerosis with TDP-43 neuropathology: a genetic and histopathological analysis. *Lancet Neurol* *7*, 409-416.

van der Zee, J., Gijssels, I., Dillen, L., Van Langenhove, T., Theuns, J., Engelborghs, S., Philtjens, S., Vandenbulcke, M., Sleegers, K., Sieben, A., *et al.* (2013). A pan-European study of the C9orf72 repeat associated with FTL: geographic prevalence, genomic instability, and intermediate repeats. *Hum Mutat* *34*, 363-373.

Vance, C., Al-Chalabi, A., Ruddy, D., Smith, B.N., Hu, X., Sreedharan, J., Siddique, T., Schelhaas, H.J., Kusters, B., Troost, D., *et al.* (2006). Familial amyotrophic lateral sclerosis with frontotemporal dementia is linked to a locus on chromosome 9p13.2-21.3. *Brain* 129, 868-876.

Vance, C., Rogelj, B., Hortobagyi, T., De Vos, K.J., Nishimura, A.L., Sreedharan, J., Hu, X., Smith, B., Ruddy, D., Wright, P., *et al.* (2009). Mutations in FUS, an RNA processing protein, cause familial amyotrophic lateral sclerosis type 6. *Science* 323, 1208-1211.

Verkerk, A.J., Pieretti, M., Sutcliffe, J.S., Fu, Y.H., Kuhl, D.P., Pizzuti, A., Reiner, O., Richards, S., Victoria, M.F., Zhang, F.P., *et al.* (1991). Identification of a gene (FMR-1) containing a CGG repeat coincident with a breakpoint cluster region exhibiting length variation in fragile X syndrome. *Cell* 65, 905-914.

Vieira, R.T., Caixeta, L., Machado, S., Silva, A.C., Nardi, A.E., Arias-Carrion, O., and Carta, M.G. (2013). Epidemiology of early-onset dementia: a review of the literature. *Clin Pract Epidemiol Ment Health* 9, 88-95.

Waite, A.J., Baumer, D., East, S., Neal, J., Morris, H.R., Ansorge, O., and Blake, D.J. (2014). Reduced C9orf72 protein levels in frontal cortex of amyotrophic lateral sclerosis and frontotemporal degeneration brain with the C9ORF72 hexanucleotide repeat expansion. *Neurobiol Aging* 35, 1779 e1775-1779 e1713.

Watts, G.D., Wymer, J., Kovach, M.J., Mehta, S.G., Mumm, S., Darvish, D., Pestronk, A., Whyte, M.P., and Kimonis, V.E. (2004). Inclusion body myopathy associated with Paget disease of bone and frontotemporal dementia is caused by mutant valosin-containing protein. *Nat Genet* 36, 377-381.

Webster, C.P., Smith, E.F., Bauer, C.S., Moller, A., Hautbergue, G.M., Ferraiuolo, L., Myszczyńska, M.A., Higginbottom, A., Walsh, M.J., Whitworth, A.J., *et al.* (2016). The C9orf72 protein interacts with Rab1a and the ULK1 complex to regulate initiation of autophagy. *EMBO J* 35, 1656-1676.

Wen, X., Tan, W., Westergard, T., Krishnamurthy, K., Markandaiah, S.S., Shi, Y., Lin, S., Shneider, N.A., Monaghan, J., Pandey, U.B., *et al.* (2014). Antisense proline-arginine RAN dipeptides linked to C9ORF72-ALS/FTD form toxic nuclear aggregates that initiate in vitro and in vivo neuronal death. *Neuron* 84, 1213-1225.

Xi, Z., Rainero, I., Rubino, E., Pinessi, L., Bruni, A.C., Maletta, R.G., Nacmias, B., Sorbi, S., Galimberti, D., Surace, E.I., *et al.* (2014). Hypermethylation of the CpG-island near the C9orf72 G(4)C(2)-repeat expansion in FTLD patients. *Hum Mol Genet* 23, 5630-5637.

Xi, Z., Zinman, L., Moreno, D., Schymick, J., Liang, Y., Sato, C., Zheng, Y., Ghani, M., Dib, S., Keith, J., *et al.* (2013). Hypermethylation of the CpG island near the G4C2 repeat in ALS with a C9orf72 expansion. *Am J Hum Genet* 92, 981-989.

Xu, Z., Poidevin, M., Li, X., Li, Y., Shu, L., Nelson, D.L., Li, H., Hales, C.M., Gearing, M., Wingo, T.S., *et al.* (2013). Expanded GGGGCC repeat RNA associated with amyotrophic lateral sclerosis and frontotemporal dementia causes neurodegeneration. *Proc Natl Acad Sci U S A* 110, 7778-7783.

Yamakawa, M., Ito, D., Honda, T., Kubo, K., Noda, M., Nakajima, K., and Suzuki, N. (2015). Characterization of the dipeptide repeat protein in the molecular pathogenesis of c9FTD/ALS. *Hum Mol Genet* 24, 1630-1645.

Yang, D., Abdallah, A., Li, Z., Lu, Y., Almeida, S., and Gao, F.B. (2015). FTD/ALS-associated poly(GR) protein impairs the Notch pathway and is recruited by poly(GA) into cytoplasmic inclusions. *Acta Neuropathol* 130, 525-535.

Yang, M., Liang, C., Swaminathan, K., Herrlinger, S., Lai, F., Shiekhhattar, R., and Chen, J.F. (2016). A C9ORF72/SMCR8-containing complex regulates ULK1 and plays a dual role in autophagy. *Sci Adv* 2, e1601167.



- Yin, S., Lopez-Gonzalez, R., Kunz, R.C., Gangopadhyay, J., Borufka, C., Gygi, S.P., Gao, F.B., and Reed, R. (2017). Evidence that C9ORF72 Dipeptide Repeat Proteins Associate with U2 snRNP to Cause Mis-splicing in ALS/FTD Patients. *Cell Rep* *19*, 2244-2256.
- Zhang, D., Iyer, L.M., He, F., and Aravind, L. (2012). Discovery of Novel DENN Proteins: Implications for the Evolution of Eukaryotic Intracellular Membrane Structures and Human Disease. *Front Genet* *3*, 283.
- Zhang, Y.J., Gendron, T.F., Grima, J.C., Sasaguri, H., Jansen-West, K., Xu, Y.F., Katzman, R.B., Gass, J., Murray, M.E., Shinohara, M., *et al.* (2016). C9ORF72 poly(GA) aggregates sequester and impair HR23 and nucleocytoplasmic transport proteins. *Nat Neurosci* *19*, 668-677.
- Zhang, Y.J., Jansen-West, K., Xu, Y.F., Gendron, T.F., Bieniek, K.F., Lin, W.L., Sasaguri, H., Caulfield, T., Hubbard, J., Daugherty, L., *et al.* (2014). Aggregation-prone c9FTD/ALS poly(GA) RAN-translated proteins cause neurotoxicity by inducing ER stress. *Acta Neuropathol* *128*, 505-524.
- Zou, Z.Y., Zhou, Z.R., Che, C.H., Liu, C.Y., He, R.L., and Huang, H.P. (2017). Genetic epidemiology of amyotrophic lateral sclerosis: a systematic review and meta-analysis. *J Neurol Neurosurg Psychiatry*.
- Zu, T., Gibbens, B., Doty, N.S., Gomes-Pereira, M., Huguet, A., Stone, M.D., Margolis, J., Peterson, M., Markowski, T.W., Ingram, M.A., *et al.* (2011). Non-ATG-initiated translation directed by microsatellite expansions. *Proc Natl Acad Sci U S A* *108*, 260-265.

## IV. Results

### 1.1 Publication 1:

Distribution of dipeptide repeat proteins in cellular models and *C9orf72* mutation cases suggests link to transcriptional silencing

published as

**Schludi MH**, May S, Grässer FA, Rentzsch K, Kremmer E, Küpper C, Klopstock T, German Consortium for Frontotemporal Lobar Degeneration, Bavarian Brain Banking Alliance, Arzberger T, Edbauer D. Distribution of dipeptide repeat proteins in cellular models and *C9orf72* mutation cases suggests link to transcriptional silencing. *Acta Neuropathol.* 2015. doi:10.1007/s00401-015-1450-z

# Distribution of dipeptide repeat proteins in cellular models and *C9orf72* mutation cases suggests link to transcriptional silencing

Martin H. Schludi<sup>1,2</sup> · Stephanie May<sup>1</sup> · Friedrich A. Grässer<sup>3</sup> · Kristin Rentzsch<sup>1</sup> · Elisabeth Kremmer<sup>1,2,4</sup> · Clemens Küpper<sup>1,2,5</sup> · Thomas Klopstock<sup>1,2,5</sup> · German Consortium for Frontotemporal Lobar Degeneration · Bavarian Brain Banking Alliance · Thomas Arzberger<sup>1,6,7</sup> · Dieter Edbauer<sup>1,2,8</sup>

Received: 2 April 2015 / Revised: 25 May 2015 / Accepted: 3 June 2015  
© The Author(s) 2015. This article is published with open access at Springerlink.com

**Abstract** A massive expansion of a GGGGCC repeat upstream of the *C9orf72* coding region is the most common known cause of amyotrophic lateral sclerosis and frontotemporal dementia. Despite its intronic localization and lack of a canonical start codon, both strands are translated into aggregating dipeptide repeat (DPR) proteins: poly-GA, poly-GP, poly-GR, poly-PR and poly-PA. To address conflicting findings on the predominant toxicity of the different DPR species in model systems, we compared the expression pattern of the DPR proteins in rat

primary neurons and postmortem brain and spinal cord of *C9orf72* mutation patients. Only poly-GA overexpression closely mimicked the p62-positive neuronal cytoplasmic inclusions commonly observed for all DPR proteins in patients. In contrast, overexpressed poly-GR and poly-PR formed nucleolar p62-negative inclusions. In patients, most of the less common neuronal intranuclear DPR inclusions were para-nucleolar and p62 positive. Neuronal nucleoli in *C9orf72* cases showed normal size and morphology regardless of the presence of poly-GR and poly-PR inclusions arguing against widespread nucleolar stress, reported in cellular models. Colocalization of para-nucleolar DPR inclusions with heterochromatin and a marker of transcriptional repression (H3K9me2) indicates a link to gene transcription. In contrast, we detected numerous intranuclear DPR inclusions not associated with nucleolar structures in ependymal and subependymal cells. In patients, neuronal inclusions of poly-GR, poly-GP and the poly-GA interacting protein Unc119 were less abundant than poly-GA inclusions, but showed similar regional and subcellular distribution. Regardless of neurodegeneration, all inclusions were most abundant in neocortex, hippocampus and thalamus, with few inclusions in brain stem and spinal cord. In the granular cell layer of the cerebellum, poly-GA and Unc119 inclusions were significantly more abundant in cases with FTLD than in cases with MND and FTLD/MND. Poly-PR

---

Clinical contributions came from members of the German Consortium for Frontotemporal Lobar Degeneration: Adrian Danek, Janine Diehl-Schmid, Klaus Fassbender, Hans Förstl, Johannes Kornhuber, Markus Otto.

---

Clinical contributions came from members of the Bavarian Brain Banking Alliance: Andres Ceballos-Baumann, Marianne Dieterich, Regina Feurecker, Armin Giese, Hans Klünemann, Alexander Kurz, Johannes Levin, Stefan Lorenzl, Thomas Meyer, Georg Nübling, Sigrun Roeber.

---

T. Arzberger and D. Edbauer are both equal senior coauthors on this work.

---

**Electronic supplementary material** The online version of this article (doi:10.1007/s00401-015-1450-z) contains supplementary material, which is available to authorized users.

---

✉ Thomas Arzberger  
thomas.arzberger@med.uni-muenchen.de

✉ Dieter Edbauer  
dieter.edbauer@dzne.de

<sup>1</sup> German Center for Neurodegenerative Diseases (DZNE), Feodor-Lynen-Str. 17, 81337 Munich, Germany

<sup>2</sup> Munich Cluster of Systems Neurology (SyNergy), Munich, Germany

<sup>3</sup> Institute of Virology, Saarland University Medical School, 66421 Homburg, Germany

<sup>4</sup> Institute of Molecular Immunology, Helmholtz Zentrum München, German Research Center for Environmental Health (GmbH), Marchioninstr. 25, 81377 Munich, Germany

<sup>5</sup> Department of Neurology, Friedrich-Baur-Institute, Ludwig-Maximilians-University, 80336 Munich, Germany

inclusions were rare throughout the brain but significantly more abundant in the CA3/4 region of FTLD cases than in MND cases. Thus, although DPR distribution is not correlated with neurodegeneration spatially, it correlates with neuropathological subtypes.

**Keywords** ALS · FTLD · Repeat disorders · *C9orf72* · DPR inclusions · Neurotoxicity

## Introduction

About 10 % of all patients with amyotrophic lateral sclerosis (ALS), frontotemporal dementia (FTD) or mixed presentation of both diseases (ALS/FTD) are caused by a massive expansion of a GGGGCC repeat upstream of the *C9orf72*-coding region [11, 18, 43]. Three main hypotheses have been proposed to explain the pathomechanism of *C9orf72* disease. First, reduced expression of the mutant allele suggests a loss of function mechanism [11, 18]. Studies in *C. elegans* and zebrafish reported motor deficits [7, 51], although loss of *C9orf72* has no obvious effect in cultured neurons and mice [25, 55]. Second, the repeat RNA may induce toxicity by sequestering endogenous RNA-binding proteins in nuclear RNA foci [16]. A large number of GGGGCC-interacting proteins have been identified, but their contribution to *C9orf72* disease has not been elucidated so far [9, 27, 37]. Additionally, formation of RNA-DNA hybrids of the expanded repeat (so-called R-loops) may contribute to toxicity by interfering with transcription [20, 54]. However, in cultured primary neurons and the fly retina even high-level expression of repeat RNA causes little or no toxicity [35, 55]. Third, although located in an intron and lacking an ATG start codon, sense and antisense transcripts of the expanded repeat are translated by an unconventional mechanism into five dipeptide repeat (DPR) protein species [1, 17, 36, 38, 60]. All DPR species are detected in neuronal inclusions throughout the central nervous system (CNS) of *C9orf72* mutation patients, predominantly in the cytoplasm. Inclusions of poly-(glycine–alanine) (poly-GA), poly-(glycine–arginine) (poly-GR) and poly-(glycine–proline) (poly-GP) proteins encoded by the sense strand are far more abundant than

poly-(proline–alanine) (poly-PA) and poly-(proline–arginine) (poly-PR) proteins encoded by the antisense strand [17, 36]. None of these mechanisms, however, has so far explained the origin of neuronal and glial TDP-43 inclusions found in almost all cases with *C9orf72* mutation, and the variable expression of dementia and motor symptoms even within the same family [16, 33]. Interestingly, the first clinical symptoms and neurodegeneration seem to arise prior to the onset of TDP-43 pathology when DPR inclusion pathology is already widespread [2, 36, 38, 42].

Recently, several groups reported toxicity of recombinantly expressed individual DPR species in cell lines, primary neurons and the fly retina. This led to a controversy about the main toxic DPR species. Several groups showed neurotoxicity of poly-GA, the most abundant DPR inclusion protein in *C9orf72* mutation patients. Poly-GA toxicity has been attributed to co-aggregation of the transport factor Unc119 [34] and impairment of the proteasome [57, 59]. However, in contrast to TDP-43 inclusions, poly-GA inclusions show no spatial correlation with neurodegeneration in patients [10, 29]. Other reports favor toxicity of the arginine-rich DPR species, poly-GR and poly-PR, by interference with global RNA metabolism and protein synthesis [23, 35, 55]. While poly-GR and poly-PR localization was not analyzed in the fly model [35], cell culture studies found overexpressed poly-GR and poly-PR (20–400 repeats) predominantly in nucleolar aggregates [23, 34, 55, 57, 59]. This is in strong contrast to the predominantly cytoplasmic localization of poly-GR and poly-PR described in patients so far [17, 36, 38, 60]. Poly-GP also has been reported to induce toxicity in cell lines, although no mechanism was proposed [60]. Only poly-PA was not toxic in any system tested. However, none of the proposed pathomechanisms has been rigorously validated in patient tissue.

Prompted by conflicting reports on the neurotoxicity of DPR proteins in vitro, we carefully compared the expression of recombinant DPR proteins in primary rat neurons of all DPR species with proposed neurotoxicity, including the predominant sense strand-derived DPR inclusions and poly-PR, in patient brain using novel monoclonal antibodies particularly focusing on nuclear and nucleolar pathology. Since toxic overexpressed arginine-rich DPRs mainly aggregate in p62-negative intranuclear inclusions, we tried to identify such inclusions in key areas of neurodegeneration in patient CNS. Additionally, we analyzed the regional distribution pattern of aggregates containing poly-GA, its interacting partner Unc119, poly-GR, poly-GP or poly-PR in brain and spinal cord of autopsy cases with *C9orf72* mutation and correlated aggregate frequency with the neuropathological diagnosis.

<sup>6</sup> Center for Neuropathology and Prion Research, Ludwig-Maximilians-University Munich, Feodor-Lynen-Str. 23, 81377 Munich, Germany

<sup>7</sup> Department of Psychiatry and Psychotherapy, Ludwig-Maximilians University Munich, Nußbaumstraße 7, 80336 Munich, Germany

<sup>8</sup> Institute for Metabolic Biochemistry, Ludwig-Maximilians University Munich, 81377 Munich, Germany

## Materials and methods

### Antibodies and reagents

The following antibodies were used: anti-nucleolin (rabbit polyclonal and mouse monoclonal, Abcam, Cambridge England), anti-p62/SQSTM1 (rabbit polyclonal, MBL, Nagoya Japan and mouse monoclonal, BD, Belgium), anti-poly-GA clone 5E9 (mouse monoclonal) [29], anti-Unc119 (rabbit polyclonal, homemade) [34], anti-fibrillarlin (rabbit polyclonal, Abcam), anti-GST (rabbit polyclonal, Eurogentec, Belgium), anti-H3K9me2 (Cell Signaling Technology, Cambridge, England), anti-HDAC6 (Santa Cruz, Dallas, Texas), anti-CUG-BP1 (Abcam), anti-PML (Abcam), anti-HSF1 (Santa Cruz), anti-CD99/MIC2 (Thermo scientific, Waltham, Massachusetts), anti-PSMC2 and anti-PSMC4 (Bethyl laboratories, Montgomery, Texas), anti-Coilin (Abcam) and anti-p53 (Ventana, Tuscon, Arizona). Poly-GR antibodies 5A2 and 5H9 have been described previously [36, 38]. The novel poly-GR-specific clone 7H1 (rat isotype IgG2c) was identified by rescreening monoclonal antibodies raised against the EBNA2 epitope GQSRGRGRGRGRGRGKGSRDK with asymmetrically dimethylated arginines [19] and screened by ELISA against biotinylated (GR)<sub>10</sub> peptides (Peps4LifeSciences, Heidelberg, Germany) as described [36]. Like clone 5H9, 7H1 detected (GR)<sub>10</sub> with asymmetrically dimethylated arginines and non-methylated arginines, but also weakly cross-reacts with (GR)<sub>10</sub> containing symmetrically dimethylated arginines (data not shown). By immunizing rats with synthetic GP<sub>10</sub> peptides the poly-GP-specific antibody 7A5 (isotype IgG2c) was raised using previously described protocols [29]. Poly-PR antibody 32B3 (isotype IgG2b) was raised against synthetic PR<sub>10</sub> peptides in mouse using the same protocol.

RNA was stained with SYTO12 and SYTO RNaselect (Life Technologies, Darmstadt, Germany) and nuclei were stained with DAPI (Roche Applied Science, Penzberg, Germany).

### DNA constructs and lentivirus production

Previously described cDNAs of GA<sub>175</sub>-GFP and GFP-GR<sub>149</sub>, GP<sub>80</sub>-V5/His and PR<sub>175</sub>-GFP with ATG start codon were cloned in a lentiviral packing vector (FhSynW2) containing the human synapsin promoter [34]. Poly-GA, poly-GR and poly-PR were expressed from synthetic genes devoid of GGGGCC repeats, while poly-GP was expressed from a ATG(GGGCCG)<sub>80</sub> construct. For poly-GR, the GFP had to be fused to the N-terminus to allow robust expression (for details see [34]). Lentivirus was produced in HEK293FT cells (Life Technologies) as described previously [15].

### Cell culture

Primary hippocampal and cortical neurons were cultured from embryonic day 19 rats and infected for transduction with lentivirus as described previously [15, 48]. For immunofluorescence, the primary neurons were fixed for 10 min in 4 % paraformaldehyde and 4 % sucrose on ice. Primary and secondary antibodies were diluted in GDB buffer (0.1 % gelatin, 0.3 % Triton X-100, 450 mM NaCl, 16 mM sodium phosphate pH 7.4). Confocal images were taken by a LSM710 confocal laser scanning system (Carl Zeiss, Jena, Germany) with a 63× oil immersion objective.

### Patient material, brain slices

Tissue samples of all autopsy cases investigated were provided by the Neurobiobank Munich, Ludwig-Maximilians-University (LMU) Munich. They were collected according to the guidelines of the local ethical committee. Demographic and neuropathological data are listed in Table 1.

### Definition of neuropathological groups

Cases with *C9orf72* mutation were stratified into frontotemporal lobar degeneration (FTLD), motoneuron disease (MND) or mixed FTLD/MND according to neuropathological criteria. FTLD was diagnosed when gliosis and/or spongy alterations were seen in the cortex of the superior

**Table 1** Demographic and neuropathological data of patients and control cases

Case no.	Sex	Age at death	Duration of disease	Neuropathological diagnosis
C9-1	Female	65	3 years	FTLD–MND
C9-2	Female	59	6 months	FTLD–MND
C9-3	Male	65	4 years	FTLD–MND
C9-4	Female	63	3 years	MND
C9-5	Female	49	8 months	MND
C9-6	Male	51	2 years	MND
C9-7	Male	72	1 years	FTLD
C9-8	Female	57	7 years	FTLD
C9-9	Male	67	Unknown	FTLD
C9-10	Male	41	6 years	FTLD–MND
C9-11	Male	56	22 months	FTLD–MND
C9-12	Male	57	3 years	FTLD–MND
C9-13	Male	57	3–4 years	FTLD–MND
C9-14	Male	74	Several years	FTLD–MND
FUS-1	Female	54	4 years	FTLD–MND–FUS
Ctrl-1	Male	60	–	–
Ctrl-2	Female	60	–	–

and/or medial frontal gyrus (Brodman areas 8/9) and/or in the cortex of the parahippocampal and/or fusiform gyrus on hemalum–eosin stainings. MND was diagnosed when either the motor cortex showed gliosis and/or spongy alterations on hemalum–eosin stainings and/or the pyramidal tract showed a microglia activation on immunohistochemical stains using the CR3/43 antibody and/or the hypoglossal nucleus and/or the anterior horn at any spinal cord level showed a loss of motoneurons and/or gliosis and/or p62-positive inclusions in motoneurons.

### Immunohistochemistry

Immunohistochemistry and immunofluorescence were performed on paraffin sections as previously described [29]. For Unc119 immunohistochemistry, paraffin sections were treated 25 min with 0.1 µg/µl proteinase K in 10 mM Tris/HCl. This pretreatment dramatically increased the number of visible Unc119 aggregates (compare [34]). Afterwards the slides were incubated with the Unc119 antibody overnight at 4 °C and detected with the DCS SuperVision 2 Kit (DCS innovative diagnostic-system, Hamburg, Germany) according to the manufacturer's instructions. An additional 0.05 µg/µl proteinase K pretreatment for 1 min before citrate retrieval was used for anti-nucleolin and H3K9me2 immunofluorescence experiments. Anti-poly-GA immunohistochemistry was performed with the Ventana BenchMark XT automated staining system (Ventana) using the UltraView Universal DAB Detection Kit (Roche). Incubation with poly-GR and poly-GP antibodies was done overnight at 4 °C, further steps were an incubation with a rabbit anti-rat antibody (1:2000) for 1 h at room temperature, and a final processing on the Ventana BenchMark XT using the UltraView Universal DAB Detection Kit (Roche). The poly-PR antibody was also incubated overnight at 4 °C and detected the following day on Ventana BenchMark XT. Images of immunohistochemical stainings were taken by CellD, Olympus BX50 Soft Imaging System (Olympus, Tokyo, Japan), confocal images on a LSM710 (Carl Zeiss) with a 40× or 63× oil immersion objective.

### RNA in situ hybridization

Paraffin sections were dewaxed in xylene and ethanol followed by microwaving in citrate pH6 buffer for 4 × 5 min. After washing with 2× SSC (0,3 M NaCl, 30 mM sodium citrate, pH7), sections were preincubated (30 min) at 65 °C in 2× SSC containing 40 % formamide and 2.5 % BSA and incubated over night at 50 °C with the Cy3(GGCCCC)<sub>4</sub> probe (Integrated DNA Technologies, Coralville, Iowa) in 2× SSC containing 0.8 mg/ml tRNA, 0.8 mg/ml salmon sperm DNA, 0.16 % BSA, 8 % dextran sulfate, 1.6 mM ribonucleoside vanadyl complex and 5 mM EDTA. After

washing with 0.5× SSC immunofluorescence was performed as described previously [29]. In all steps, RNase-free Milli-Q ultrapurified water was used.

### Semi-quantitative analysis of inclusion pathology

Frequency of poly-GA, poly-GR, poly-GP and Unc119 inclusion pathology was analyzed separately for neuronal cytoplasmic inclusions (NCI), neuronal intranuclear inclusions (NII) and dystrophic neurites (DN) in a semi-quantitative manner for 36 different CNS regions of five representative cases (C9-1 to 5) with *C9orf72* mutation with a Zeiss Axioplan microscope. In neocortical regions, in the granular and molecular cell layers of the cerebellum and in spinal cord, each type of inclusion pathology was considered as “few” if less than half of 12 representative visual fields (using a 20× objective) showed at least one inclusion, as “some” if more than half but not all visual fields showed at least one inclusion, as “many” if in every visual field at least 4 inclusions were detectable and as “abundant” if each visual field showed more than 20 aggregates. This method was also used for counting dystrophic neurites in all regions. In structures of hippocampus, subcortical nuclei, brain stem and the Purkinje cell layer of the cerebellum, NCIs and NIIs were considered as “few” if less than 2 % of the neurons contained aggregates, “some” if 3–25 % of the neurons contained aggregates, “many” if 25–50 % of the neurons contained aggregates and “abundant” if more than 50 % of the neurons contained aggregates.

### Quantitative analysis of inclusion pathology

The following areas with high loads of DPR protein aggregates but diverging neurodegenerative vulnerability were selected for quantification of NCIs and NIIs: cortex of the superior frontal gyrus, motor cortex, striate area of the occipital cortex, granular cell layer of the dentate gyrus, cornu ammonis regions 3/4, granular cell layer of the cerebellum, molecular cell layer of the cerebellum (superior part).

In all cases with *C9orf72* mutation, 3–12 pictures adjacent to each other were taken from a representative area of each region of interest with a digital camera (Olympus Cam SC30) at an Olympus BX41 microscope using a 40× objective for cerebellar granular cell layer and a 20× objective for all other regions. Three to four pictures were taken from each cerebellar and hippocampal region. In neocortex, pictures were taken in a columnar orientation covering all six cell layers. The inclusions of one such column represented by 6–12 adjacent pictures were counted. All NCIs and NIIs were manually counted on each digital picture separately using the CellCounter plugin in Fiji ImageJ. For each region in each case, the total number of inclusions was

divided by the number of pictures taken, and the average value was determined. Finally, the average of the values for each region was determined in each neuropathological group (FTLD, MND, FTLN/MND) separately.

## Statistics

Statistical analysis was performed with GraphPad Prism software (version 6.01). The groups with neuropathological diagnosis MND, FTLN and FTLN/MND were compared and analyzed by two-way ANOVA followed by Tukey's post hoc test. Nucleolus size (Feret diameter) was quantified from confocal images, taken on a LSM710 with a 40× oil immersion objective, using Fiji ImageJ particle analyzer and statistically evaluated by an unpaired *t* test followed by an *F*-test to compare variances. Multiple comparison of the size of the nucleoli in the frontal cortex was done by one-way ANOVA followed by Tukey's post hoc test. Significance level was set at  $p < 0.05$  (two sided).

## Results

### Intranuclear poly-GR and poly-PR inclusions are nucleolar in cell models, but para-nucleolar in patients

To compare DPRs expressed from synthetic genes and DPR inclusions in *C9orf72* mutation patients under optimal conditions, we raised novel monoclonal antibodies. Rat poly-GP antibody 7A5, rat poly-GR antibody 7H1 and mouse poly-PR antibody 32B3 specifically detected the respective 15-mer DPRs fused to GST (Fig. S1a). 7A5 and 7H1 robustly detected SDS-insoluble aggregates in frontal cortex of patients but not of controls cases (Fig. S1b). In patients, poly-GR antibody 7H1 detected more neuronal cytoplasmic inclusions than the previously used clone 5H9 (Fig. S1c). The monoclonal poly-GP and poly-PR antibodies also allowed a more sensitive detection of poly-GP and poly-PR inclusions than our previous polyclonal antibodies [36, 38]. With the new antibodies, poly-GR and poly-GP aggregates were found in various brain areas and in spinal cord motoneurons of *C9orf72* mutation patients, but not of control cases (Fig. S2a, b). Poly-PR inclusions were much less common in all brain regions (Fig. S2c). Despite a recent report of preferential aggregation of poly-PR in spinal cord motoneurons [8], we found no such inclusions with both the mouse poly-PR antibody 32B3 and our rabbit polyclonal antibody [39].

To analyze the DPR proteins in vitro, we transduced rat hippocampal neurons with a lentivirus expressing GFP-GR<sub>149</sub>, PR<sub>175</sub>-GFP, GA<sub>175</sub>-GFP or GP<sub>80</sub>-V5/His for 7 days. Consistent with previous results [34, 57, 59], GFP-GR<sub>149</sub> showed a diffuse cytoplasmic distribution and often formed

nuclear aggregates that colocalized with nucleolin, a key component of the nucleolus (Fig. 1a, first row). PR<sub>175</sub>-GFP showed more pronounced nuclear and nucleolar localization and the majority of nucleoli appeared fragmented (Fig. 1a, second row). GA<sub>175</sub>-GFP formed compact mainly cytoplasmic and some intranuclear inclusions that did not colocalize with nucleolin (Fig. 1a, third row). GP<sub>80</sub>-V5/His expression was diffusely distributed throughout the neurons with some enrichment in the nucleus (Fig. 1a, fourth row). Lentiviral expression of the four DPR constructs in cortical neurons fully confirmed the localization found in hippocampal neurons (Fig. S3).

In contrast to transduced hippocampal neurons, poly-GR and poly-PR antibodies labeled mainly cytoplasmic inclusions in *C9orf72* mutation patients (Fig. S2a, c), an observation consistent with previous reports [17, 36, 38, 60]. However, a fraction of neurons also contained small poly-GR and poly-PR inclusions in the nucleus (Fig. 1b, first and second row). Quantitative analysis revealed that 78 % of the poly-GR NIIs were attached to the nucleoli, whereas the remaining NIIs were randomly distributed (Fig. 1b, first row, Fig. S4a). In contrast to GFP-GR<sub>149</sub> and PR<sub>175</sub>-GFP expressing neurons, we never saw a colocalization of poly-GR or poly-PR and nucleolin in three *C9orf72* cases investigated. Immunofluorescence with two other monoclonal poly-GR antibodies (5H9 and 5A2) [36, 38] confirmed these results (Fig. S4b). Moreover, poly-GR did not colocalize with fibrillarin, another nucleolar marker (Fig. S4c). Intranuclear poly-GA and poly-GP showed a very similar pattern of para-nucleolar inclusions in *C9orf72* mutation patients (Fig. 1b, rows three and four; Fig. S4a). Thus, current cellular DPR models cannot fully replicate the pattern of intranuclear aggregates found in patient tissue.

### Para-nucleolar DPR aggregates colocalize with silent DNA

To elucidate the nature of the para-nucleolar DPR compartment, we analyzed colocalization with several marker proteins (data not shown). However, none of the markers for Marinesco bodies (HDAC6), the perinuclear compartment (CUG-BP1, PML, HSF1 and CD99), clastosomes (proteasomal subunits PSMC2 and PSMC4) and nucleolar caps (fibrillarin, coilin and PML) colocalized with para-nucleolar DPR inclusions, indicating they represent a unique compartment. Moreover, the para-nucleolar DPR protein aggregates were also not colocalized with the nuclear GGGGCC RNA foci in frontal cortex or cerebellum (Fig. S4d/e). However, many para-nucleolar DPR inclusions colocalized with heterochromatin detected by the DNA-binding dye DAPI in patients (Fig. 2a), which was not observed for poly-GA, poly-GR, poly-PR or poly-GP overexpressed in primary neurons (Fig. 1a). Para-nucleolar DPR inclusions

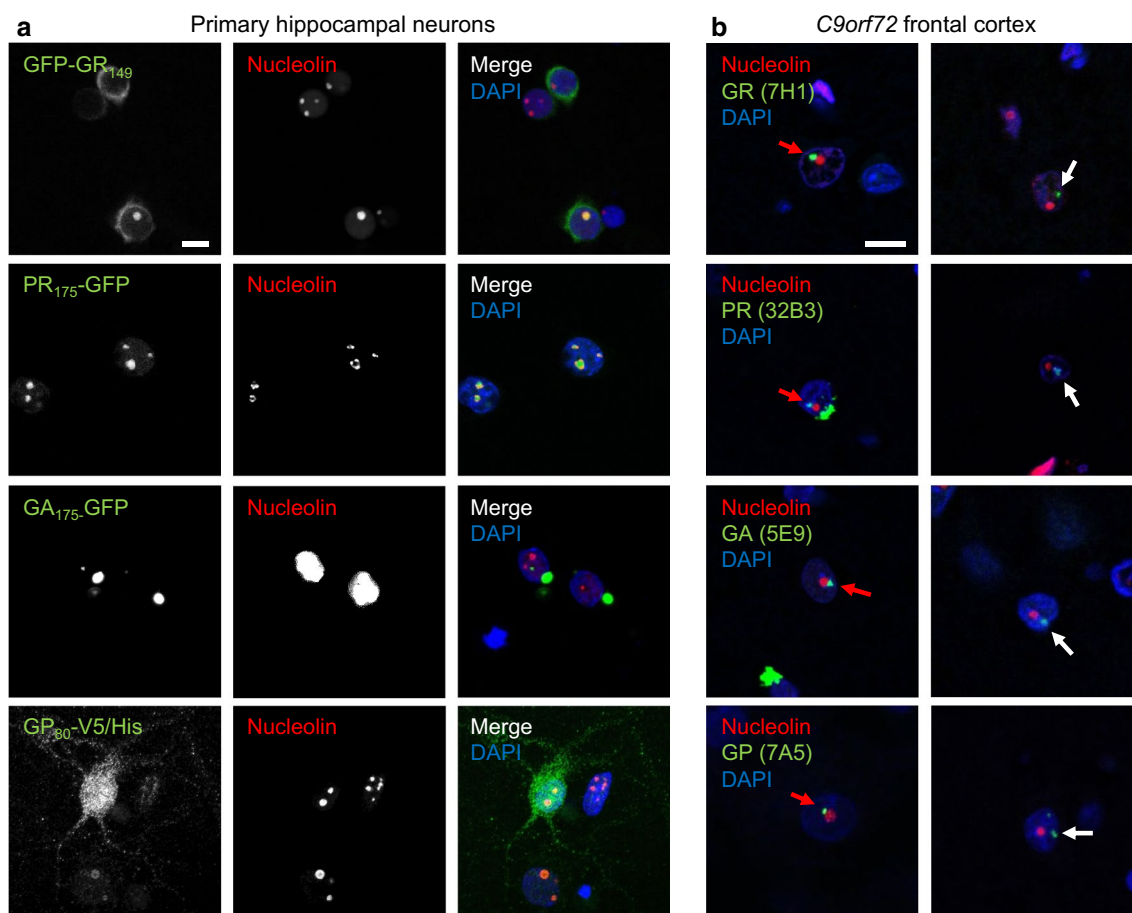


**Fig. 1** Differential localization of intranuclear DPR inclusions in transduced primary neurons and in neurons of cases with *C9orf72* mutation. Double immunofluorescence for different DPR proteins (green) and nucleolin (red), a marker for the nucleolus, in primary neurons (**a**) and in frontal cortex of cases with *C9orf72* mutation (**b**). Nuclei are labeled with DAPI. Single confocal sections containing the nucleolus are shown. **a** Primary neurons transduced with lentivirus expressing either GFP-GR<sub>149</sub>, PR<sub>175</sub>-GFP, GA<sub>175</sub>-GFP or GP<sub>80</sub>-V5/His (DIV6 + 7). Note that poly-GR and poly-PR but not poly-

GA intranuclear inclusions are localized in the nucleolus. Poly-GA forms mainly compact cytoplasmic inclusions. Poly-GP expression is mainly pan-nuclear and also cytosolic. **b** In cortical areas of cases with *C9orf72* mutation neuronal intranuclear poly-GA, poly-GR and poly-GP inclusions are mostly localized adjacent to the nucleolus (red arrows) or less frequently randomly distributed (white arrows). No colocalization of DPR proteins with the nucleolus is observed. Scale bars represent 10  $\mu$ m

were also labeled by the RNA-binding dyes SYTO12 and SYTO RNaselect, but no RNA enrichment was observed compared to the nucleolus (Fig. 2b). Since all RNA dyes also cross-react with DNA to some extent, we focused on the specific enrichment of heterochromatin DNA in para-nucleolar DPR inclusions. Colocalization was even more pronounced with an antibody for histone 3 dimethylated at lysine 9 (H3K9me2), a signal for transcriptional silencing (Fig. 2c). This may link para-nucleolar DPR proteins to transcriptional changes induced by the expanded *C9orf72* repeat DNA and RNA [20].

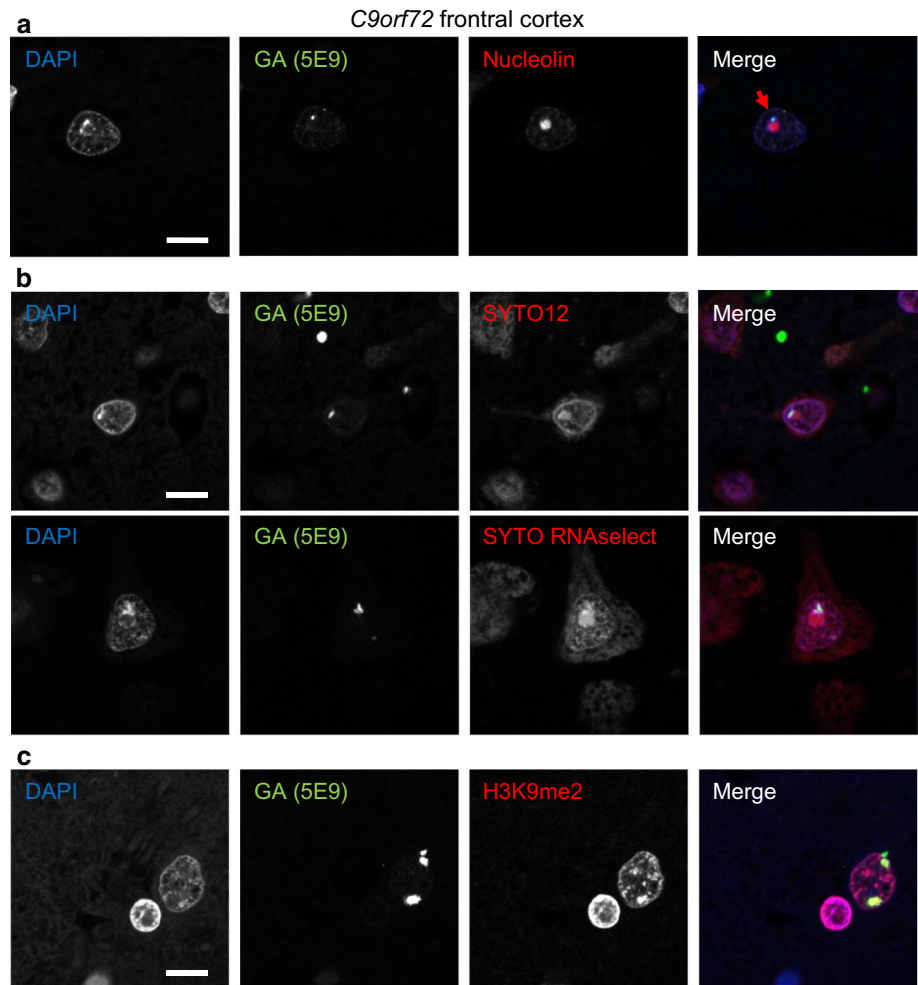
Since arginine-rich DPR proteins and transcription of the expanded repeat have been shown to induce nucleolar stress in cellular models [20, 50], we also investigated

nucleolar size and morphology. Nucleolin stainings of the CA3/4 layer of the hippocampus, a region with abundant DPR pathology, revealed no differences in nucleolus shape and size between *C9orf72* patients and controls (Fig. S5a, b). In the frontal cortex of *C9orf72* FTLD cases, the size of the nucleoli did not differ from nucleoli of healthy controls regardless, whether the cells contained cytoplasmic or para-nucleolar or no DPR inclusions (Fig. S5c).

Nucleolar stress typically results in nucleolar p53 accumulation [26], which we did not observe in *C9orf72* cases (Fig. S5d). Thus, the expanded hexanucleotide repeat DNA and/or RNA may interfere with transcriptional processes without inducing overt nucleolar stress in the hippocampus and cortical areas.



**Fig. 2** Para-nucleolar poly-GA inclusions colocalize with transcriptionally silenced DNA. Immunofluorescence for poly-GA proteins with the indicated antibodies and dyes to label DNA or RNA in frontal cortex of cases with *C9orf72* mutation. **a** Para-nucleolar poly-GA inclusions are enriched for heterochromatin labeled with the DNA-specific dye DAPI (*arrow*). **b** Para-nucleolar poly-GA inclusions are also stained with RNA-selective dyes SYTO12 and SYTO RNaselect. Note that both dyes also show chromatin staining similar to DAPI indicating cross-reactivity with DNA. **c** Nuclear poly-GA inclusions colocalize with histone 3 dimethylated at lysine 9 (H3K9me2), a marker for transcriptionally inactive DNA. Scale bars represent 10  $\mu$ m



### Overexpressed and patient poly-GR, poly-PR and poly-GP show different p62 labeling

p62 is found in many inclusion bodies of neurodegenerative diseases. Although most inclusions of all DPR species colocalize with p62 in *C9orf72* patients [36, 38], we and others had only found a colocalization of p62 with overexpressed poly-GA but not with other overexpressed DPR species in HEK293 cells [34, 57]. We therefore tested p62 co-aggregation in primary hippocampal neurons with lentiviral expression of GA<sub>175</sub>-GFP, GFP-GR<sub>149</sub>, PR<sub>175</sub>-GFP, GP<sub>80</sub>-V5/His. Consistent with previous results, most cytoplasmic and intranuclear GA<sub>175</sub>-GFP inclusions were strongly co-labeled with p62 antibodies (Fig. 3a, first row), while GFP-GR<sub>149</sub> and PR<sub>175</sub>-GFP inclusions were negative for p62 (Fig. 3a, second row and Fig. S6a). GP<sub>80</sub>-V5/His was diffusely expressed with enrichment in the nucleus without obvious p62 colocalization (Fig. 3a, third row). These results were confirmed in cortical neurons transduced with the same DPR constructs (Fig. S6b).

We wondered whether such p62-negative poly-GR inclusions occur in patients, particularly in the nucleolus. In frontal cortex, double immunostaining revealed a strong colocalization of poly-GR and p62 in the cytosol and the nucleus, similar to poly-GA (Fig. 3b, first and second row, Fig. S7a, first row). Only very few poly-GR inclusions in the cytosol (Fig. 3b, second row) as well as in the nucleus (Fig. S7a, second row) were not labeled with p62. Similarly, the vast majority of poly-GP and poly-PR inclusions co-stained with p62 (Fig. 3b, third row and Fig. S7b).

Moreover, double immunostaining of p62 and nucleolin revealed no colocalization of ubiquitinated inclusions and the nucleolus (Fig. 3c). However, occasionally p62 labeling was observed next to the nucleolus, which was consistent with the findings for specific DPR antibodies (Fig. 1b). Together, these findings indicate that in patients with *C9orf72* mutation most intranuclear DPRs aggregate in a p62-positive para-nucleolar compartment and not directly within the nucleolus.

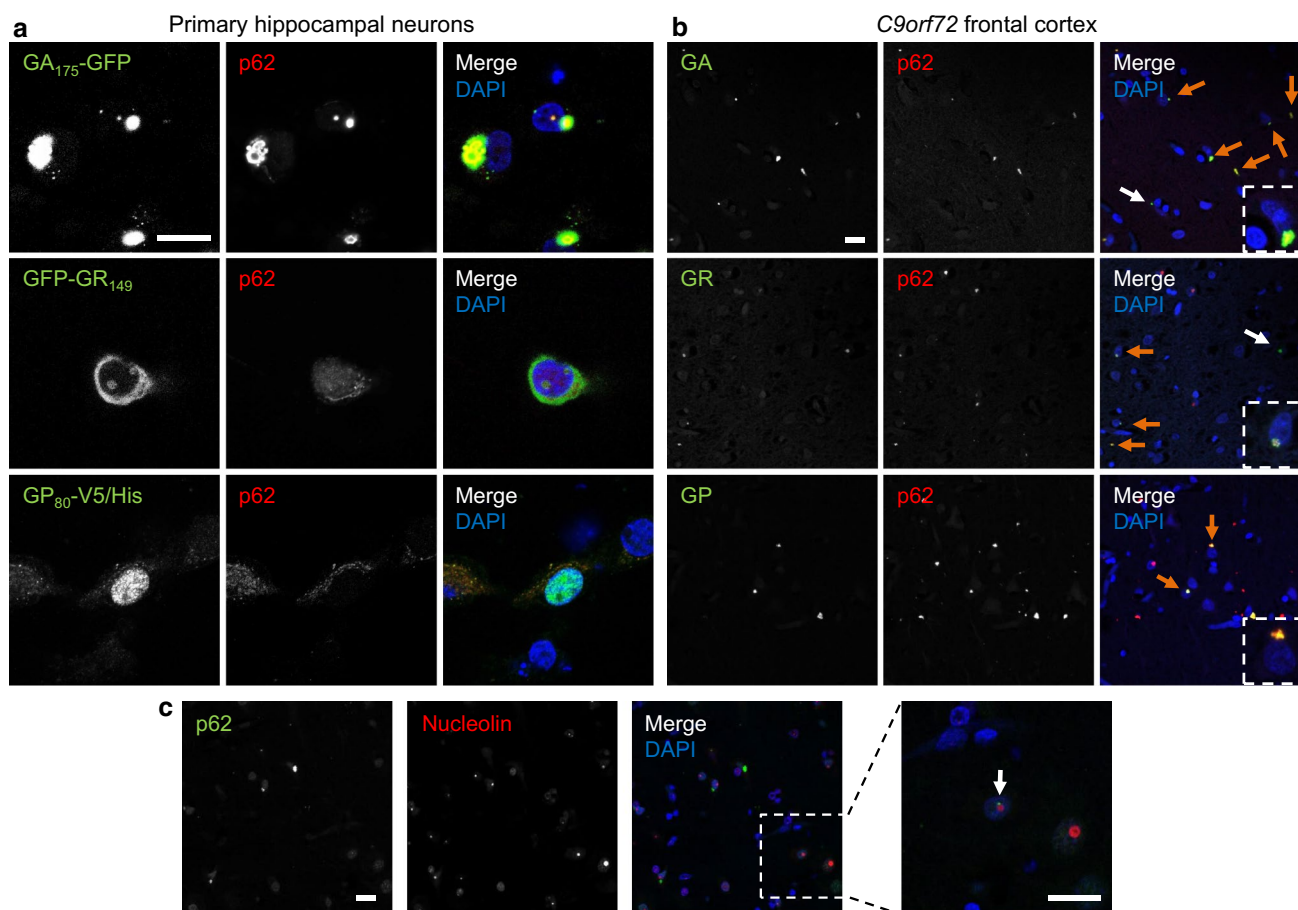


**Fig. 3** Differential colocalization of DPR and p62 inclusions in cases with *C9orf72* mutation and cell culture. Double immunofluorescence for DPR proteins and p62. Nuclei are labeled with DAPI. **a** In primary hippocampal neurons transduced with GA<sub>175</sub>-GFP, GFP-GR<sub>149</sub> or GP<sub>80</sub>-V5/His (DIV6 + 7) p62 co-aggregates with cytoplasmic and intranuclear poly-GA inclusions, but not with poly-GR and poly-GP. In contrast to poly-GA inclusions, poly-GR and poly-GP aggregates

appear less compact or granular. **b** In frontal cortex of *C9orf72* mutation patients almost all poly-GA and poly-GR and all poly-GP inclusions are positive for p62 (orange arrows). Poly-GA and poly-GR inclusions without p62 labeling are rare (white arrows). **c** Intranuclear p62 aggregates show the same distribution pattern as DPR inclusions and are mostly para-nucleolar (arrow). Scale bars represent 20 μm

### Poly-GR and poly-GP inclusion types resemble poly-GA pathology and also occur in glia

To further analyze the correlation of DPR inclusions with neurodegeneration, we characterized the spectrum of poly-GR, poly-GP and poly-PR pathology in *C9orf72* mutation patients. Poly-GR (7H1), poly-GP (7A5) and poly-PR (32B3) antibodies labeled predominantly NCIs throughout the brain, which showed the characteristic star-shaped appearance in pyramidal cells of the hippocampal formation and cortical neurons (Fig. 4a–c). Additionally, NIIs and “pre-inclusions” with diffuse cytoplasmic staining were also detected with all three DPR antibodies (Fig. 4d–i). Only poly-GR and poly-GP antibodies also detected DNIs (Fig. 4j, k). Additionally, poly-GP antibodies occasionally visualized diffuse pan-nuclear DPR expression (Fig. 4l), resembling the pattern of recombinant poly-GP expression in neurons (Figs. 1a, 3a, S3).

Although DPR proteins had previously been described exclusively in neurons, we noticed intranuclear inclusions in ependymal cells of the spinal cord central canal in *C9orf72* cases with MND most prominently with poly-GA antibodies (Fig. 4m, n), but also with poly-GR and poly-GP antibodies (Fig. 4o, p). Such glial inclusions were not detected in an FTLD–MND–FUS case confirming antibody specificity (Fig. S7c). Strikingly, the vast majority of these inclusions were intranuclear, while most neuronal DPR inclusions were cytoplasmic. In contrast to neuronal intranuclear DPR inclusions, the ependymal inclusions were not associated to the nucleolus (Fig. S7d). We observed further glial intranuclear poly-GA inclusions in ependymal and subependymal cells lining the lateral ventricle (Fig. 4q). Thus, not only TDP-43 pathology but also DPR pathology extends to glial cells in *C9orf72* mutation patients.

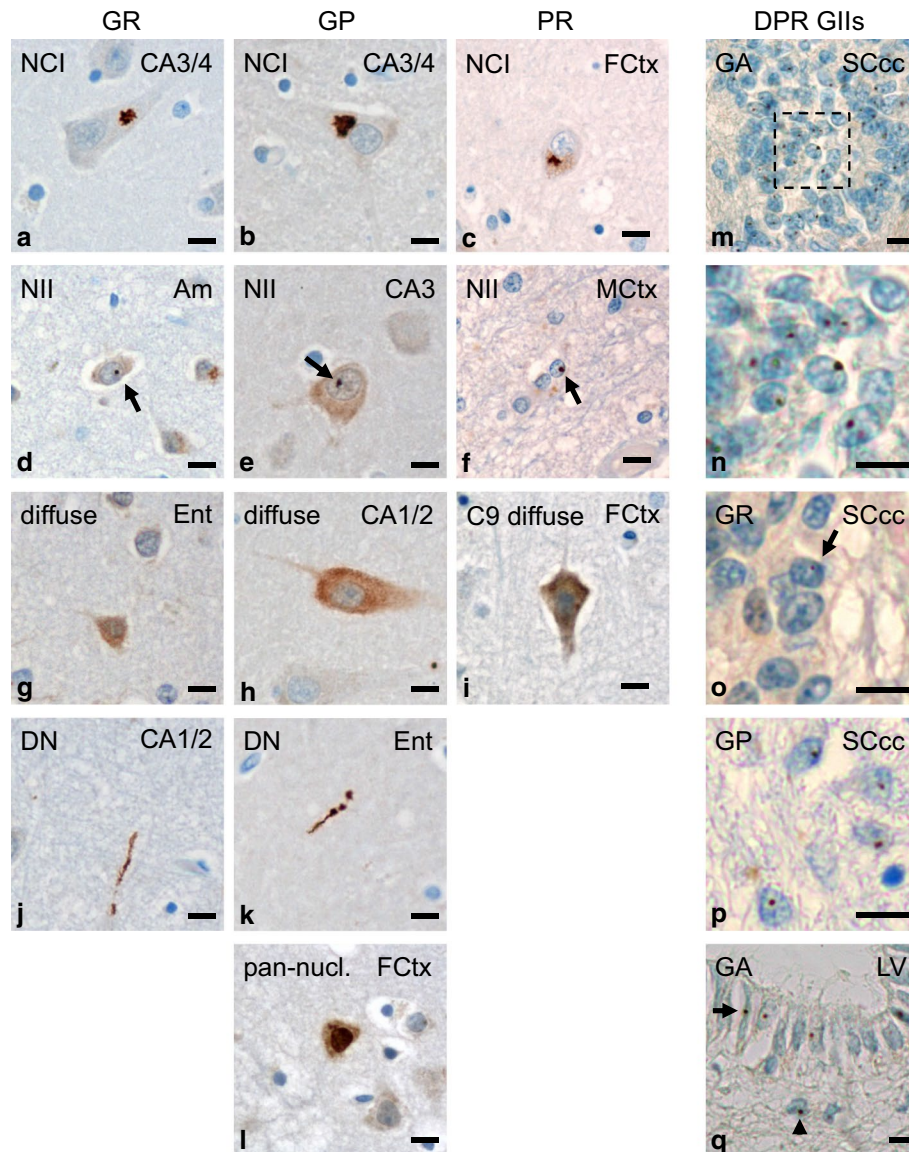


**Fig. 4** Spectrum of DPR pathology in neurons and glial cells of patients with *C9orf72* mutation. **a–l** Immunohistochemistry with novel monoclonal antibodies for poly-GR (clone 7H1), poly-GP (clone 7A5) and poly-PR (clone 32B3) in cases with *C9orf72* mutation. Poly-GR, poly-GP and poly-PR mainly form compact characteristic star-like cytoplasmic (**a–c**) or small round intranuclear inclusions (**arrows** in **d–f**) in neurons and show a diffuse granular cytoplasmic staining (**g–i**). Furthermore there are poly-GR and poly-GP aggregates in dystrophic neurites (**j, k**); note that dystrophic neurites with poly-PR could not be detected. Solely for poly-GP, a diffuse pan-nuclear staining is also found (**l**). **m–q** Immunohistochemistry with indicated DPR antibodies shows glial intranuclear inclusions in

*C9orf72* cases. In ependymal cells of spinal cord central canal intranuclear inclusions of poly-GA (**m, n** detail of **m**), and less frequently of poly-GR (**o**) and poly-GP (**p**) are detectable; further glial intranuclear inclusions of poly-GA are present in ependymal (**arrow**) and subependymal (**arrowhead**) cells of the lateral ventricle wall at level of accumbens nucleus (**q**). *Scale bars* represent 20  $\mu$ m. *Am* amygdala, *CA* cornu ammonis region, *DN* dystrophic neurite, *Ent* entorhinal cortex, *FCtx* frontal cortex, *GII* glial intranuclear inclusion, *MCtx* primary motor cortex, *LV* wall of lateral ventricle, *NCI* neuronal cytoplasmic inclusion, *NII* neuronal intranuclear inclusion, *SC* spinal cord, *SCcc* spinal cord central canal

Taken together, the poly-GR and poly-GP inclusion pattern resembled that of poly-GA in *C9orf72* mutation patients [10, 29, 38]. Poly-PR inclusions were very rare and were not found in DNs. The identification of different types of inclusions in neuronal and glial cells suggests cell type-dependent differences in DPR aggregation or degradation.

### Spectrum and distribution of DPR inclusions

To further elucidate the spectrum of DPR pathology in *C9orf72* mutation patients, we analyzed the load of NCI, NII and DN pathology in 36 CNS regions using monoclonal antibodies for poly-GA (clone 5E9), poly-GR (clone

7H1) and poly-GP (clone 7A5) in five representative cases with comprehensive tissue collection, including two MND cases and three FTLD/MND cases (C9-1 to C9-5, see Table 1). Overall poly-PR distribution pattern appeared similar (not shown), but the number of inclusions was too low for a reliable semi-quantitative analysis.

In all brain regions, DPR inclusion pathology in form of NCIs, NIIs and DNs was most abundant for poly-GA (Fig. 5a) and less distinct for poly-GR and poly-GP (Fig. 5b, c; Table S1). Regardless of the neuropathological diagnosis, all cases showed the strongest DPR pathology in neocortex, hippocampus and cerebellum. DPR inclusions were also abundant in amygdala and thalamus. Few inclusions were visible in basal ganglia, brain stem and spinal cord. Overall, DNs with poly-GR aggregates were less frequent than those with poly-GA or poly-GP aggregates. The highest density of poly-GA or poly-GP containing DNs was seen in the molecular layer of the cerebellum. Despite the abundant intranuclear inclusions of overexpressed poly-GR in various cell models, poly-GR NIIs were even less frequent than poly-GA and poly-GP NIIs in *C9orf72* mutation patients. Poly-GR NIIs were most abundant in the thalamus compared to poly-GR NCIs. Thus, the pattern of poly-GA, poly-GR and poly-GP inclusions pathology is consistent with previous less detailed reports [1, 29, 36]. The biggest difference between the three sense strand-derived DPR species was the almost complete lack of poly-GR DNs throughout the CNS.

### Poly-PR but not poly-GR inclusions show different distribution in FTLD and MND cases

To better analyze the correlation of poly-GR and poly-PR pathology with neurodegeneration, we focused on seven key regions that are variably affected in *C9orf72* mutation patients. We counted the number of inclusions in a defined number of visual fields in three neocortical regions (cortex of the medial frontal gyrus, motor cortex striate area of the occipital cortex), two hippocampal regions (granular cell layer of the dentate gyrus, pyramidal cell layer of cornu ammonis regions 3 and 4) and the granular and molecular cell layers of the cerebellar cortex (for details see methods). Compared to the semi-quantitative analysis (Fig. 5), we used a larger cohort of 14 patients, including three MND cases, three FTLD cases and eight patients with combined FTLD/MND (Table 1). Strikingly, poly-GR load was similar in occipital cortex, which is not affected by neurodegeneration in any of the three patient groups, and in frontal cortex, which is degenerated in FTLD and FTLD/MND cases, but not in MND cases (Fig. 6a; Table S2). In contrast, DPR abundance was less in the motor cortex than in frontal or occipital cortex, although we did not have material for comparison from patients without

neuropathological signs of MND. Overall, poly-GR inclusions showed a very similar distribution pattern among all three patient subgroups, suggesting that poly-GR aggregation does not spatially correlate with neurodegeneration in *C9orf72* mutation patients.

Poly-PR inclusions were scarce throughout the CNS with the highest frequency in the hippocampus. In three cases (MND and FTLD/MND, 6 sections each), we found no poly-PR in spinal cord motoneurons. Poly-PR was significantly more abundant in the CA3/4 region of FTLD cases compared to MND cases (Fig. 6b). Thus, poly-PR, but not poly-GR, distribution differs between *C9orf72* disease subtypes, although it is not spatially correlated with neurodegeneration.

### Spectrum of Unc119 inclusion pathology

Next, we analyzed the distribution of Unc119, a transport factor for myristoylated proteins, which co-aggregates with poly-GA [34]. In our previous analyses, Unc119 inclusions were more prominent in regions affected by prominent neurodegeneration in three *C9orf72* mutation patients, but staining intensity and inclusions density varied considerably between patients. To improve detection of Unc119 inclusions, we tested several conditions for antigen retrieval (see method section for details). Brief proteinase K treatment completely removed the diffuse Unc119 staining in the neuronal soma of patients and controls, but dramatically increased visible Unc119 inclusion pathology in *C9orf72* mutation patients (Fig. 7). Using this improved staining protocol, we identified abundant Unc119 inclusions not only in the frontal cortex, the dentate gyrus but also in the cerebellum (Fig. 7a–c). Rare Unc119 inclusions were also seen in the cytoplasm of spinal cord motoneurons (Fig. 7d) and in the nuclei of central canal ependymal cells (Fig. 7e). No Unc119 inclusions were found in control cases (Fig. 7f–j). The spectrum of proteinase K resistant Unc119 pathology ranged from predominant NCIs to less abundant NIIs and DNs and to rare diffuse aggregates (Fig. 7k–n). Moreover, para-nucleolar Unc119 inclusions colocalizing with poly-GA were found, indicating that Unc119 can be recruited into the nucleus by poly-GA aggregates (Fig. S8). Overall, the pattern of Unc119 pathology in cases with *C9orf72* mutation strongly resembled the pattern of DPR pathology.

### Regional distribution of poly-GA and Unc119 inclusions differs between MND and FTLD cases

To analyze the correlation of Unc119 aggregation and neurodegeneration, we extended our analysis to further CNS regions in the five representative cases (C9-1 to C9-5, see Table 1). We found many Unc119 inclusions throughout

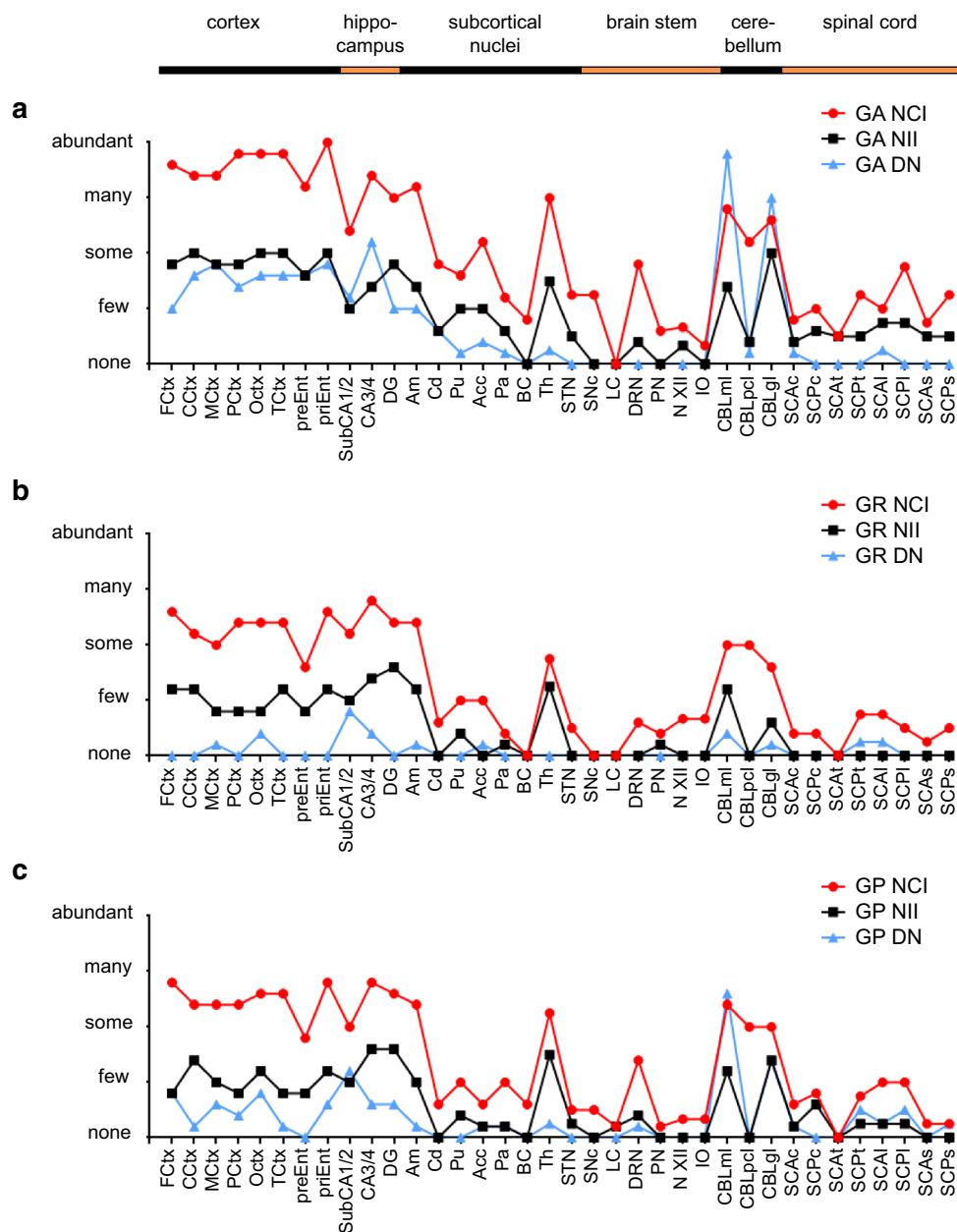


**Fig. 5** Regional distribution pattern of neuronal poly-GA, poly-GR and poly-GP inclusion pathology in cases with *C9orf72* mutation. Semi-quantitative immunohistochemical analyses for poly-GA (a), poly-GR (b) and poly-GP (c) neuronal cytoplasmic inclusions (NCI), neuronal intranuclear inclusions (NII) and dystrophic neurites (DN) in representative cortical, hippocampal, subcortical, brain stem, cerebellar and spinal cord areas of five *C9orf72* mutation patients reveal a predominance of poly-GA aggregates for all types of aggregates in all areas. Highest densities of poly-GA, poly-GR and poly-GP aggregates are seen in cortical areas, hippocampus, amygdaloid nuclei, thalamus and cerebellum. Note that poly-GR-positive DNs are rarely found outside the hippocampus. Categories for semi-quantitative analysis (none, few, some, many, abundant) are explained in detail in the “Materials and methods” section. *Acc* accumbens nucleus, *Am* amygdaloid nuclei, *BC* basal nucleus of Meynert compact part, *CA3/4* cornu ammonis fields 3/4, *CBLgl* cerebellar granular cell layer,

*CBLml* cerebellar molecular cell layer, *CBLpcl* cerebellar Purkinje cell layer, *CCtx* cortex of cingulate gyrus, *Cd* caudate nucleus, *DG* dentate gyrus, *DRN* dorsal raphe nuclei, *FCtx* frontal cortex, *IO* inferior olive, *LC* locus coeruleus, *MCtx* primary motor cortex, *N XII* hypoglossal nucleus, *OCtx* occipital cortex, *Pa* pallidum, *PCtx* parietal cortex, *PN* pontine nuclei of pons, *preEnt* lamina principalis externa of entorhinal cortex, *priEnt* lamina principalis interna of entorhinal cortex, *Pu* putamen, *SCAc* anterior horn of cervical spinal cord, *SCAl* anterior horn of lumbar spinal cord, *SCAs* anterior horn of sacral spinal cord, *SCAt* anterior horn of thoracic spinal cord, *SCPc* posterior horn of cervical spinal cord, *SCPI* anterior horn of lumbar spinal cord, *SCPp* posterior horn of lumbar spinal cord, *SCPp* posterior horn of thoracic spinal cord, *SNc* substantia nigra compact part, *STN* subthalamic nucleus, *SubCA1/2* subiculum plus cornu ammonis fields 1/2, *TCtx* temporal cortex, *Th* thalamus

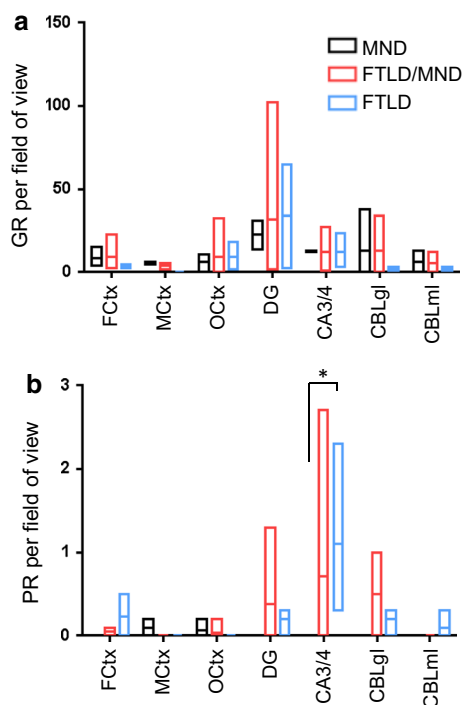


**Fig. 6** Quantitative assessment of poly-GR and poly-PR inclusion pathology in selected brain areas of *C9orf72* cases with different neuropathological phenotypes. The graphs show the minimum, mean and maximum number of poly-GR and poly-PR inclusions averaged per visual field. **a** There is no significant difference in the average number of cytoplasmic and intranuclear neuronal poly-GR inclusions per visual field (20× objective, 40× for cerebellar granular cell layer) between *C9orf72* cases with motoneuron disease (MND,  $n = 2-3$ ), cases with frontotemporal lobar degeneration (FTLD,  $n = 3$ , no MtCtx) and cases with a combination of frontotemporal lobar degeneration and motoneuron disease (FTLD/MND,  $n = 4-8$ ) in brain areas with highest poly-GR load. **b** Poly-PR inclusions are only common in hippocampus and cerebellum of FTLD and FTLD/MND cases, but absent in MND cases, reaching statistical significance in CA3/CA4 (ANOVA,  $p = 0.0103$ ). The quantitative analysis is explained in detail in the “Materials and methods” section. The data for individual cases are presented in Table S2. CA3/4 cornu ammonis fields 3/4, CBLgl cerebellar granular cell layer, CBLml cerebellar molecular cell layer, DG dentate gyrus, FCtx frontal cortex, MCtx primary motor cortex, OCtx occipital cortex

the neocortex, hippocampus and thalamus (Fig. 8a; Table S1). In contrast to findings using our previous staining protocol, Unc119 inclusions were now also frequent in the cerebellum. Overall, Unc119 distribution closely resembled poly-GA distribution (Fig. 5a), although Unc119 inclusions were less frequent in all brain regions (Fig. 8a). Unc119 NIIs were most prominent in the dentate gyrus and completely absent in the brain stem.

A quantitative analysis of the complete patient cohort revealed no difference in the poly-GA and Unc119 frequency in cortical regions and hippocampus between the MND, FTLD or FTLD/MND patients (Fig. 8b, c; Table

S2). As for poly-GR (Fig. 6a), the poly-GA load was similar in the non-degenerating occipital cortex and the degenerating frontal cortex of FTLD and FTLD/MND patients (Fig. 8b). Unexpectedly, poly-GA and Unc119 inclusions were significantly more common in the cerebellar granular cell layer of FTLD patients compared to MND or FTLD/MND patients (Fig. 8b, c). Interestingly, these patients showed a trend towards lower levels of poly-GR inclusions (Fig. 6a), suggesting differential translation or aggregation of these DPR species in the cerebellum. These findings are consistent with an emerging role of the cerebellum in the pathophysiology of *C9orf72* disease [13, 14, 30–32, 52, 56].

## Discussion

With this study, we provide the first quantitative analysis of the three major DPR species poly-GA, poly-GR and poly-GP as well as poly-PR in a neuropathologically characterized cohort of *C9orf72* mutation patients using monoclonal antibodies. Despite ample in vitro evidence especially for poly-GA, poly-GR and poly-PR toxicity [23, 34, 35, 50, 55, 57, 59, 60], we could not identify a spatial correlation between DPR inclusion pathology and neurodegeneration in patients, although poly-GA and poly-PR showed different distribution in MND and FTLD cases. Different localization and aggregation behavior especially of poly-GR and poly-PR proteins in cellular models and patients may explain the poor translatability of the in vitro results. The newly identified para-nucleolar aggregation of DPR proteins in heterochromatin structures in patient neurons hints for repeat-associated alterations in transcription.

## Subcellular localization of DPR proteins

In patients, poly-GA, poly-GR, poly-GP and poly-PR showed remarkably similar regional and subcellular expression patterns, suggesting that these proteins are co-translated in most cells and then co-aggregate in p62-positive inclusions [38]. In transduced primary neurons, only poly-GA expression gives rise to p62-positive compact cytoplasmic inclusions. Consistent with previous reports overexpressed poly-GR and poly-PR predominantly localized to the nucleolus and was p62 negative in primary neuron culture [34, 50, 57]. However, in patients with *C9orf72* mutation, poly-GR and poly-PR inclusions were predominantly cytoplasmic, and we did not find a single nucleolar inclusion. Overexpression of poly-GP in neurons resulted either in diffuse cytoplasmic or more often diffuse pan-nuclear accumulation similar to previous reports [57]. We found both expression patterns in patients, although compact NCIs were much more common.

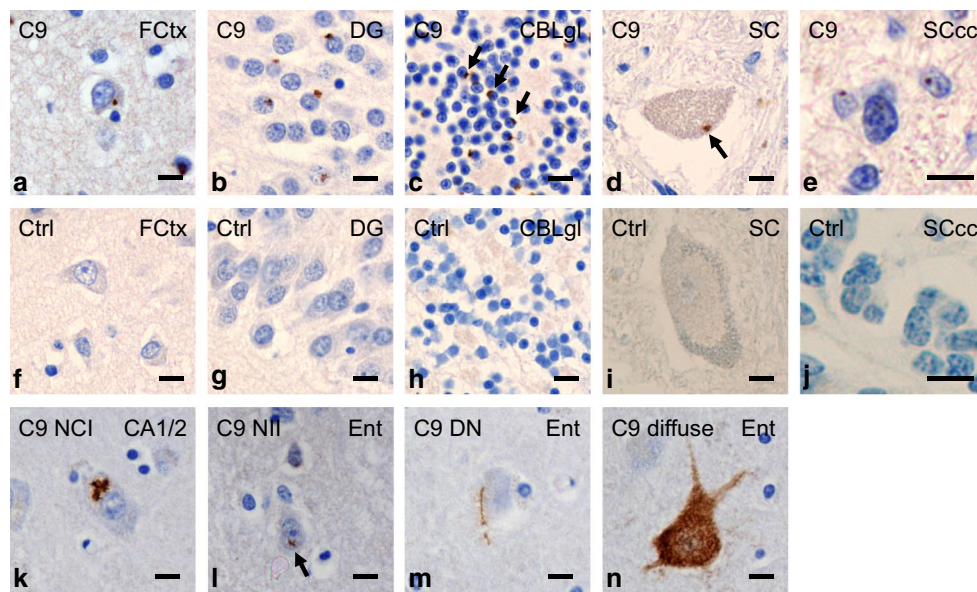


**Fig. 7** Spectrum of Unc119 pathology in cases with *C9orf72* mutation resembles poly-GA pathology. Immunohistochemistry with a polyclonal rabbit antibody against Unc119. In *C9orf72* mutation cases, numerous Unc119 inclusions are seen in neurons of various brain areas (a–c), rarely in motoneurons of spinal cord (d) and in ependymal cells of spinal cord central canal (e); examples of cytoplasmic inclusions are marked by arrows. (f–j) Corresponding areas of control cases do not contain such inclusions and the proteinase K pretreatment removes all soluble Unc119 staining in cases and con-

trols. (k–n) The types of Unc119 aggregates are similar to those of DPR proteins. There are often star-like neuronal cytoplasmic inclusions (NCI) (k), neuronal intranuclear inclusions (NII, pointed by arrow in l), compact aggregates in dystrophic neurites (DN) (m) and diffuse granular cytoplasmic aggregates in neurons (n). Scale bars represent 20  $\mu$ m. *C9* case with *C9orf72* mutation, *CA1/2* cornu ammonis fields 1/2, *CBLgl* granular cell layer of cerebellum, *Ctrl* control case, *DG* dentate gyrus, *Ent* entorhinal cortex, *FCtx* frontal cortex, *SC* spinal cord, *SCcc* spinal cord central canal

We noticed abundant poly-GA pathology in ependymal cells of the spinal cord central canal and the lateral ventricle. Poly-GP and poly-GR were detected at a lesser extent. While TDP-43 pathology and RNA foci have been detected in neurons and glia [17], DPR proteins had been described only in neurons and in Sertoli cells of testis so far [1, 38]. In contrast to neurons, ependymal cells harbor almost exclusively intranuclear inclusions. The pathogenic role of glial DPR inclusions remains unclear, since it does not extend to astrocytes and oligodendrocytes [29]. However, trophic support from ependymal cells has been linked to ALS either directly or via altering neurogenesis [6, 12]. Moreover, poly-GP has been detected in the CSF, which may reflect neuronal death or active secretion [47]. Additionally, ependymal cells may release DPR proteins into the CSF more efficiently than neurons.

Since the localization of DPR aggregates is already differing between neurons and glia in patients, cell type-specific effects may contribute to the aberrant expression pattern of overexpressed poly-GR and poly-GP in cellular models. Further explanations may be the faster expression kinetics and the lack of expression of the other DPR species and hexanucleotide repeat RNA in most current model systems. Since aberrantly localized DPR proteins may invoke different toxic pathways, future studies of cellular and

animal models of DPR toxicity will benefit from the careful analysis of the subcellular localization of the aggregates.

#### Para-nucleolar DPR aggregates and nucleolar stress

While intranuclear DPR inclusions appear randomly distributed throughout the nucleus in glia, we noticed that intranuclear inclusions in neurons are predominantly para-nucleolar. To elucidate the function of para-nucleolar DPR aggregates, we tested several markers for known nucleolus-associated compartments. Robust co-staining with p62 is reminiscent of the ubiquitinated Marinesco bodies, found in the aging brain particularly in neuromelanin containing neurons of the substantia nigra [3, 40]. However, the para-nucleolar DPR inclusions lack the characteristic eosinophilic staining and we could not detect colocalization with HDAC6, which had previously been identified in Marinesco bodies [40]. The “perinucleolar compartment” has been implicated in RNA polymerase III-dependent transcription [41], but the marker proteins CUG-BP1, PML, HSF1 and CD99 did not colocalize with DPR NIIs. In cells with elevated proteasomal activity, proteasomes congregate in “clastosomes” close to the nucleolus [24], but the para-nucleolar DPRs were negative for proteasomal subunits PSMC2 and PSMC4. Block of transcription leads to a

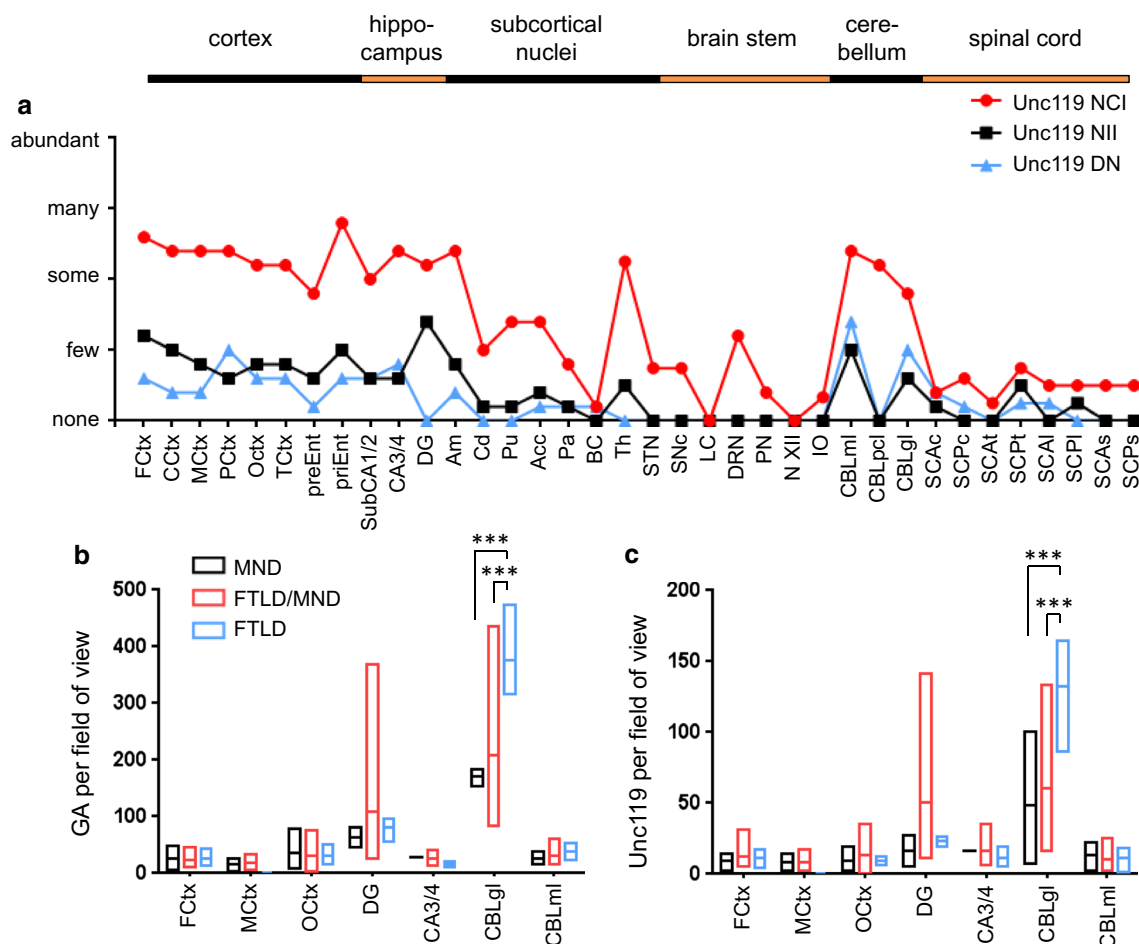


**Fig. 8** Distribution of poly-GA and Unc119 inclusion pathology depends on pathological subtypes. **a** Semi-quantitative analysis of Unc119 neuronal cytoplasmic inclusions (NCI), neuronal intranuclear inclusions (NII) and dystrophic neurites (DN) in representative cortical, hippocampal, subcortical, brain stem, cerebellar and spinal cord areas of five *C9orf72* mutation patients. The regional distribution of Unc119 inclusions resembles the pattern of poly-GA pathology (Fig. 5), albeit at overall lower abundance. Semi-quantitative analysis is explained in detail in the “Materials and methods” section. Abbreviations as in Fig. 5. **b, c** Quantitative analysis of NCI and NII of poly-GA and Unc119 pathology by immunohistochemistry in *C9orf72* mutation patients with MND ( $n = 2-3$ ), FTLD ( $n = 3$ , no

MtCtx) and combined FTLD/MND ( $n = 4-8$ ) cases as in Fig. 6. The graphs show the minimum, mean and maximum number of poly-GA and Unc119 inclusions averaged per visual field. Poly-GA distributions are significantly different between FTLD, FTLD/MND and MND patients in granular layer of cerebellum ( $p_{\text{FTLD vs. FTLD/MND}} = 0.0003$ ,  $p_{\text{FTLD vs. MND}} = 0.0003$ ) (**b**). Similarly, the frequency of Unc119 inclusions is different in the granular layer of cerebellum in FTLD patients compared with FTLD/MND and MND ( $p_{\text{FTLD vs. FTLD/MND}} = 0.0005$ ,  $p_{\text{FTLD vs. MND}} = 0.0008$ ) (**c**). Quantitative analysis is explained in detail in the “Materials and methods” section, the data for individual cases are presented in Table S2. Abbreviations as in Fig. 6

segregation of nucleolar subcompartments and formation of the so-called “nucleolar caps”, but the marker proteins fibrillarin, PML and coilin were not detected in DPR inclusions [45].

Colocalization of para-nucleolar DPR proteins with heterochromatin in DAPI staining and with H3K9me2, a prominent marker of transcriptional repression, suggests a link between DPRs and transcriptional regulation. This is most consistent with transcriptional stalling and nucleolar stress due to formation of RNA-DNA hybrids (so-called R-loops) from hexanucleotide repeats [20]. Importantly, H3K9 dimethylation has been linked to R-loop-induced

transcriptional silencing [46]. This potential link of DPR proteins with DNA/RNA-based disease mechanisms may also explain why para-nucleolar DPR aggregates were not found in transduced neurons expressing DPR proteins from synthetic genes. We found no colocalization of para-nucleolar DPR inclusions with GGGGCC repeat RNA foci. Consistent with previous reports, there was rather an inverse correlation of foci and (cytoplasmic) DPR inclusions [17]. Nucleolar stress is typically associated with nucleolar enlargement and nucleolar accumulation of p53 particularly when it is caused by proteasomal inhibition [21, 26]. Interestingly, two groups reported proteasomal impairment



by poly-GA in vitro [57, 59]. However, we detected no nucleolar accumulation of p53 and no change in nucleolar size and morphology in *C9orf72* patients. Thus, neither the *C9orf72* mutant allele nor cytoplasmic or para-nucleolar DPR inclusions affected nucleolar size in the brain.

### Correlation of DPR and Unc119 inclusion pathology with neuropathological subtypes

Our cohort of 14 *C9orf72* mutation patients represents the whole spectrum of clinical and neuropathological subtypes, including three cases each with either MND or FTLD and eight cases with a mixed disease. We chose five representative cases with comprehensive tissue collection for the semi-quantitative analysis of 36 CNS regions of the sense strand-derived DPR species and Unc119. We had previously shown that poly-GA sequesters Unc119, a protein that regulates trafficking of lipidated cargo proteins, such as transducin  $\alpha$  in the retina [34, 58]. Loss of Unc119 is neurotoxic and Unc119 overexpression rescues poly-GA toxicity in vitro. Using improved antigen retrieval with proteinase K, we could detect Unc119 in about 40 % of poly-GA inclusions in all analyzed brain regions. Although these data corroborate Unc119 as a specific component of poly-GA inclusions, selective co-aggregation of Unc119 cannot easily explain selective vulnerability in certain brain regions. However, proteinase K pretreatment precludes analyzing the residual soluble Unc119 in affected cells. Identification of Unc119 cargos essential for neuronal survival and analysis of their localization in *C9orf72* patients will be necessary to determine functional Unc119 inactivation and its correlation to neurodegeneration.

In all patients, DPR and Unc119 pathology showed a stereotypic expression pattern with highest abundance in cortex, hippocampus, thalamus and cerebellum. In contrast to previous semi-quantitative studies restricted to poly-GA pathology [10, 29], we performed a quantitative analysis of poly-GA, poly-GR, poly-PR and Unc119 pathology in seven critical brain regions in all 14 patients. The amount of poly-GA, poly-GR, poly-PR and Unc119 aggregates was similar in frontal cortex, motor cortex and occipital cortex, although the latter is not affected by neurodegeneration in *C9orf72* mutation patients. Moreover, the extent of DPR pathology in frontal cortex and motor cortex did not correlate with neurodegeneration in FTLD or MND cases. Interestingly, poly-GA and poly-PR, the DPR species with the strongest toxic effects in cell culture, showed distinct depositions in FTLD vs. MND cases with *C9orf72* mutation cases [34, 35, 55, 57, 59]. Poly-PR aggregates were significantly more common in the CA3/4 region of FTLD than of MND cases. Due to the very low frequency of poly-PR inclusions, the pathophysiological relevance remains unclear. Interestingly, nuclear foci of antisense repeat RNA

have recently been linked to motor neuron degeneration [8]. Poly-GA and Unc119 pathology was significantly higher in the cerebellar granular cell layer of FTLD patients compared to MND and FTLD/MND patients. At the same time, there was a trend for lower poly-GR pathology in FTLD patients, which suggests that the composition of the DPR inclusions in these patients is significantly altered, although it is unclear if and how this is related to pathogenesis. In our previous study, focusing on poly-GA pathology no similar correlation was observed [29], but both studies differ in staging of the cases (clinically vs. neuropathologically) and in analyzing the extent of DPR pathology (semi-quantitative vs. quantitative approaches). Interestingly, there is considerable somatic heterogeneity in the length of the expanded *C9orf72* repeat and only the repeat length in the cerebellum but not in the frontal cortex is inversely correlated with disease duration, arguing for an underappreciated role of the cerebellum in the pathogenesis of FTLD [49, 52].

Overall, our data do not support a spatial correlation of DPR inclusions with neurodegeneration, although DPR proteins can clearly induce neurotoxicity in various model systems. Several explanations are possible:

1. DPR inclusions are not actually involved in the *C9orf72* pathomechanism but only TDP-43 inclusions. The strongest counterarguments are rare *C9orf72* cases without TDP-43 pathology and abundant DPR pathology [2, 36, 38, 42]. In addition, DPR pathology seems to precede TDP-43 pathology, although it is not spatially correlated [2, 33]. Moreover, introducing stop codons into the GGGGCC repeat expansion prevented toxicity in the fly model, strongly arguing for a critical role of DPR proteins [35]. Methylation in the *C9orf72* promoter region is associated with reduced RNA foci and DPR pathology and prolonged disease duration presumably by inhibition of repeat transcription, which supports a toxic gain of function pathomechanism [4, 28, 44].
2. Soluble DPR proteins, rather than inclusions, may cause neurodegeneration. Although diffuse poly-GA coalesces into inclusions in cell culture systems [59], it remains unclear whether DPR proteins in cells with diffuse staining patterns cause enhanced toxicity. Soluble poly-GR/PR may interfere with the overall cellular RNA metabolism [23]. Intercellular spreading of DPR proteins may trigger pathogenic mechanisms leading to TDP-43 phosphorylation or seed TDP-43 aggregation in a non-cell autonomous manner. Spreading and seeding have been reported for other intracellular aggregating proteins in neurodegenerative diseases, but have not been claimed to be the main source of toxicity [22, 53].

3. Finally and most likely, a combination of DNA•RNA hybrids, RNA foci and protein toxicity, together with a potential *C9orf72* haploinsufficiency and unknown cell type-specific susceptibility factors are responsible for the selective neurodegeneration in certain brain regions in *C9orf72* mutation carriers. This is supported by a very recent mouse model showing TDP-43 pathology, neurodegeneration, RNA foci and DPR proteins upon high-level viral expression of the GGGGCC repeat [5].

This interaction of DNA/RNA toxicity and DPR toxicity may be represented by the newly described para-nucleolar DPR aggregates. Thus, models expressing both repeat RNA and DPR proteins and constant comparison with pathological analysis of patient samples are needed to elucidate the cause of neurodegeneration in *C9orf72* repeat expansion carriers, and how this can lead to either FTL or MND.

**Acknowledgments** We thank Mrs. B. Kraft, Mrs. I. Pigur and Mr. M. Schmidt for excellent technical assistance. We thank C. Lehmer, K. Mori, Y. Ohki, D. Orozco and B. Schmid for critical comments and technical advice. DE was supported by the Helmholtz Young Investigator program HZ-NG-607 and the Hans und Ilse Breuer Foundation. DE, MD and TK received funding from the Munich Cluster of Systems Neurology (SyNergy). The research leading to these results has received funding from the European Research Council under the European Union's Seventh Framework Programme FP7/2014-2019 under Grant agreement No. 617198 [DPR-MODELS] to DE.

**Open Access** This article is distributed under the terms of the Creative Commons Attribution 4.0 International License (<http://creativecommons.org/licenses/by/4.0/>), which permits unrestricted use, distribution, and reproduction in any medium, provided you give appropriate credit to the original author(s) and the source, provide a link to the Creative Commons license, and indicate if changes were made.

## References

- Ash PE, Bieniek KF, Gendron TF, Caulfield T, Lin WL, DeJesus-Hernandez M, van Blitterswijk MM, Jansen-West K, Paul JW 3rd, Rademakers R, Boylan KB, Dickson DW, Petrucelli L (2013) Unconventional translation of C9ORF72 GGGGCC expansion generates insoluble polypeptides specific to c9FTD/ALS. *Neuron*. doi:10.1016/j.neuron.2013.02.004
- Baborie A, Griffiths TD, Jaros E, Perry R, McKeith IG, Burn DJ, Masuda-Suzukake M, Hasegawa M, Rollinson S, Pickering-Brown S, Robinson AC, Davidson YS, Mann DM (2014) Accumulation of dipeptide repeat proteins predates that of TDP-43 in frontotemporal lobar degeneration associated with hexanucleotide repeat expansions in C9ORF72 gene. *Neuropathol Appl Neurobiol*. doi:10.1111/nan.12178
- Beach TG, Walker DG, Sue LI, Newell A, Adler CC, Joyce JN (2004) Substantia nigra Marinesco bodies are associated with decreased striatal expression of dopaminergic markers. *J Neuro-pathol Exp Neurol* 63:329–337
- Belzil VV, Bauer PO, Prudencio M, Gendron TF, Stetler CT, Yan IK, Pregent L, Daugherty L, Baker MC, Rademakers R, Boylan K, Patel TC, Dickson DW, Petrucelli L (2013) Reduced C9orf72 gene expression in c9FTD/ALS is caused by histone trimethylation, an epigenetic event detectable in blood. *Acta Neuropathol* 126:895–905. doi:10.1007/s00401-013-1199-1
- Chew J, Gendron TF, Prudencio M, Sasaguri H, Zhang YJ, Castanedes-Casey M, Lee CW, Jansen-West K, Kurti A, Murray ME, Bieniek KF, Bauer PO, Whitelaw EC, Rousseau L, Stankowski JN, Stetler C, Daugherty LM, Perkerson EA, Desaro P, Johnston A, Overstreet K, Edbauer D, Rademakers R, Boylan KB, Dickson DW, Fryer JD, Petrucelli L (2015) C9ORF72 repeat expansions in mice cause TDP-43 pathology, neuronal loss, and behavioral deficits. *Science*. doi:10.1126/science.aaa9344
- Chi L, Ke Y, Luo C, Li B, Gozal D, Kalyanaraman B, Liu R (2006) Motor neuron degeneration promotes neural progenitor cell proliferation, migration, and neurogenesis in the spinal cords of amyotrophic lateral sclerosis mice. *Stem Cells* 24:34–43. doi:10.1634/stemcells.2005-0076
- Ciura S, Lattante S, Le Ber I, Latouche M, Tostivint H, Brice A, Kabashi E (2013) Loss of function of C9orf72 causes motor deficits in a zebrafish model of amyotrophic lateral sclerosis. *Ann Neurol* 74:180–187. doi:10.1002/ana.23946
- Cooper-Knock J, Higginbottom A, Stopford MJ, Highley JR, Ince PG, Wharton SB, Pickering-Brown S, Kirby J, Hautbergue GM, Shaw PJ (2015) Antisense RNA foci in the motor neurons of C9ORF72-ALS patients are associated with TDP-43 proteinopathy. *Acta Neuropathol*. doi:10.1007/s00401-015-1429-9
- Cooper-Knock J, Walsh MJ, Higginbottom A, Robin Highley J, Dickman MJ, Edbauer D, Ince PG, Wharton SB, Wilson SA, Kirby J, Hautbergue GM, Shaw PJ (2014) Sequestration of multiple RNA recognition motif-containing proteins by C9orf72 repeat expansions. *Brain* 137:2040–2051. doi:10.1093/brain/awu120
- Davidson YS, Barker H, Robinson AC, Thompson JC, Harris J, Troakes C, Smith B, Al-Saraj S, Shaw C, Rollinson S, Masuda-Suzukake M, Hasegawa M, Pickering-Brown S, Snowden JS, Mann DM (2014) Brain distribution of dipeptide repeat proteins in frontotemporal lobar degeneration and motor neurone disease associated with expansions in C9ORF72. *Acta Neuropathol Commun* 2:70. doi:10.1186/2051-5960-2-70
- DeJesus-Hernandez M, Mackenzie IR, Boeve BF, Boxer AL, Baker M, Rutherford NJ, Nicholson AM, Finch NA, Flynn H, Adamson J, Kouri N, Wojtas A, Sengdy P, Hsiung GY, Karydas A, Seeley WW, Josephs KA, Coppola G, Geschwind DH, Wszolek ZK, Feldman H, Knopman DS, Petersen RC, Miller BL, Dickson DW, Boylan KB, Graff-Radford NR, Rademakers R (2011) Expanded GGGGCC hexanucleotide repeat in noncoding region of C9ORF72 causes chromosome 9p-linked FTD and ALS. *Neuron* 72:245–256. doi:10.1016/j.neuron.2011.09.011
- Dodge JC, Treleaven CM, Fidler JA, Hester M, Haidet A, Handy C, Rao M, Eagle A, Matthews JC, Taksir TV, Cheng SH, Shihabuddin LS, Kaspar BK (2010) AAV4-mediated expression of IGF-1 and VEGF within cellular components of the ventricular system improves survival outcome in familial ALS mice. *Mol Ther* 18:2075–2084. doi:10.1038/mt.2010.206
- Downey LE, Fletcher PD, Golden HL, Mahoney CJ, Augustus JL, Schott JM, Rohrer JD, Beck J, Mead S, Rossor MN, Crutch SJ, Warren JD (2014) Altered body schema processing in frontotemporal dementia with C9ORF72 mutations. *J Neurol Neurosurg Psychiatry* 85:1016–1023. doi:10.1136/jnnp-2013-306995
- Downey LE, Mahoney CJ, Rossor MN, Crutch SJ, Warren JD (2012) Impaired self-other differentiation in frontotemporal dementia due to the C9ORF72 expansion. *Alzheimers Res Ther* 4:42. doi:10.1186/alzrt145
- Fleck D, van Bebber F, Colombo A, Galante C, Schwenk BM, Rabe L, Hampel H, Novak B, Kremmer E, Tahirovic S, Edbauer D, Lichtenthaler SF, Schmid B, Willem M, Haass C (2013) Dual cleavage of neuregulin 1 type III by BACE1

- and ADAM17 liberates its EGF-like domain and allows paracrine signaling. *J Neurosci* 33:7856–7869. doi:[10.1523/JNEUROSCI.3372-12.2013](https://doi.org/10.1523/JNEUROSCI.3372-12.2013)
16. Gendron TF, Belzil VV, Zhang YJ, Petrucelli L (2014) Mechanisms of toxicity in C9FTLD/ALS. *Acta Neuropathol* 127:359–376. doi:[10.1007/s00401-013-1237-z](https://doi.org/10.1007/s00401-013-1237-z)
  17. Gendron TF, Bieniek KF, Zhang YJ, Jansen-West K, Ash PE, Caulfield T, Daugherty L, Dunmore JH, Castaneda-Casey M, Chew J, Cosio DM, van Blitterswijk M, Lee WC, Rademakers R, Boylan KB, Dickson DW, Petrucelli L (2013) Antisense transcripts of the expanded C9ORF72 hexanucleotide repeat form nuclear RNA foci and undergo repeat-associated non-ATG translation in c9FTD/ALS. *Acta Neuropathol* 126:829–844. doi:[10.1007/s00401-013-1192-8](https://doi.org/10.1007/s00401-013-1192-8)
  18. Gijssels I, Van Langenhove T, van der Zee J, Slegers K, Philtjens S, Kleinberger G, Janssens J, Bettens K, Van Cauwenbergh C, Pereson S, Engelborghs S, Sieben A, De Jonghe P, Vandenberghe R, Santens P, De Bleeker J, Maes G, Baumer V, Dillen L, Joris G, Cuijt I, Corsmit E, Elinck E, Van Dongen J, Vermeulen S, Van den Broeck M, Vaerenberg C, Mattheijssens M, Peeters K, Robberecht W, Cras P, Martin JJ, De Deyn PP, Cruts M, Van Broeckhoven C (2012) A C9orf72 promoter repeat expansion in a Flanders-Belgian cohort with disorders of the frontotemporal lobar degeneration-amyotrophic lateral sclerosis spectrum: a gene identification study. *Lancet Neurol* 11:54–65. doi:[10.1016/S1474-4422\(11\)70261-7](https://doi.org/10.1016/S1474-4422(11)70261-7)
  19. Gross H, Barth S, Palermo RD, Mamiani A, Hennard C, Zimmer-Strobl U, West MJ, Kremmer E, Grasser FA (2010) Asymmetric Arginine dimethylation of Epstein-Barr virus nuclear antigen 2 promotes DNA targeting. *Virology* 397:299–310. doi:[10.1016/j.virol.2009.11.023](https://doi.org/10.1016/j.virol.2009.11.023)
  20. Haeusler AR, Donnelly CJ, Periz G, Simko EA, Shaw PG, Kim MS, Maragakis NJ, Troncoso JC, Pandey A, Sattler R, Rothstein JD, Wang J (2014) C9orf72 nucleotide repeat structures initiate molecular cascades of disease. *Nature* 507:195–200. doi:[10.1038/nature13124](https://doi.org/10.1038/nature13124)
  21. Hetman M, Pietrzak M (2012) Emerging roles of the neuronal nucleolus. *Trends Neurosci* 35:305–314. doi:[10.1016/j.tins.2012.01.002](https://doi.org/10.1016/j.tins.2012.01.002)
  22. Jucker M, Walker LC (2011) Pathogenic protein seeding in Alzheimer disease and other neurodegenerative disorders. *Ann Neurol* 70:532–540. doi:[10.1002/ana.22615](https://doi.org/10.1002/ana.22615)
  23. Kwon I, Xiang S, Kato M, Wu L, Theodoropoulos P, Wang T, Kim J, Yun J, Xie Y, McKnight SL (2014) Poly-dipeptides encoded by the C9orf72 repeats bind nucleoli, impede RNA biogenesis, and kill cells. *Science* 345:1139–1145. doi:[10.1126/science.1254917](https://doi.org/10.1126/science.1254917)
  24. Lafarga M, Berciano MT, Pena E, Mayo I, Castano JG, Bohmann D, Rodrigues JP, Tavanez JP, Carmo-Fonseca M (2002) Clastosome: a subtype of nuclear body enriched in 19S and 20S proteasomes, ubiquitin, and protein substrates of proteasome. *Mol Biol Cell* 13:2771–2782. doi:[10.1091/mbc.E02-03-0122](https://doi.org/10.1091/mbc.E02-03-0122)
  25. Lagier-Tourenne C, Baughn M, Rigo F, Sun S, Liu P, Li HR, Jiang J, Watt AT, Chun S, Katz M, Qiu J, Sun Y, Ling SC, Zhu Q, Polymenidou M, Drenner K, Artates JW, McAlonis-Downes M, Markmiller S, Hutt KR, Pizzo DP, Cady J, Harms MB, Baloh RH, Vandenberg SR, Yeo GW, Fu XD, Bennett CF, Cleveland DW, Ravits J (2013) Targeted degradation of sense and antisense C9orf72 RNA foci as therapy for ALS and frontotemporal degeneration. *Proc Natl Acad Sci* 110:E4530–E4539. doi:[10.1073/pnas.1318835110](https://doi.org/10.1073/pnas.1318835110)
  26. Latonen L, Moore HM, Bai B, Jaamaa S, Laiho M (2011) Proteasome inhibitors induce nucleolar aggregation of proteasome target proteins and polyadenylated RNA by altering ubiquitin availability. *Oncogene* 30:790–805. doi:[10.1038/ncr.2010.469](https://doi.org/10.1038/ncr.2010.469)
  27. Lee YB, Chen HJ, Peres JN, Gomez-Deza J, Attig J, Stalekar M, Troakes C, Nishimura AL, Scotter EL, Vance C, Adachi Y, Sardone V, Miller JW, Smith BN, Gallo JM, Ule J, Hirth F, Rogelj B, Houart C, Shaw CE (2013) Hexanucleotide repeats in ALS/FTD form length-dependent RNA foci, sequester RNA binding proteins, and are neurotoxic. *Cell Rep* 5:1178–1186. doi:[10.1016/j.celrep.2013.10.049](https://doi.org/10.1016/j.celrep.2013.10.049)
  28. Liu EY, Russ J, Wu K, Neal D, Suh E, McNally AG, Irwin DJ, Van Deerlin VM, Lee EB (2014) C9orf72 hypermethylation protects against repeat expansion-associated pathology in ALS/FTD. *Acta Neuropathol* 128:525–541. doi:[10.1007/s00401-014-1286-y](https://doi.org/10.1007/s00401-014-1286-y)
  29. Mackenzie IR, Arzberger T, Kremmer E, Troost D, Lorenzl S, Mori K, Weng SM, Haass C, Kretschmar HA, Edbauer D, Neumann M (2013) Dipeptide repeat protein pathology in C9ORF72 mutation cases: clinico-pathological correlations. *Acta Neuropathol* 126:859–879. doi:[10.1007/s00401-013-1181-y](https://doi.org/10.1007/s00401-013-1181-y)
  30. Mahoney CJ, Beck J, Rohrer JD, Lashley T, Mok K, Shakespeare T, Yeatman T, Warrington EK, Schott JM, Fox NC, Rossor MN, Hardy J, Collinge J, Revesz T, Mead S, Warren JD (2012) Frontotemporal dementia with the C9ORF72 hexanucleotide repeat expansion: clinical, neuroanatomical and neuropathological features. *Brain* 135:736–750. doi:[10.1093/brain/awr361](https://doi.org/10.1093/brain/awr361)
  31. Mahoney CJ, Downey LE, Ridgway GR, Beck J, Clegg S, Blair M, Finnegan S, Leung KK, Yeatman T, Golden H, Mead S, Rohrer JD, Fox NC, Warren JD (2012) Longitudinal neuroimaging and neuropsychological profiles of frontotemporal dementia with C9ORF72 expansions. *Alzheimers Res Ther* 4:41. doi:[10.1186/alzrt144](https://doi.org/10.1186/alzrt144)
  32. Mahoney CJ, Simpson IJ, Nicholas JM, Fletcher PD, Downey LE, Golden HL, Clark CN, Schmitz N, Rohrer JD, Schott JM, Zhang H, Ourselin S, Warren JD, Fox NC (2015) Longitudinal diffusion tensor imaging in frontotemporal dementia. *Ann Neurol* 77:33–46. doi:[10.1002/ana.24296](https://doi.org/10.1002/ana.24296)
  33. Mann DM (2015) Dipeptide repeat protein toxicity in frontotemporal lobar degeneration and in motor neurone disease associated with expansions in C9ORF72—a cautionary note. *Neurobiol Aging* 36:1224–1226. doi:[10.1016/j.neurobiolaging.2014.10.011](https://doi.org/10.1016/j.neurobiolaging.2014.10.011)
  34. May S, Hornburg D, Schludi MH, Arzberger T, Rentzsch K, Schwenk BM, Grasser FA, Mori K, Kremmer E, Banzhaf-Strathmann J, Mann M, Meissner F, Edbauer D (2014) C9orf72 FTD/ALS-associated Gly-Ala dipeptide repeat proteins cause neuronal toxicity and Unc119 sequestration. *Acta Neuropathol* 128:485–503. doi:[10.1007/s00401-014-1329-4](https://doi.org/10.1007/s00401-014-1329-4)
  35. Mizielińska S, Gronke S, Niccoli T, Ridler CE, Clayton EL, Devoy A, Moens T, Norona FE, Woollacott IO, Pietrzyk J, Cleverley K, Nicoll AJ, Pickering-Brown S, Dols J, Cabecinha M, Hendrich O, Fratta P, Fisher EM, Partridge L, Isaacs AM (2014) C9orf72 repeat expansions cause neurodegeneration in *Drosophila* through arginine-rich proteins. *Science* 345:1192–1194. doi:[10.1126/science.1256800](https://doi.org/10.1126/science.1256800)
  36. Mori K, Arzberger T, Grasser FA, Gijssels I, May S, Rentzsch K, Weng SM, Schludi MH, van der Zee J, Cruts M, Van Broeckhoven C, Kremmer E, Kretschmar HA, Haass C, Edbauer D (2013) Bidirectional transcripts of the expanded C9orf72 hexanucleotide repeat are translated into aggregating dipeptide repeat proteins. *Acta Neuropathol* 126:881–893. doi:[10.1007/s00401-013-1189-3](https://doi.org/10.1007/s00401-013-1189-3)
  37. Mori K, Lammich S, Mackenzie IR, Forne I, Zilow S, Kretschmar H, Edbauer D, Janssens J, Kleinberger G, Cruts M, Herms J, Neumann M, Van Broeckhoven C, Arzberger T, Haass C (2013) hnRNP A3 binds to GGGGCC repeats and is a constituent of p62-positive/TDP43-negative inclusions in the hippocampus of patients with C9orf72 mutations. *Acta Neuropathol*. doi:[10.1007/s00401-013-1088-7](https://doi.org/10.1007/s00401-013-1088-7)

38. Mori K, Weng SM, Arzberger T, May S, Rentzsch K, Kremmer E, Schmid B, Kretzschmar HA, Cruts M, Van Broeckhoven C, Haass C, Edbauer D (2013) The C9orf72 GGGGCC repeat is translated into aggregating dipeptide-repeat proteins in FTL/ALS. *Science*. doi:[10.1126/science.1232927](https://doi.org/10.1126/science.1232927)
39. Nakagawa T, Feliu-Mojer MI, Wulf P, Lois C, Sheng M, Hoogenraad CC (2006) Generation of lentiviral transgenic rats expressing glutamate receptor interacting protein 1 (GRIP1) in brain, spinal cord and testis. *J Neurosci Methods* 152:1–9
40. Odagiri S, Tanji K, Mori F, Kakita A, Takahashi H, Kamitani T, Wakabayashi K (2012) Immunohistochemical analysis of Marinesco bodies, using antibodies against proteins implicated in the ubiquitin-proteasome system, autophagy and aggresome formation. *Neuropathology* 32:261–266. doi:[10.1111/j.1440-1789.2011.01267.x](https://doi.org/10.1111/j.1440-1789.2011.01267.x)
41. Pollock C, Huang S (2010) The perinucleolar compartment. *Cold Spring Harb Perspect Biol* 2:a000679. doi:[10.1101/cshperspect.a000679](https://doi.org/10.1101/cshperspect.a000679)
42. Proudfoot M, Gutowski NJ, Edbauer D, Hilton DA, Stephens M, Rankin J, Mackenzie IR (2014) Early dipeptide repeat pathology in a frontotemporal dementia kindred with C9ORF72 mutation and intellectual disability. *Acta Neuropathol* 127:451–458. doi:[10.1007/s00401-014-1245-7](https://doi.org/10.1007/s00401-014-1245-7)
43. Renton AE, Majounie E, Waite A, Simon-Sanchez J, Rollinson S, Gibbs JR, Schymick JC, Laaksvirta H, van Swieten JC, Myllykangas L, Kalimo H, Paetau A, Abramzon Y, Remes AM, Kaganovich A, Scholz SW, Duckworth J, Ding J, Harmer DW, Hernandez DG, Johnson JO, Mok K, Rytan M, Trabzuni D, Guerreiro RJ, Orrell RW, Neal J, Murray A, Pearson J, Jansen IE, Sondervan D, Seelaar H, Blake D, Young K, Halliwell N, Callister JB, Toulson G, Richardson A, Gerhard A, Snowden J, Mann D, Neary D, Nalls MA, Peuralinna T, Jansson L, Isoviita VM, Kaivorinne AL, Holtta-Vuori M, Ikonen E, Sulkava R, Benatar M, Wu J, Chio A, Restagno G, Borghero G, Sabatelli M, Heckerman D, Rogaeva E, Zinman L, Rothstein JD, Sendtner M, Drepper C, Eichler EE, Alkan C, Abdullaev Z, Pack SD, Dutra A, Pak E, Hardy J, Singleton A, Williams NM, Heutink P, Pickering-Brown S, Morris HR, Tienari PJ, Traynor BJ (2011) A hexanucleotide repeat expansion in C9ORF72 is the cause of chromosome 9p21-linked ALS-FTD. *Neuron* 72:257–268. doi:[10.1016/j.neuron.2011.09.010](https://doi.org/10.1016/j.neuron.2011.09.010)
44. Russ J, Liu EY, Wu K, Neal D, Suh E, Irwin DJ, McMillan CT, Harms MB, Cairns NJ, Wood EM, Xie SX, Elman L, McCluskey L, Grossman M, Van Deerlin VM, Lee EB (2015) Hypermethylation of repeat expanded C9orf72 is a clinical and molecular disease modifier. *Acta Neuropathol* 129:39–52. doi:[10.1007/s00401-014-1365-0](https://doi.org/10.1007/s00401-014-1365-0)
45. Shav-Tal Y, Blechman J, Darzacq X, Montagna C, Dye BT, Patton JG, Singer RH, Zipori D (2005) Dynamic sorting of nuclear components into distinct nucleolar caps during transcriptional inhibition. *Mol Biol Cell* 16:2395–2413. doi:[10.1091/mbc.E04-11-0992](https://doi.org/10.1091/mbc.E04-11-0992)
46. Skourti-Stathaki K, Kamieniarz-Gdula K, Proudfoot NJ (2014) R-loops induce repressive chromatin marks over mammalian gene terminators. *Nature* 516:436–439. doi:[10.1038/nature13787](https://doi.org/10.1038/nature13787)
47. Su Z, Zhang Y, Gendron TF, Bauer PO, Chew J, Yang WY, Fostvedt E, Jansen-West K, Belzil VV, Desaro P, Johnston A, Overstreet K, Oh SY, Todd PK, Berry JD, Cudkovicz ME, Boeve BF, Dickson D, Floeter MK, Traynor BJ, Morelli C, Ratti A, Silani V, Rademakers R, Brown RH, Rothstein JD, Boylan KB, Petrucelli L, Disney MD (2014) Discovery of a biomarker and lead small molecules to target r(GGGGCC)-associated defects in c9FTD/ALS. *Neuron* 83:1043–1050. doi:[10.1016/j.neuron.2014.07.041](https://doi.org/10.1016/j.neuron.2014.07.041)
48. Tada T, Simonetta A, Batterton M, Kinoshita M, Edbauer D, Sheng M (2007) Role of Septin cytoskeleton in spine morphogenesis and dendrite development in neurons. *Curr Biol* 17:1752–1758
49. Tan RH, Devenney E, Dobson-Stone C, Kwok JB, Hodges JR, Kiernan MC, Halliday GM, Hornberger M (2014) Cerebellar integrity in the amyotrophic lateral sclerosis-frontotemporal dementia continuum. *PLoS One* 9:e105632. doi:[10.1371/journal.pone.0105632](https://doi.org/10.1371/journal.pone.0105632)
50. Tao Z, Wang H, Xia Q, Li K, Jiang X, Xu G, Wang G, Ying Z (2015) Nucleolar stress and impaired stress granule formation contribute to C9orf72 RAN translation-induced cytotoxicity. *Hum Mol Genet*. doi:[10.1093/hmg/ddv005](https://doi.org/10.1093/hmg/ddv005)
51. Therrien M, Rouleau GA, Dion PA, Parker JA (2013) Deletion of C9ORF72 results in motor neuron degeneration and stress sensitivity in *C. elegans*. *PLoS One* 8:e83450. doi:[10.1371/journal.pone.0083450](https://doi.org/10.1371/journal.pone.0083450)
52. van Blitterswijk M, DeJesus-Hernandez M, Niemantsverdriet E, Murray ME, Heckman MG, Diehl NN, Brown PH, Baker MC, Finch NA, Bauer PO, Serrano G, Beach TG, Josephs KA, Knopman DS, Petersen RC, Boeve BF, Graff-Radford NR, Boylan KB, Petrucelli L, Dickson DW, Rademakers R (2013) Association between repeat sizes and clinical and pathological characteristics in carriers of C9ORF72 repeat expansions (Xpansize-72): a cross-sectional cohort study. *Lancet Neurol* 12:978–988. doi:[10.1016/S1474-4422\(13\)70210-2](https://doi.org/10.1016/S1474-4422(13)70210-2)
53. Walker LC, Diamond MI, Duff KE, Hyman BT (2013) Mechanisms of protein seeding in neurodegenerative diseases. *JAMA Neurol* 70:304–310. doi:[10.1001/jamaneurol.2013.1453](https://doi.org/10.1001/jamaneurol.2013.1453)
54. Wang J, Haeusler AR, Simko EA (2015) Emerging role of RNA\*DNA hybrids in C9orf72-linked neurodegeneration. *Cell Cycle* 14:526–532. doi:[10.1080/15384101.2014.995490](https://doi.org/10.1080/15384101.2014.995490)
55. Wen X, Tan W, Westergard T, Krishnamurthy K, Markandiah SS, Shi Y, Lin S, Shneider NA, Monaghan J, Pandey UB, Pasinelli P, Ichida JK, Trotti D (2014) Antisense proline-arginine RAN dipeptides linked to C9ORF72-ALS/FTD form toxic nuclear aggregates that initiate in vitro and in vivo neuronal death. *Neuron* 84:1213–1225. doi:[10.1016/j.neuron.2014.12.010](https://doi.org/10.1016/j.neuron.2014.12.010)
56. Whitwell JL, Weigand SD, Boeve BF, Senjem ML, Gunter JL, DeJesus-Hernandez M, Rutherford NJ, Baker M, Knopman DS, Wszolek ZK, Parisi JE, Dickson DW, Petersen RC, Rademakers R, Jack CR Jr, Josephs KA (2012) Neuroimaging signatures of frontotemporal dementia genetics: C9ORF72, tau, progranulin and sporadic. *Brain* 135:794–806. doi:[10.1093/brain/aws001](https://doi.org/10.1093/brain/aws001)
57. Yamakawa M, Ito D, Honda T, Kubo KI, Noda M, Nakajima K, Suzuki N (2014) Characterization of the dipeptide repeat protein in the molecular pathogenesis of c9FTD/ALS. *Hum Mol Genet*. doi:[10.1093/hmg/ddu576](https://doi.org/10.1093/hmg/ddu576)
58. Zhang H, Constantine R, Vorobiev S, Chen Y, Seetharaman J, Huang YJ, Xiao R, Montelione GT, Gerstner CD, Davis MW, Inana G, Whitby FG, Jorgensen EM, Hill CP, Tong L, Baehr W (2011) UNC119 is required for G protein trafficking in sensory neurons. *Nat Neurosci* 14:874–880. doi:[10.1038/nn.2835](https://doi.org/10.1038/nn.2835)
59. Zhang YJ, Jansen-West K, Xu YF, Gendron TF, Bieniek KF, Lin WL, Sasaguri H, Caulfield T, Hubbard J, Daugherty L, Chew J, Belzil VV, Prudencio M, Stankowski JN, Castanedes-Casey M, Whitelaw E, Ash PE, DeTure M, Rademakers R, Boylan KB, Dickson DW, Petrucelli L (2014) Aggregation-prone c9FTD/ALS poly(GA) RAN-translated proteins cause neurotoxicity by inducing ER stress. *Acta Neuropathol* 128:505–524. doi:[10.1007/s00401-014-1336-5](https://doi.org/10.1007/s00401-014-1336-5)
60. Zu T, Liu Y, Banez-Coronel M, Reid T, Pletnikova O, Lewis J, Miller TM, Harms MB, Falchook AE, Subramony SH, Ostrow LW, Rothstein JD, Troncoso JC, Ranum LP (2013) RAN proteins and RNA foci from antisense transcripts in C9ORF72 ALS and frontotemporal dementia. *Proc Natl Acad Sci* 110:E4968–E4977. doi:[10.1073/pnas.1315438110](https://doi.org/10.1073/pnas.1315438110)

**Online Supplemental Materials**

**Distribution of dipeptide repeat proteins in cellular models and *C9orf72* mutation cases suggests link to transcriptional silencing**

Martin H. Schludi, Stephanie May, Friedrich A. Grässer, Kristin Rentzsch, Elisabeth Kremmer, Clemens Küpper, Thomas Klopstock, German Consortium for Frontotemporal Lobar Degeneration, Bavarian Brain Banking Alliance, Thomas Arzberger, Dieter Edbauer

**Includes:**

Supplemental Figures S1-S8

Supplemental Tables S1-S2

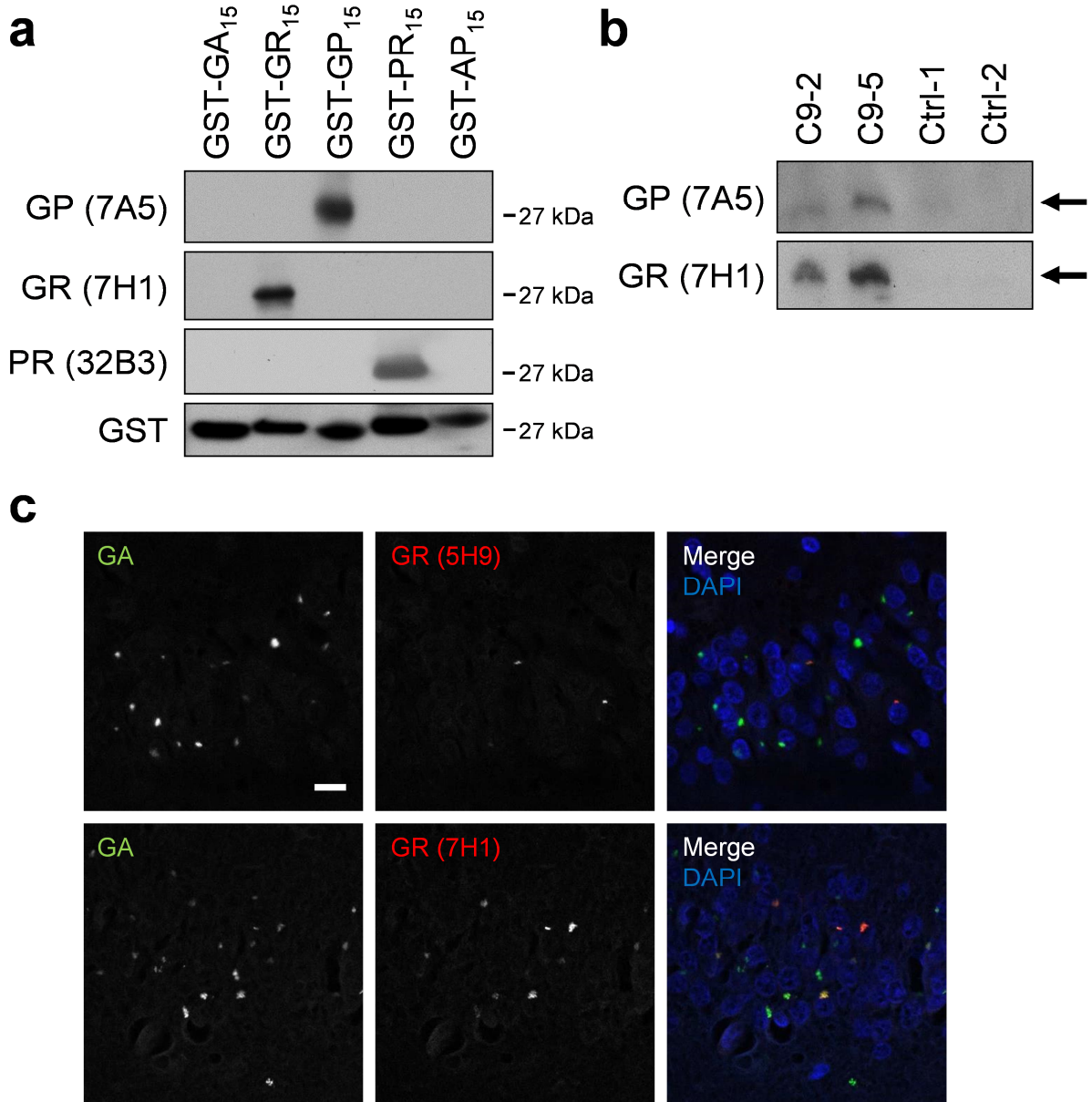


**Figure S1: Monoclonal poly-GR and poly-GP antibodies are specific**

(a) Immunoblot of 200 ng recombinant GST-GA<sub>15</sub>, GST-GR<sub>15</sub>, GST-GP<sub>15</sub>, GST-PR<sub>15</sub> and GST-AP<sub>15</sub> fusion proteins with indicated antibodies as described previously (Mori et al, 2013a). (b) Immunoblot of the insoluble fraction of cerebellum shows poly-GP and poly-GR aggregates at the top of the gel (arrows) in *C9orf72* cases (C9) but not in healthy controls (Ctrl). Frontal cortex samples were prepared by boiling the Triton X-100 (1 %) and SDS (2 %) insoluble fraction in 4x Laemmli buffer (containing 8 % SDS) as described previously (Mori et al, 2013c). poly-PR inclusions are very rare and can only be detected by immunostaining. (c) Double immunofluorescence showing coaggregation of poly-GA and poly-GR in the dentate gyrus of hippocampus. Poly-GA is used as a reference for the total number of DPR inclusions. poly-GR antibody 7H1 shows more inclusions pathology than antibody 5H9. Scale bar represents 20  $\mu$ m.

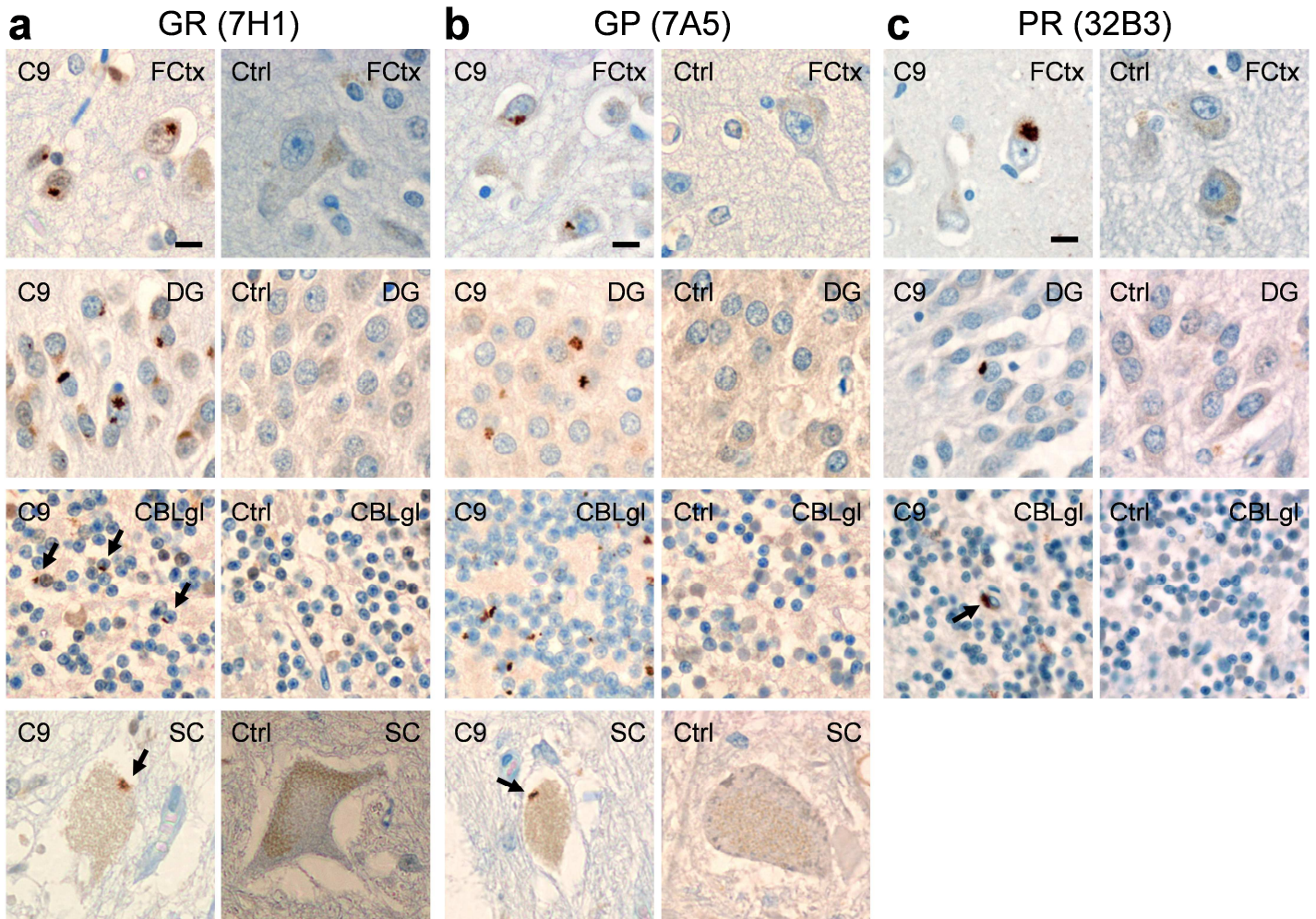


**Figure S2: Poly-GR, poly-GP and poly-PR aggregates are specific for patients with *C9orf72* mutations.**

Immunohistochemistry with novel monoclonal antibodies for (a) poly-GR (rat clone 7H1) and (b) poly-GP (rat clone 7A5), shows abundant inclusions in various brain regions of patients with *C9orf72* mutations (C9). Many aggregates are seen in the frontal cortex (FCtx), dentate gyrus of hippocampus (DG) and granular cell layer of cerebellum (CBLgl). Rarely, motoneurons in the spinal cord (SC) contain small intracytoplasmic poly-GR and poly-GP aggregates which are mainly localized at the edge of the cells. No inclusions are seen in a control brain (Ctrl). (c) Mouse poly-PR antibody 32B3 detects similar *C9orf72*-specific inclusions in FCtx, DG and CBLgl, but with much lower abundance. Poly-PR inclusions in motoneurons of the spinal cord were not detectable. Scale bar represents 20  $\mu\text{m}$ .

## Primary cortical neurons

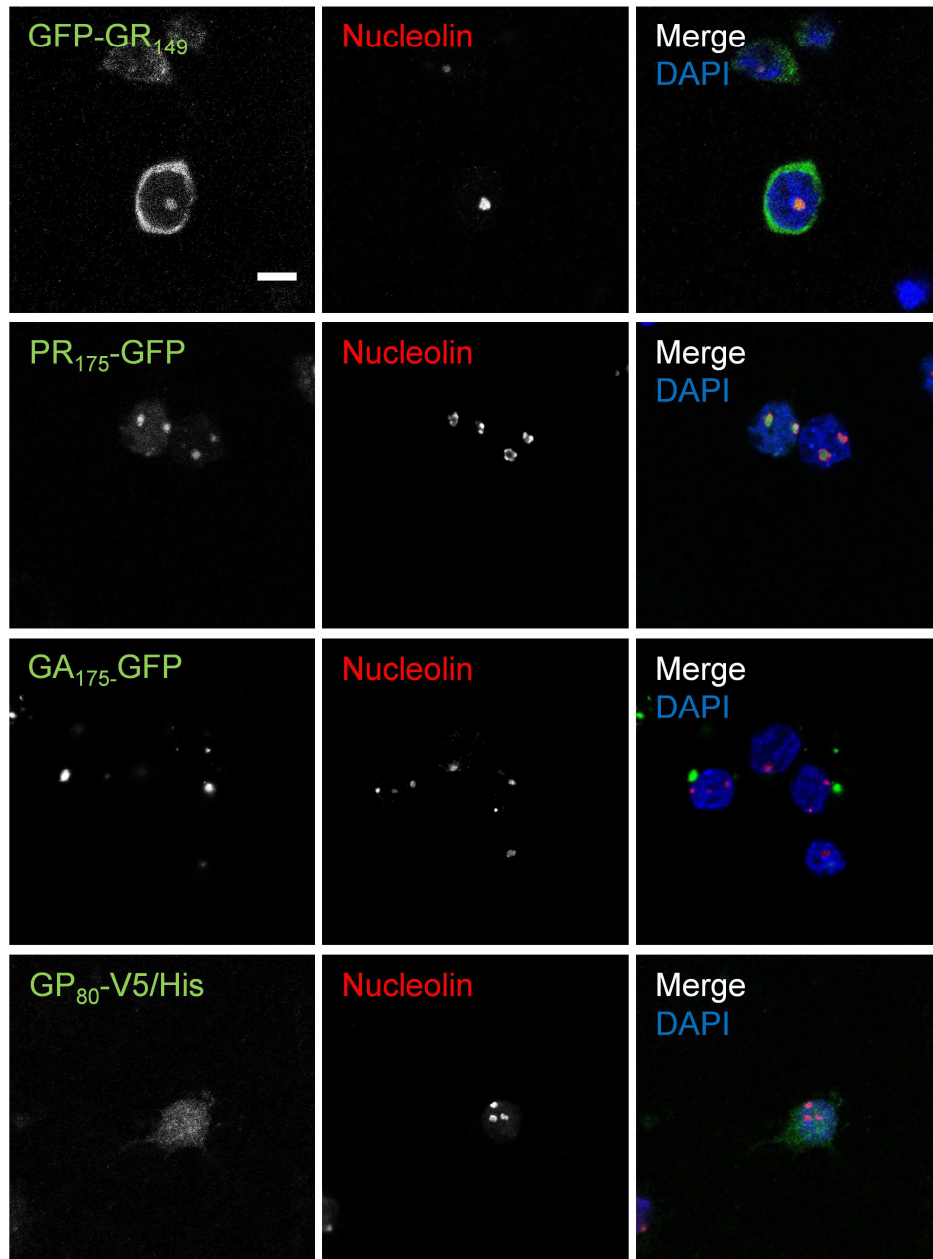


**Figure S3: Expression pattern of DPR proteins in primary cortical neurons**

Primary cortical neurons transduced with lentivirus expressing either GFP-GR<sub>149</sub>, PR<sub>175</sub>-GFP, GA<sub>175</sub>-GFP or GP<sub>80</sub>-V5/His (DIV6+7). Double immunofluorescence for different DPR proteins and nucleolin. Nuclei are labeled with DAPI. Single confocal sections containing the nucleolus are shown. The expression pattern of all DPR species strongly resembles the pattern seen in hippocampal neurons (Fig. 1a). Neurons expressing PR<sub>175</sub>-GFP often have fragmented nucleoli. Scale bar represent 10  $\mu$ m.



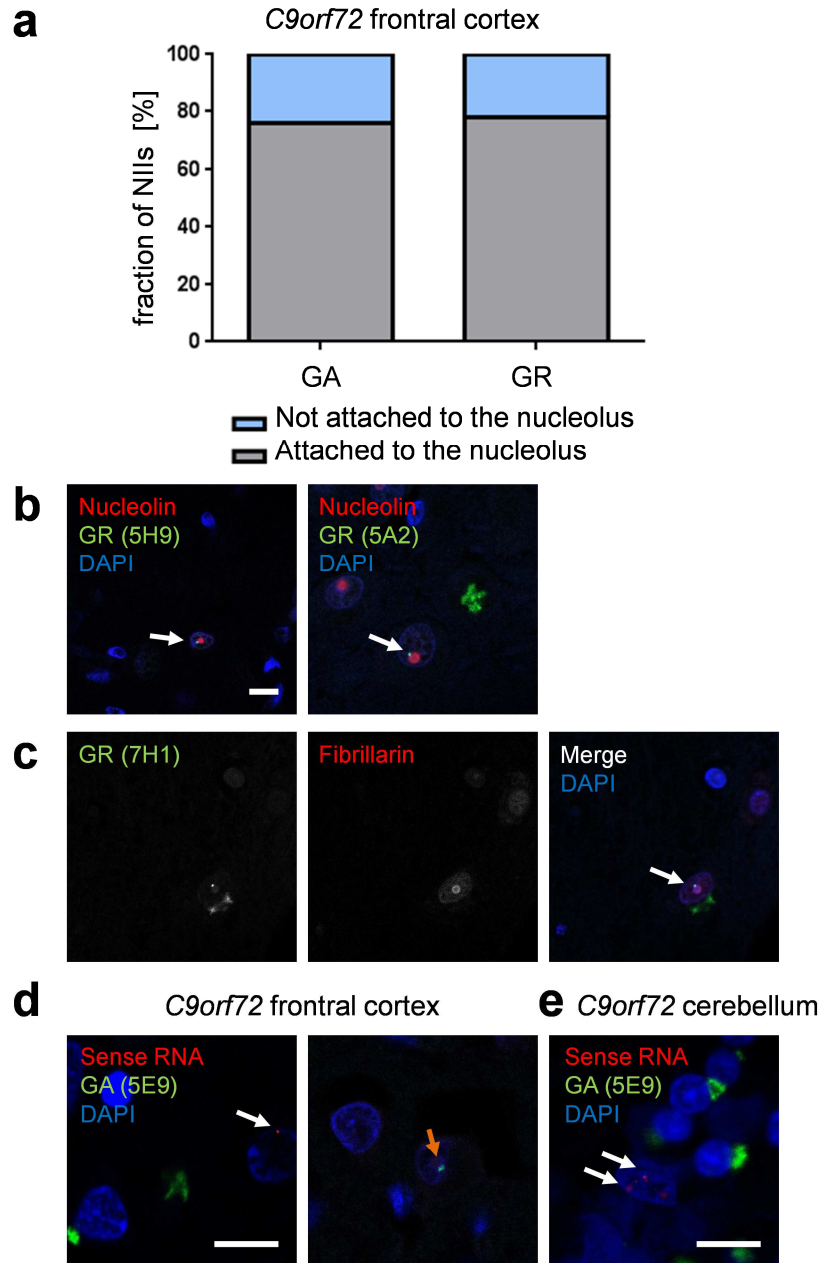


**Figure S4: Poly-GR antibodies detect para-nucleolar aggregates**

(a) Quantitative analysis of the localization of poly-GA and poly-GR NIIs was performed on double immunofluorescence stains with nucleolin in cortical areas of two *C9orf72* patients and two controls. 76% of poly-GA NIIs and 78% of poly-GR NIIs are attached to the nucleolus (50 NIIs each were analyzed). (b) Para-nucleolar poly-GR aggregates (arrows) are detected by two additional monoclonal poly-GR antibodies (5H9 and 5A2) as shown by double immunofluorescence with nucleolin. (c) Para-nucleolar poly-GR aggregates (arrow) are detected using fibrillarlin as an alternative marker for nucleoli. Scale bars represent 20  $\mu\text{m}$ . (d, e) Combined GGGGCC-specific *in situ* hybridization and poly-GA immunofluorescence shows no colocalization of RNA foci (white arrows) and para-nucleolar DPR inclusions (orange arrow).

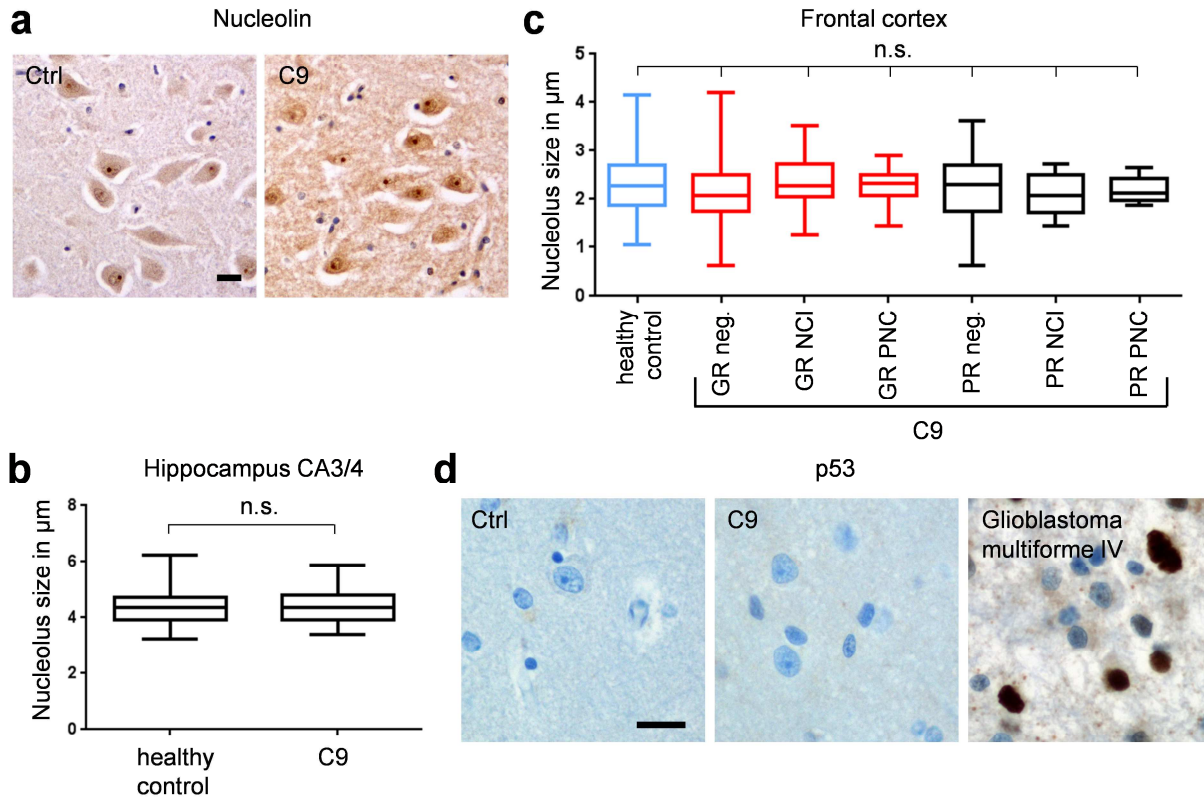


**Figure S5: Analysis of nucleolar stress in *C9orf72* cases**

Analysis of the hallmarks of nucleolar stress in *C9orf72* mutation patients (C9) and controls (Ctrl). **(a)** Immunohistochemistry with a nucleolin antibody reveals no difference in the shape of the nucleoli in neurons of the CA3/4 region between cases with *C9orf72* mutation and control cases. **(b)** Quantitative analysis of the average nucleolus size in the CA3/4 region performed on nucleolin immunofluorescence images reveals no difference between *C9orf72* patients and controls as well ( $n_{\text{ctrl}}=45$ ,  $n_{\text{C9}}=55$  nucleoli from two control cases and four *C9orf72* patients). The detailed analysis is described in the methods section. **(c)** Quantitative analysis of nucleolus size performed on nucleolin and poly-GR or poly-PR double immunofluorescence images in the frontal cortex. In *C9orf72* patients nucleolus size was analyzed separately for cells without DPR inclusions, with neuronal cytoplasmic inclusions (NCI) or inclusions in a para-nucleolar compartment (PNC) using MetaMorph software.  $n_{\text{ctrl}}=91$ ,  $n_{\text{GR NCI}}=40$ ,  $n_{\text{GR PNC}}=12$ ,  $n_{\text{GR neg.}}=126$ ,  $n_{\text{PR NCI}}=12$ ,  $n_{\text{PR PNC}}=5$ ,  $n_{\text{PR neg.}}=78$  nucleoli were investigated from two control cases and two *C9orf72* patients. Box plot shows mean, first and third quartile. Whiskers represent minimum and maximum. **(d)** Immunohistochemistry of frontal cortex using p53 antibodies in *C9orf72* patients, a healthy control and a case with glioblastoma as a positive control. Stress-indicative nucleolar accumulation of p53 in the nucleolus is not detected in *C9orf72* cases. Scale bars represent 20  $\mu\text{m}$ .

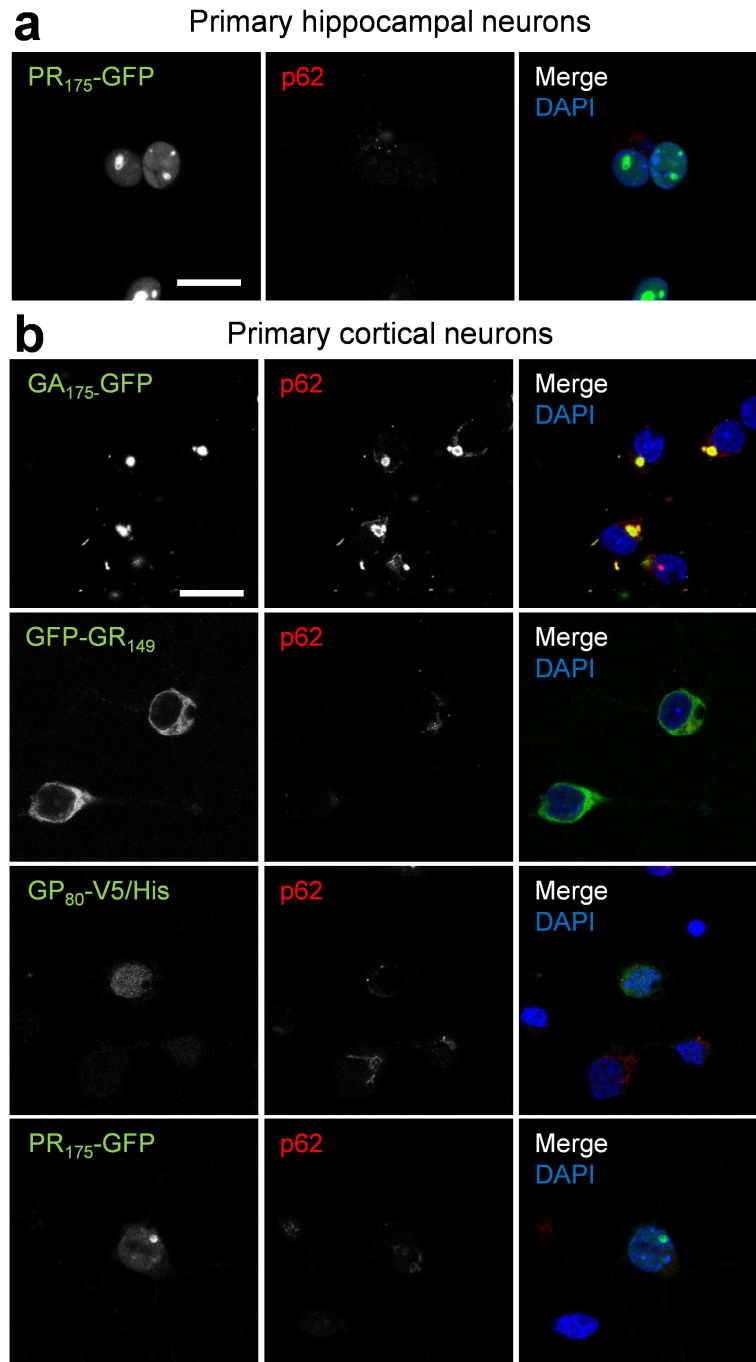


**Figure S6: Colocalization of DPR proteins with p62 in primary neurons**

Double immunofluorescence for DPR proteins and p62. Nuclei are labeled with DAPI. **(a)** PR<sub>175</sub>-GFP expressed in primary hippocampal neurons does not colocalize with p62 (DIV6+7). **(b)** Primary cortical neurons transduced with GA<sub>175</sub>-GFP, GFP-GR<sub>149</sub>, GP<sub>80</sub>-V5/His or PR<sub>175</sub>-GFP (DIV6+7). p62 co-aggregates only with cytoplasmic and intranuclear poly-GA inclusions, but not with poly-GR, poly-GP and poly-GR. Scale bars represent 20  $\mu$ m.

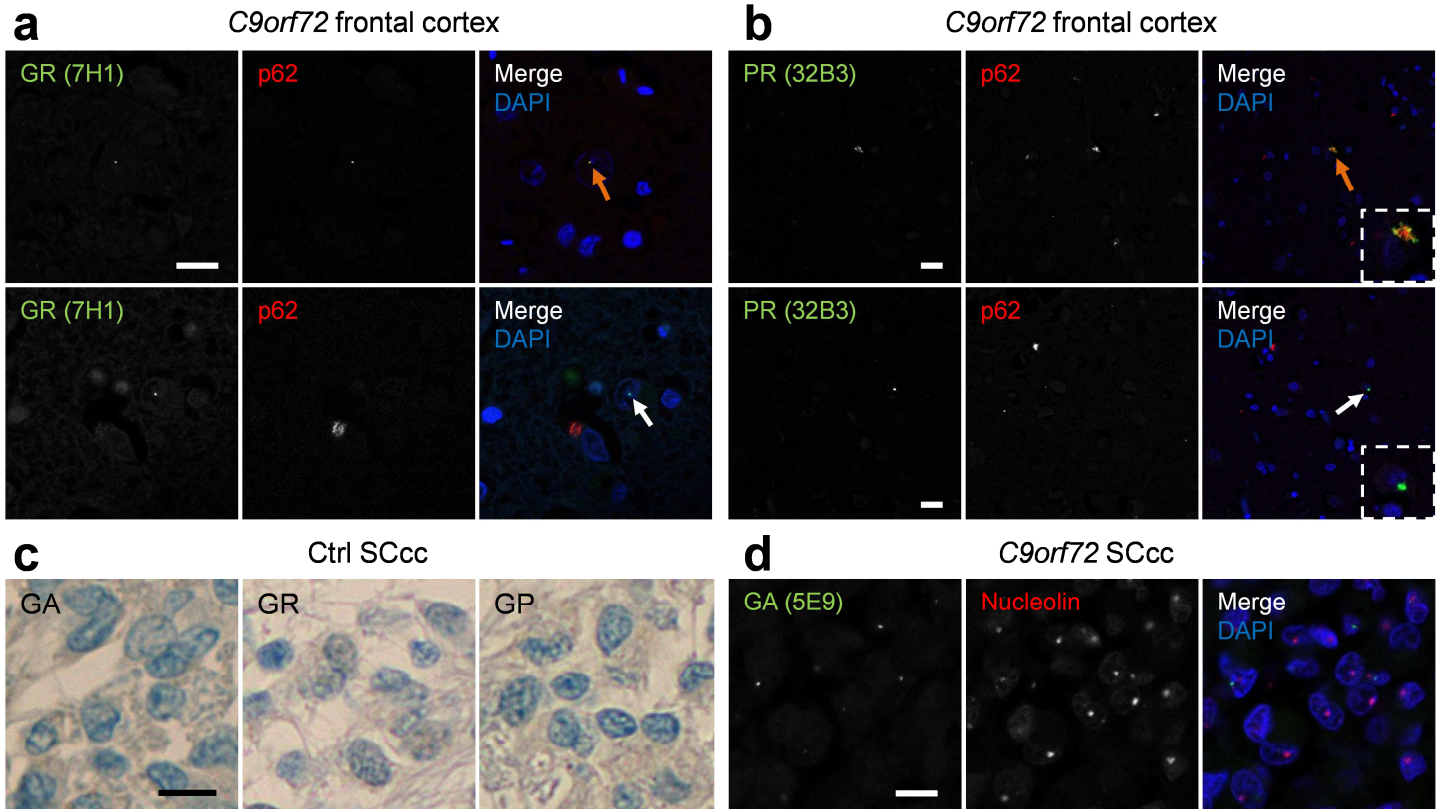


**Figure S7: p62 negative DPR inclusions are rare. DPR aggregates in the central canal of the spinal cord are not found in control cases and do not localize close to the nucleolus in *C9orf72* patients**

(a) Double immunofluorescence with poly-GR (7H1) and p62 in frontal cortex. Aside from p62 positive intranuclear inclusions (orange arrow), p62 negative intranuclear poly-GR inclusions also exist (white arrow), but are very rare. (b) In frontal cortex of *C9orf72* mutation patients most poly-PR inclusions are positive for p62 (orange arrow). Rarely a p62 negative poly-PR inclusion can be found (white arrows). (c) Immunohistochemistry with antibodies against poly-GA (5E9), poly-GR (7H1) and poly-GP (7A5) shows no DPR inclusions in the central canal of the spinal cord (SCcc) in an FTLD-MND-FUS case (FUS-1). (d) Double immunofluorescence with poly-GA and nucleolin shows that DPR inclusions are randomly distributed within the nuclei in SCcc glial cells. Scale bars represent 20 μm.

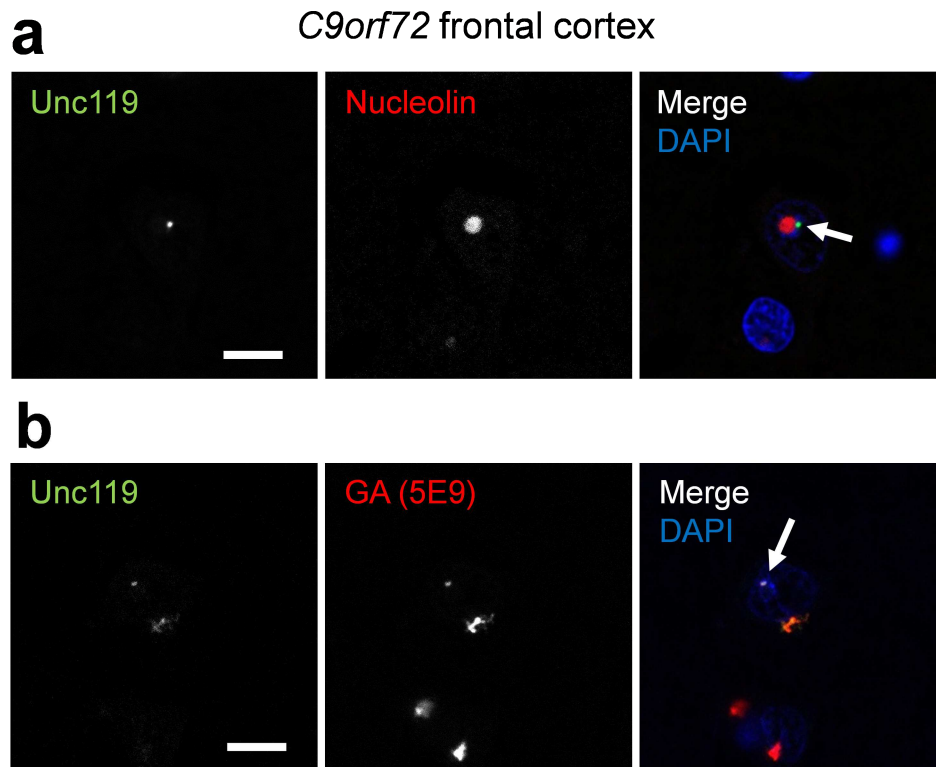


**Figure S8: Unc119 is colocalized with poly-GA in para-nucleolar inclusions**

Double immunofluorescence with Unc119 and nucleolin, poly-GA or p62 in frontal cortex. **(a)** Some Unc119 inclusions show para-nucleolar localization (arrow). **(b)** Intranuclear Unc119 is colocalized with poly-GA (arrow).

**Table S1: Semiquantitative assessment of DPR and Unc119 pathology in five C9orf72 cases**

Raw data for Fig. 5 and 8a. The numbers represent the categories „none“ (0), „few“ (1), „some“ (2), „many“ (3) and „abundant“ (4). The analysis is described in detail in the method section. Abbreviations as in Fig. 5.

**GA immunoreactive inclusions**

Case no.	FCtx			MCtx			CCtx			PCTx			TCtx			Octx			DG			CA3/4			SubCA1/2				
	NCI	NII	DN	NCI	NII	DN	NCI	NII	DN	NCI	NII	DN	NCI	NII	DN	NCI	NII	DN	NCI	NII	DN	NCI	NII	DN	NCI	NII	DN	NCI	NII
C9-1	4	2	2	3	2	1	3	2	1	4	2	1	4	2	1	3	2	1	3	1	2	3	1	2	2	1	0		
C9-2	4	2	1	4	2	2	4	2	2	4	2	2	4	2	2	4	2	1	4	2	3	4	2	3	3	1	2		
C9-3	3	2	1	3	1	2	3	2	2	3	1	1	3	2	2	3	2	2	3	2	2	2	1	2	2	1	1		
C9-4	3	1	0	3	2	2	3	2	1	4	2	2	4	2	2	4	2	1	3	1	1	3	1	2	2	1	1		
C9-5	4	2	1	4	2	2	4	2	2	4	2	1	4	2	2	4	2	2	3	2	1	3	2	2	3	1	2		
Mean	3,6	1,8	1,0	3,4	1,8	1,8	3,4	2,0	1,6	3,8	1,8	1,4	3,8	2,0	1,6	3,8	2,0	1,6	3,0	1,8	1,0	3,0	1,4	2,2	2,4	1,0	1,2		
CBLgI	CBLmI			CBLpI			Cd			Pu			Acc			Pa			BC			priEnt							
	NCI	NII	DN	NCI	NII	DN	NCI	NII	DN	NCI	NII	DN	NCI	NII	DN	NCI	NII	DN	NCI	NII	DN	NCI	NII	DN	NCI	NII	DN	NCI	NII
C9-1	3	2	3	2	2	4	2	0	0	2	1	0	2	1	0	2	1	0	1	0	0	1	0	0	4	2	1		
C9-2	4	4	4	4	2	4	3	1	0	3	1	1	2	1	0	3	1	0	1	0	0	1	0	0	4	2	2		
C9-3	2	1	3	3	1	4	2	1	1	1	0	0	1	1	0	2	1	0	0	0	0	0	0	0	4	2	2		
C9-4	2	1	3	2	1	4	2	0	0	1	0	1	1	1	0	1	1	1	1	0	0	1	0	0	4	2	2		
C9-5	3	2	2	3	1	3	2	0	0	2	1	1	2	1	1	3	1	1	1	0	1	0	0	4	2	2			
Mean	2,8	2,0	3,0	2,8	1,4	3,8	2,2	0,4	0,2	1,8	0,6	0,6	1,6	1,0	0,2	2,2	1,0	0,4	1,2	0,6	0,2	0,8	0,0	0,0	4,0	2,0	1,8		
preEnt	Am			Th			Snc			STN			LC			DRN			PN			N XII							
	NCI	NII	DN	NCI	NII	DN	NCI	NII	DN	NCI	NII	DN	NCI	NII	DN	NCI	NII	DN	NCI	NII	DN	NCI	NII	DN	NCI	NII	DN	NCI	NII
C9-1	3	1	1	3	2	1	4	2	0	1	1	0	0	0	0	2	0	0	1	0	0	1	0	0	0	0	0		
C9-2	4	1	2	4	2	2	4	2	0	1	1	0	1	0	0	2	1	0	1	0	0	1	0	0	1	0	0		
C9-3	3	2	2	3	1	1	2	1	0	1	0	0	1	0	0	1	0	0	1	0	0	1	0	0	4	2	2		
C9-4	3	2	1	3	1	0	3	1	0	1	0	0	1	0	0	2	0	0	2	0	0	0	0	0	4	2	2		
C9-5	3	2	2	3	1	1	3	2	1	2	1	1	2	0	0	2	1	0	2	1	0	0	0	0	4	2	2		
Mean	3,2	1,6	1,6	3,2	1,4	1,0	3,0	1,5	0,3	1,3	0,5	0,0	1,3	0,0	0,0	1,8	0,4	0,0	0,6	0,0	0,0	0,6	0,0	0,0	0,7	0,3	0,0		
IO	SCAC			SCPC			SCAT			SCPT			SCAI			SCPI			SCAS			SCPs							
	NCI	NII	DN	NCI	NII	DN	NCI	NII	DN	NCI	NII	DN	NCI	NII	DN	NCI	NII	DN	NCI	NII	DN	NCI	NII	DN	NCI	NII	DN	NCI	NII
C9-1	0	0	0	0	0	0	1	0	0	0	0	0	2	0	0	2	0	0	1	0	0	1	0	0	1	0	0		
C9-2	1	0	0	1	2	1	2	2	0	2	2	0	2	2	0	2	2	0	2	2	0	1	2	0	1	2	0		
C9-3				1	0	0	1	0	0	0	0	0	0	0	0	0	0	0	0	0	0	0	0	0	1	0	0		
C9-4	0	0	0	1	0	0	0	0	0	0	0	0	1	1	0	2	1	0	1	0	0	1	0	0	2	0	0		
C9-5	0	0	0	1	0	0	1	1	0	0	0	0	1	0	0	1	0	0	1	0	0	1	0	0	2	0	0		
Mean	0,3	0,0	0,0	0,8	0,4	0,2	1,0	0,6	0,0	0,5	0,5	0,0	1,0	0,8	0,3	1,8	0,8	0,0	0,8	0,5	0,0	0,8	0,5	0,0	1,3	0,5	0,0		

**GR immunoreactive inclusions**

Case no.	FCtx			MCtx			CCtx			PCtx			TCtx			Octx			DG			CA3/4			SubCA1/2		
	NCI	NII	DN	NCI	NII	DN	NCI	NII	DN	NCI	NII	DN	NCI	NII	DN	NCI	NII	DN	NCI	NII	DN	NCI	NII	DN	NCI	NII	DN
C9-1	3	1	0	2	1	0	2	2	0	2	1	0	2	1	0	3	2	0	3	2	0	3	2	0	2	1	1
C9-2	3	2	0	2	1	0	3	1	0	3	1	0	3	1	0	3	2	0	3	2	0	4	2	0	3	1	0
C9-3	2	1	0	2	0	0	2	1	0	2	0	0	2	1	0	2	0	1	2	1	0	2	1	1	2	1	1
C9-4	2	1	0	2	1	0	2	1	0	2	1	0	2	1	0	2	1	0	2	1	0	3	1	0	2	1	0
C9-5	3	1	0	2	1	1	2	1	0	3	1	0	3	2	0	2	2	0	2	2	0	2	1	1	2	1	2
Mean	2,6	1,2	0,0	2,0	0,8	0,2	2,2	1,2	0,0	2,4	0,8	0,0	2,4	1,2	0,0	2,4	0,8	0,4	2,4	1,6	0,0	2,8	1,4	0,4	2,2	1,0	0,8
	CBLgl			CBLml			CBLpcl			Cd			Pu			Acc			Pa			BC			priEnt		
	NCI	NII	DN	NCI	NII	DN	NCI	NII	DN	NCI	NII	DN	NCI	NII	DN	NCI	NII	DN	NCI	NII	DN	NCI	NII	DN	NCI	NII	DN
C9-1	2	1	0	2	1	0	2	0	0	1	0	0	1	1	0	0	0	0	0	0	0	0	0	0	3	2	0
C9-2	2	1	0	2	1	1	2	0	0	1	0	0	1	0	0	1	0	0	1	0	0	0	0	0	3	1	0
C9-3	1	0	0	2	1	1	2	0	0	1	0	0	1	0	0	1	0	0	0	0	0	0	0	0	2	1	0
C9-4	1	0	0	2	1	0	2	0	0	0	0	0	1	1	0	1	0	1	0	0	0	0	0	0	2	1	0
C9-5	2	1	1	2	2	0	2	0	0	0	0	0	1	0	0	1	1	0	1	1	0	0	0	0	3	1	0
Mean	1,6	0,6	0,2	2,0	1,2	0,4	2,0	0,0	0,0	0,6	0,0	0,0	1,0	0,0	0,2	0,4	0,2	0,0	0,4	0,2	0,0	0,0	0,0	0,0	2,6	1,2	0,0
	preEnt			Am			Th			Snc			STN			LC			DRN			PN			NXII		
	NCI	NII	DN	NCI	NII	DN	NCI	NII	DN	NCI	NII	DN	NCI	NII	DN	NCI	NII	DN	NCI	NII	DN	NCI	NII	DN	NCI	NII	DN
C9-1	2	1	0	2	1	0	3	2	0	1	0	0	0	0	0	0	0	0	1	0	0	0	0	0	0	0	0
C9-2	2	1	0	3	2	1	1	1	0	0	0	0	0	0	0	1	0	0	1	0	0	0	0	0	1	0	0
C9-3	1	1	0	2	1	0	1	1	0	0	0	0	0	0	0	1	0	0	1	0	0	1	1	0	2	1	0
C9-4	1	0	0	2	1	0	1	1	0	0	0	0	0	0	0	0	0	0	0	0	0	0	0	0	2	1	0
C9-5	2	1	0	3	1	0	2	1	0	1	0	0	0	0	0	1	0	0	1	0	0	1	0	0	1	0	0
Mean	1,6	0,8	0,0	2,4	1,2	0,2	1,8	1,3	0,0	0,5	0,0	0,0	0,0	0,0	0,0	0,6	0,0	0,0	0,4	0,2	0,0	0,4	0,2	0,0	0,7	0,0	0,0
	IO			SCAc			SCPc			SCAt			SCPt			SCAI			SCPI			SCAs			SCPs		
	NCI	NII	DN	NCI	NII	DN	NCI	NII	DN	NCI	NII	DN	NCI	NII	DN	NCI	NII	DN	NCI	NII	DN	NCI	NII	DN	NCI	NII	DN
C9-1	1	0	0	0	0	0	0	0	0	0	0	0	1	0	0	1	0	0	0	0	0	0	0	0	1	0	0
C9-2	0	0	0	1	0	0	0	0	0	0	0	0	0	0	0	1	0	0	1	0	0	0	0	0	0	0	0
C9-3				0	0	0	1	0	0																		
C9-4				1	0	0	1	0	0	0	0	0	1	0	1	0	0	0	1	0	0	0	0	0	0	0	0
C9-5	1	0	0	0	0	0	0	0	0	0	0	0	1	0	0	0	0	1	0	0	0	0	0	0	1	0	0
Mean	0,7	0,0	0,0	0,4	0,0	0,0	0,4	0,0	0,0	0,0	0,0	0,0	0,8	0,0	0,3	0,5	0,0	0,0	0,3	0,0	0,0	0,3	0,0	0,0	0,5	0,0	0,0

**GP immunoreactive inclusions**

Case no.	FCtx			MCtx			CCtx			PCtx			TCtx			Octx			DG			CA3/4			SubCA1/2					
	NCI	NII	DN	NCI	NII	DN	NCI	NII	DN	NCI	NII	DN	NCI	NII	DN	NCI	NII	DN	NCI	NII	DN	NCI	NII	DN	NCI	NII	DN			
C9-1	3	1	0	3	1	1	2	1	0	2	1	1	2	1	0	3	1	1	3	2	1	3	1	1	3	1	1	2	1	1
C9-2	3	1	1	2	1	1	3	2	0	2	1	0	3	2	0	3	2	1	3	2	1	3	2	1	4	2	1	2	1	2
C9-3	2	0	1	2	1	0	2	1	0	2	0	0	3	0	0	2	1	1	2	1	0	2	1	0	2	2	0	2	1	0
C9-4	3	1	1	3	1	1	2	1	0	3	1	0	2	0	0	3	1	1	2	1	0	2	1	0	2	1	0	2	1	1
C9-5	3	1	1	2	1	0	3	2	1	3	1	1	3	1	1	2	1	0	3	2	1	3	2	1	3	2	1	2	1	2
Mean	2,8	0,8	0,8	2,4	1,0	0,6	2,4	1,4	0,2	2,4	0,8	0,4	2,6	0,8	0,2	2,6	1,2	0,8	2,6	1,6	0,6	2,6	1,6	0,6	2,8	1,6	0,6	2,0	1,0	1,2
	CBLgl			CBLml			CBLpcl			Cd			Pu			Acc			Pa			BC			priEnt					
	NCI	NII	DN	NCI	NII	DN	NCI	NII	DN	NCI	NII	DN	NCI	NII	DN	NCI	NII	DN	NCI	NII	DN	NCI	NII	DN	NCI	NII	DN	NCI	NII	DN
C9-1	2	2	1	2	1	3	2	0	0	1	1	0	1	1	0	1	1	0	1	0	1	1	0	1	0	0	0	3	1	1
C9-2	3	2	2	4	1	3	2	0	0	1	1	0	1	1	0	1	0	0	1	0	0	1	0	0	1	0	0	3	2	0
C9-3	2	1	2	2	1	2	2	0	0	1	0	0	1	0	0	1	0	0	1	0	0	1	0	0	1	0	0	3	1	1
C9-4	1	0	0	2	1	2	2	0	0	0	0	0	1	0	0	1	1	0	1	1	0	1	1	0	1	0	0	2	1	0
C9-5	2	2	2	2	2	3	2	0	0	0	0	0	1	0	0	1	0	0	1	0	0	1	0	0	0	0	0	3	1	1
Mean	2,0	1,4	1,4	2,4	1,2	2,6	2,0	0,0	0,0	0,6	0,0	0,0	1,0	0,4	0,0	0,6	0,2	0,2	1,0	0,2	0,2	1,0	0,2	0,2	0,6	0,0	0,0	2,8	1,2	0,6
	preEnt			Am			Th			Snc			STN			LC			DRN			PN			NXII					
	NCI	NII	DN	NCI	NII	DN	NCI	NII	DN	NCI	NII	DN	NCI	NII	DN	NCI	NII	DN	NCI	NII	DN	NCI	NII	DN	NCI	NII	DN	NCI	NII	DN
C9-1	2	1	0	2	1	1	3	2	0	2	1	0	0	0	0	2	0	0	0	0	0	2	0	1	0	0	0	0	0	0
C9-2	2	1	0	3	1	0	3	2	0	2	1	0	0	0	0	1	0	0	1	0	0	1	0	0	0	0	0	1	0	0
C9-3	2	1	0	2	1	0	2	2	1	0	0	0	1	0	0	0	0	0	1	1	0	1	1	0	0	0	0	0	0	0
C9-4	1	0	0	2	1	0	2	1	0	0	0	0	1	0	0	0	1	0	2	0	0	2	0	0	0	0	0	0	0	0
C9-5	2	1	0	3	1	0	2	1	0	0	0	0	0	0	0	1	0	0	1	1	0	1	1	0	1	0	0	0	0	0
Mean	1,8	0,8	0,0	2,4	1,0	0,2	2,3	1,5	0,3	0,5	0,3	0,0	0,5	0,0	0,0	0,2	0,2	0,0	1,4	0,4	0,2	1,4	0,4	0,2	0,2	0,0	0,0	0,3	0,0	0,0
	IO			SCAc			SCPc			SCAT			SCPT			SCAI			SCPI			SCAs			SCPs					
	NCI	NII	DN	NCI	NII	DN	NCI	NII	DN	NCI	NII	DN	NCI	NII	DN	NCI	NII	DN	NCI	NII	DN	NCI	NII	DN	NCI	NII	DN	NCI	NII	DN
C9-1	0	0	0	0	0	1	1	1	0	0	0	0	1	0	1	1	0	1	1	0	2	1	0	2	0	0	0	0	0	0
C9-2	1	0	0	1	1	0	1	1	0	0	0	0	1	1	1	1	1	0	1	1	0	1	1	0	0	0	0	0	0	0
C9-3				1	0	0	1	0	0																					
C9-4	0	0	0	0	0	0	0	0	0	0	0	0	0	0	0	1	0	0	1	0	0	1	0	0	0	0	0	0	0	0
C9-5	0	0	0	1	0	0	1	1	0	0	0	0	1	0	0	1	0	0	1	0	0	1	0	0	1	0	0	1	0	1
Mean	0,3	0,0	0,0	0,6	0,2	0,2	0,8	0,6	0,0	0,0	0,0	0,0	0,8	0,3	0,5	1,0	0,3	0,3	1,0	0,3	0,5	1,0	0,3	0,5	0,3	0,0	0,0	0,3	0,0	0,3



**Unc119 immunoreactive inclusions**

Case no.	FCtx			MCtx			CCtx			PCtx			TCtx			Octx			DG			CA3/4			SubCA1/2		
	NCI	NII	DN	NCI	NII	DN	NCI	NII	DN	NCI	NII	DN	NCI	NII	DN	NCI	NII	DN	NCI	NII	DN	NCI	NII	DN	NCI	NII	DN
C9-1	3	2	1	2	1	0	2	1	0	2	1	1	2	1	1	2	1	0	2	1	0	2	1	0	2	1	0
C9-2	3	1	1	3	1	0	3	1	0	3	1	1	2	1	0	3	2	0	3	1	1	3	1	1	2	1	1
C9-3	2	1	0	2	1	1	2	1	1	2	1	1	2	1	1	2	0	1	2	1	0	2	1	1	2	1	0
C9-4	2	1	0	2	0	0	2	1	0	2	0	1	2	1	1	2	1	0	2	1	0	3	0	0	2	0	0
C9-5	3	1	1	3	1	1	3	1	1	3	0	1	3	1	1	3	1	0	2	2	0	2	0	2	2	0	2
Mean	2,6	1,2	0,6	2,4	0,8	0,4	2,4	1,0	0,4	2,4	0,6	1,0	2,2	0,8	0,6	2,2	1,4	0,0	2,4	0,6	0,8	2,4	0,6	0,8	2,0	0,6	0,6
	CBLgl			CBLml			CBLpcl			Cd			Pu			Acc			Pa			BC			priEnt		
	NCI	NII	DN	NCI	NII	DN	NCI	NII	DN	NCI	NII	DN	NCI	NII	DN	NCI	NII	DN	NCI	NII	DN	NCI	NII	DN	NCI	NII	DN
C9-1	2	0	1	2	1	2	2	0	0	1	0	0	1	0	0	1	0	0	0	0	0	0	0	0	3	1	1
C9-2	2	1	2	3	1	2	3	0	0	2	1	0	2	1	0	1	1	0	1	0	1	0	1	0	3	1	0
C9-3	2	1	1	2	1	1	2	0	0	1	0	0	1	0	0	1	0	0	0	0	0	0	0	0	3	1	1
C9-4	1	0	0	2	1	0	2	0	0	0	0	0	1	0	0	1	0	0	1	0	0	9	0	0	2	1	0
C9-5	2	1	1	3	1	2	2	0	0	1	0	0	2	0	0	0	0	1	0	0	0	0	0	0	3	1	1
Mean	1,8	0,6	1,0	2,4	1,0	1,4	2,2	0,0	0,0	1,0	0,2	0,0	1,4	0,2	0,0	0,8	0,2	0,2	2,0	0,0	0,2	2,0	0,0	0,2	2,8	1,0	0,6
	preEnt			Am			Th			Snc			STN			LC			DRN			PN			NXII		
	NCI	NII	DN	NCI	NII	DN	NCI	NII	DN	NCI	NII	DN	NCI	NII	DN	NCI	NII	DN	NCI	NII	DN	NCI	NII	DN	NCI	NII	DN
C9-1	2	0	0	2	1	0	3	1	0	1	0	0	0	0	0	1	0	0	0	0	0	0	0	0	0	0	0
C9-2	2	1	0	3	1	1	2	1	0	1	0	0	1	0	0	2	0	0	1	0	0	1	0	0	0	0	0
C9-3	2	1	1	2	1	0	2	1	0	1	0	0	0	0	0	1	0	0	0	0	0	0	0	0	0	0	0
C9-4	1	0	0	2	0	0	2	0	0	0	0	0	1	0	0	1	0	0	1	0	0	0	0	0	0	0	0
C9-5	2	1	0	3	1	1	2	0	0	1	0	0	1	0	0	1	0	0	1	0	0	1	0	0	0	0	0
Mean	1,8	0,6	0,2	2,4	0,8	0,4	2,3	0,5	0,0	0,8	0,0	0,0	0,0	0,0	0,0	1,2	0,0	0,0	0,4	0,0	0,0	0,4	0,0	0,0	0,0	0,0	0,0
	IO			SCAc			SCPc			SCAT			SCPT			SCAI			SCPI			SCAs			SCP's		
	NCI	NII	DN	NCI	NII	DN	NCI	NII	DN	NCI	NII	DN	NCI	NII	DN	NCI	NII	DN	NCI	NII	DN	NCI	NII	DN	NCI	NII	DN
C9-1	0	0	0	1	0	1	1	0	0	0	0	0	0	1	1	0	0	0	0	0	0	0	0	0	1	0	0
C9-2	1	0	0	1	1	1	0	0	0	0	0	0	1	0	0	1	0	0	1	0	0	1	0	0	0	0	0
C9-3				0	0	0	1	0	0																		
C9-4				0	0	0	0	0	0	0	0	0	1	1	0	0	1	0	0	0	0	0	1	0	0	0	0
C9-5	0	0	0	0	0	0	1	0	0	1	0	0	1	0	0	1	0	0	1	0	0	1	0	0	1	0	0
Mean	0,3	0,0	0,0	0,4	0,2	0,4	0,6	0,0	0,2	0,3	0,0	0,0	0,8	0,5	0,3	0,5	0,0	0,3	0,5	0,0	0,3	0,5	0,0	0,0	0,5	0,0	0,0

**Table S2: Quantitative assessment of DPR and Unc119 pathology in 14 *C9orf72* cases**

Raw data for the quantitative analysis of inclusion pathology in 14 *C9orf72* mutation cases shown in Fig. 6, 8a and 8b. Three to twelve pictures were taken from representative areas of each region. In cortical areas pictures were taken in a columnar orientation covering layer I to VI. The total number of inclusions was divided by the number of pictures taken. For details see methods section, for abbreviations Fig. 6.

<b>GR (NCI + NII)</b>							
Case no.	FCtx	MCtx	OCtx	DG	CA3/4	CBLgl	CBLml
C9-1	11.5	5.1	6.0	48.5	10.0	29.5	6.0
C9-2	17.4	5.0	22.8	102.0	16.7	20.0	9.7
C9-3	3.4	1.5	3.5	6.7	14.7	8.0	5.7
C9-4	4.0	6.0	6.6	14.0	12.0	0.7	0.7
C9-5	15.2	5.0	11.0	31.0	13.0	37.5	13.0
C9-6	7.1		0.5			1.7	4.7
C9-7	4.1		18.3	64.7	23.7	3.7	2.3
C9-8	2.6		2.0	2.7	3.3	1.0	3.0
C9-9	5.0		6.8	34.7	10.0	0.3	1.0
C9-10	2.4		0.0	18.7	27.7	0.0	3.0
C9-11	2.5		0.3	2.0	1.0	1.3	0.7
C9-12	7.0		1.6	13.0	7.0	1.0	0.0
C9-13	22.6		32.4			34.3	12.7
C9-14	7.0	5.4	9.0	30.0	10.3	10.0	7.7
<b>PR (NCI + NII)</b>							
Case no.	FCtx	MCtx	OCtx	DG	CA3/4	CBLgl	CBLml
C9-1	0.1	0.0	0.2	1.3	2.7	0.0	0.0
C9-2	0.1	0.0	0.0	0.7	1.0	0.3	0.0
C9-3	0.1	0.0	0.0	0.0	0.0	1.0	0.0
C9-4	0.0	0.2	0.2	0.0	0.0	0.0	0.0
C9-5	0.0	0.0	0.0	0.0	0.0	0.0	0.0
C9-6	0.0		0.0			0.0	0.0
C9-7	0.0		0.0	0.3	2.3	0.3	0.3
C9-8	0.5		0.0	0.0	0.7	0.0	0.0
C9-9	0.2		0.0	0.3	0.3	0.3	0.0
C9-10	0.0		0.0			0.3	0.0
C9-11	0.0		0.0	0.0	0.3	1.0	0.0
C9-12	0.0		0.0	0.3	0.3	0.7	0.0
C9-13	0.1		0.1			0.7	0.0
C9-14	0.0	0.0	0.0	0.0	0.0	0.0	0.0
<b>GA (NCI + NII)</b>							
Case no.	FCtx	MCtx	OCtx	DG	CA3/4	CBLgl	CBLml
C9-1	10.6	6.5	9.8	70.7	30.7	85.3	16.0
C9-2	46.7	34.8	75.5	368.3	40.3	364.3	61.0
C9-3	14.6	14.0	16.2	26.0	13.0	83.0	17.7
C9-4	6.7	4.6	7.9	47.0	29.7	180.0	15.0
C9-5	48.6	25.4	79.1	80.3	28.0	183.7	39.0
C9-6	23.7		21.5			153.3	26.0
C9-7	20.0		15.2	94.0	21.3	338.5	24.0
C9-8	44.8		51.8	95.0	19.0	473.0	54.3
C9-9	14.0		24.0	56.3	11.5	315.0	35.0
C9-10	34.2		55.5	112.7	40.0	123.0	58.3
C9-11	30.8		3.3	47.0	12.7	283.0	31.0
C9-12	20.2		19.4	55.0	21.0	179.0	20.7
C9-13	25.2		46.2			437.3	29.0
C9-14	16.4	15.4	26.5	87.0	17.7	119.0	15.0

<b>Unc119 (NCI + NII)</b>							
Case no.	FCtx	MCtx	OCtx	DG	CA3/4	CBLgl	CBLml
C9-1	5.9	2.5	3.2	16.0	7.0	16.0	6.0
C9-2	16.8	17.7	16.0	141.5	27.7	133.0	25.7
C9-3	6.2	4.4	5.0	13.7	8.3	20.0	3.3
C9-4	2.0	2.0	2.2	5.8	16.6	7.3	2.7
C9-5	14.2	14.8	19.6	27.3	16.0	100.3	22.3
C9-6	12.8		6.5			39.0	15.0
C9-7	11.8		12.0	24.3	19.7	164.7	15.0
C9-8	17.0		10.2	26.3	10.3	146.0	18.0
C9-9	4.3		6.1	19.5	5.0	86.3	1.5
C9-10	31.6		35.5	138.3	35.0	61.0	18.7
C9-11	10.2		0.7	11.3	6.0	27.7	2.3
C9-12	8.0		9.6	18.0	17.3	85.7	4.3
C9-13	12.2		24.6			114.0	10.3
C9-14	11.3	10.0	12.5	18.0	12.0	25.0	10.7

## **1.2 Contribution to the publication**

As first author of this publication, I contributed to the study design and had major contributions to the experimental work. In detail, I performed all experiments shown in this publication except of immunohistochemistry or immunofluorescence staining of figure 4m/n/q, S3, S6b and demographic/neuropathological patient/control data shown in table 1.


## 2.1 Publication 2:

Spinal poly-GA inclusions in a *C9orf72* mouse model trigger motor deficits and inflammation without neuron loss

published as

**Schludi MH**, Becker L, Garrett L, Gendron TF, Zhou Q, Schreiber F, Popper B, Dimou L, Strom TM, Winkelmann J, von Thaden A, Rentzsch K, May S, Michaelson M, Schwenk BM, Tan J, Schoser B, Dieterich M, Petrucelli L, Höltner SM, Wurst W, Fuchs H, Gailus-Durner V, Hrabe de Angelis M, Klopstock T, Arzberger T, Edbauer D. Spinal poly-GA inclusions in a *C9orf72* mouse model trigger motor deficits and inflammation without neuron loss. *Acta Neuropathol.* 2017. doi:10.1007/s00401-017-1711-0

# Spinal poly-GA inclusions in a *C9orf72* mouse model trigger motor deficits and inflammation without neuron loss

Martin H. Schludi<sup>1,2</sup> · Lore Becker<sup>3</sup> · Lillian Garrett<sup>3,4</sup> · Tania F. Gendron<sup>5</sup> · Qihui Zhou<sup>1,2</sup> · Franziska Schreiber<sup>1</sup> · Bastian Popper<sup>6</sup> · Leda Dimou<sup>7,8</sup> · Tim M. Strom<sup>9</sup> · Juliane Winkelmann<sup>2,10,11,12</sup> · Anne von Thaden<sup>1</sup> · Kristin Rentzsch<sup>1</sup> · Stephanie May<sup>1</sup> · Meike Michaelsen<sup>1</sup> · Benjamin M. Schwenk<sup>1</sup> · Jing Tan<sup>10</sup> · Benedikt Schoser<sup>13</sup> · Marianne Dieterich<sup>1,2,13</sup> · Leonard Petrucelli<sup>5</sup> · Sabine M. Hölder<sup>3,4</sup> · Wolfgang Wurst<sup>1,2,4,14</sup> · Helmut Fuchs<sup>3</sup> · Valerie Gailus-Durner<sup>3</sup> · Martin Hrabe de Angelis<sup>3,15,16</sup> · Thomas Klopstock<sup>1,2,13</sup> · Thomas Arzberger<sup>1,2,17,18</sup> · Dieter Edbauer<sup>1,2,19</sup> 

Received: 9 January 2017 / Revised: 4 April 2017 / Accepted: 4 April 2017  
© The Author(s) 2017. This article is an open access publication

**Abstract** Translation of the expanded (ggggcc)<sub>n</sub> repeat in *C9orf72* patients with amyotrophic lateral sclerosis (ALS) and frontotemporal dementia (FTD) causes abundant poly-GA inclusions. To elucidate their role in pathogenesis, we generated transgenic mice expressing codon-modified (GA)<sub>149</sub> conjugated with cyan fluorescent protein (CFP). Transgenic mice progressively developed poly-GA inclusions predominantly in motoneurons and interneurons of the spinal cord and brain stem and in deep cerebellar nuclei. Poly-GA co-aggregated with p62, Rad23b and the newly identified Mif2, in both mouse and patient samples. Consistent with the expression pattern, 4-month-old

transgenic mice showed abnormal gait and progressive balance impairment, but showed normal hippocampus-dependent learning and memory. Apart from microglia activation we detected phosphorylated TDP-43 but no neuronal loss. Thus, poly-GA triggers behavioral deficits through inflammation and protein sequestration that likely contribute to the prodromal symptoms and disease progression of *C9orf72* patients.

**Keywords** ALS · FTL · FTD · MND · *C9orf72* · Neurodegeneration · Neurological disorder · Mouse model

**Electronic supplementary material** The online version of this article (doi:10.1007/s00401-017-1711-0) contains supplementary material, which is available to authorized users.

✉ Dieter Edbauer  
dieter.edbauer@dzne.de

<sup>1</sup> German Center for Neurodegenerative Diseases (DZNE) Munich, Feodor-Lynen-Straße 17, 81377 Munich, Germany

<sup>2</sup> Munich Cluster for System Neurology (SyNergy), Feodor-Lynen-Straße 17, 81377 Munich, Germany

<sup>3</sup> German Mouse Clinic, Institute of Experimental Genetics, German Research Center for Environmental Health, Helmholtz Zentrum München, Ingolstädter Landstrasse 1, 85764 Neuherberg, Germany

<sup>4</sup> Institute of Developmental Genetics, German Research Center for Environmental Health, Helmholtz Zentrum München, Ingolstädter Landstrasse 1, 85764 Neuherberg, Germany

<sup>5</sup> Department of Neuroscience, Mayo Clinic, 4500 San Pablo Road, Jacksonville, FL 32224, USA

<sup>6</sup> Department of Anatomy and Cell Biology, Biomedical Center, Ludwig-Maximilians-University Munich, Großhaderner Str. 9, 82152 Planegg-Martinsried, Germany

<sup>7</sup> Physiological Genomics, Biomedical Center, Ludwig-Maximilians-University Munich, Großhaderner Str. 9, 82152 Planegg-Martinsried, Germany

<sup>8</sup> Molecular and Translational Neuroscience, Department of Neurology, University of Ulm, Albert-Einstein-Allee 11, 89081 Ulm, Germany

<sup>9</sup> Institut für Humangenetik, Helmholtz Zentrum München, 85764 Munich, Germany

<sup>10</sup> Institut für Neurogenomik, Helmholtz Zentrum München, 85764 Munich, Germany

<sup>11</sup> Neurologische Klinik, Klinikum rechts der Isar, Technische Universität München, 81675 Munich, Germany

<sup>12</sup> Institut für Humangenetik, Klinikum rechts der Isar, Technische Universität München, 81675 Munich, Germany

<sup>13</sup> Department of Neurology, Friedrich-Baur-Institute, Klinikum der Ludwig-Maximilians-Universität München, Ziemssenstr. 1a, 80336 Munich, Germany

## Introduction

A (ggggcc)<sub>n</sub> hexanucleotide repeat expansion upstream of the coding region of *C9orf72* is the most common genetic cause of amyotrophic lateral sclerosis (ALS) and frontotemporal dementia (FTD), with some patients showing symptoms of both diseases [7]. Patients usually carry several hundred or thousand ggggcc repeats compared to less than 30 in the general population. The repeat expansion inhibits *C9orf72* expression, and sense and antisense transcripts may cause toxicity by sequestering RNA-binding proteins in nuclear foci [6, 28]. Moreover, both sense and antisense repeat transcripts are translated from all reading frames into aggregating dipeptide repeat (DPR) proteins (poly-GA, -GP, -GR, -PA, and -PR) [1, 22, 23, 40]. The relative contribution of these putative pathomechanisms, and their link to the co-occurring TDP-43 pathology present in patients with *C9orf72* ALS/FTD, are under intense debate.

Generating mouse models for *C9orf72* repeat expansion diseases has been surprisingly challenging [13]. Complete loss of *C9orf72* does not cause neurodegeneration, but does affect autophagy, particularly in the immune system, and leads to splenomegaly [15, 25]. High level viral expression of a relatively short (ggggcc)<sub>66</sub> repeat expansion leads to rapid neurodegeneration accompanied by DPR and TDP-43 pathology [5]. In contrast, expressing lower levels of an expanded repeat in its endogenous context leads to variable results. Two BAC transgenic mouse lines showed the characteristic RNA foci and DPR inclusions of *C9orf72* ALS/FTD, but no neuron loss or behavioral symptoms [24, 26], while two similar mouse models additionally showed cognitive symptoms [15, 19]. The more dramatic effects in the viral system may be due to higher expression levels and altered processing of exonic repeat expression [34]. Together, these models strongly support gain of function toxicity as the main cause of *C9orf72* ALS/FTD, but

cannot differentiate the contribution of sense and antisense RNA transcripts and the five DPR species. Viral expression of the most abundant DPR species, poly-GA, in the mouse brain causes mild neurodegeneration and cognitive symptoms without TDP-43 pathology, but this system showed no expression in the spinal cord [37]. In patients, DPR proteins are less common in the spinal cord than in the brain, but they are also found in upper and lower motoneurons [31].

To elucidate the specific contribution of poly-GA to disease pathogenesis, we aimed to generate a transgenic mouse model with poly-GA expression levels comparable to *C9orf72* ALS/FTD patients. We chose a *Thy1*-based expression vector for neuron-specific expression of poly-GA [9]. Here, we report in-depth pathological and phenotypic analyses of these mice focusing on the motor system.

## Methods

### Generation of *Thy1* (GA)<sub>149</sub>-CFP mice

We inserted a multiple cloning site into the pUC18 based murine *Thy1.2* vector using synthetic oligonucleotides [9]. This allowed us to insert a cDNA encoding (GA)<sub>149</sub>, 31 amino acids corresponding to the 3' region of the poly-GA reading frame in patients [22] and cyan fluorescent protein (CFP) (sequence shown in Fig. S1a). Compared to the previous (GA)<sub>149</sub>-GFP construct [21] only the fluorescent protein had been changed. Linearized vector was injected into C57BL/6-derived zygotes and transferred into pseudopregnant CD1 females (PolyGene). GA-CFP mice were kept in the C57BL/6N background. Mice were PCR genotyped using the following primers (tccaggagcgtaccatcttc; gtgctcaggtagtggtgtc). We confirmed maintenance of the full length transgene with PCR amplification (Expand Long Template PCR System, Roche, 11681842001; gatccaagctgccaccatg; tctagctctgccactccaag) and sequencing.

The transgene integration site was determined by whole genome sequencing according to standard protocols using the TruSeq DNA PCR-Free Library Preparation Kit and an Illumina HiSeq 4000 with 150 bp paired-end reads resulting in about 58× coverage from two lanes. Sequences mates mapping to different chromosomes were analyzed using the Integrative Genomics Viewer (IGV) [33].

### Immunohistochemistry of mouse and patient tissue

After killing, 1-, 3-, 6-, and 12-month-old mice were transcardially perfused with 1% sterile PBS and tissue was then formalin fixated for 2 days. Histological stainings were performed on 5–8 μm thick sections from paraffin-embedded tissue. For spinal cord tissue, an additional decalcification step with 5% formic acid for 5 days was performed after formalin fixation. After

<sup>14</sup> Chair of Developmental Genetics, Technische Universität München, Freising-Weihenstephan, Germany

<sup>15</sup> Chair of Experimental Genetics, School of Life Science Weihenstephan, Technische Universität München, Alte Akademie 8, 85354 Freising, Germany

<sup>16</sup> German Center for Diabetes Research (DZD), Ingolstädter Landstr. 1, 85764 Neuherberg, Germany

<sup>17</sup> Center for Neuropathology and Prion Research, Ludwig-Maximilians-University Munich, Feodor-Lynen-Straße 23, 81377 Munich, Germany

<sup>18</sup> Department of Psychiatry and Psychotherapy, Ludwig-Maximilians University Munich, Nußbaumstraße 7, 80336 Munich, Germany

<sup>19</sup> Institute for Metabolic Biochemistry, Ludwig-Maximilians-University Munich, Feodor-Lynen-Straße 17, 81337 Munich, Germany

deparaffinization in xylene and dehydration in graded ethanol, the paraffin sections were treated with citrate buffer (pH 6) for 20 min in the microwave. Mlf2 IHC staining was more prominent when the citrate retreatment was followed by 20 min incubation in 80% formic acid or 5–25 min incubation with 0.1 µg/µl proteinase K in 10 mM Tris/HCl pH 7.6 at 37 °C. Afterwards the slides were incubated with primary antibody overnight at 4 °C. For ChAT, an additional incubation with rabbit anti-goat-IgG was performed the next day for 1 h at room temperature. The slides were detected by the DCS SuperVision 2 Kit (DCS innovative diagnostic-system, Hamburg, Germany) according to the manufacturer's instructions. Iba1 and GFAP immunohistochemistry was performed with the Ventana BenchMark XT automated staining system (Ventana) using the UltraView Universal DAB Detection Kit (Roche). For Nissl staining, the deparaffinized slides were incubated in 70% ethanol overnight. After 30 min in Cresyl violet and 1 min in 96% ethanol the slides were processed in 100% ethanol with glacial acetic acid. Bright-field images were taken by CellID, Olympus BX50 Soft Imaging System (Olympus, Tokyo, Japan).

For immunofluorescence, after deparaffinization and citrate antigen retrieval, the slides were incubated with primary antibody overnight at 4 °C and the following day incubated for 1 h at room temperature with secondary Alexa Fluor labeled antibodies. For Mlf2 immunofluorescence staining, a 1 min treatment at 37 °C with 0.05 µg/µl proteinase K in 10 mM Tris/HCl pH 7.6 was necessary before citrate antigen retrieval. After the nuclei were counterstained with DAPI, the slices were incubated for 1 min in 0.2% Sudan black B and mounted with Fluoromount Aqueous Mounting Medium (Sigma, F4680). Fluorescent images were taken using a LSM710 confocal laser scanning system (Carl Zeiss, Jena, Germany) with 20x or 40x/63x oil immersion objectives.

### Antibodies

α-GFP (1:1000, Clonotect 632592), α-GA clone 5F2 [20] (purified mouse monoclonal, WB unlabeled 1:50; IHC HRP labeled 5F2 1:2500, labeled by AbD Serotec HRP-labeling Kit LNK002P; biotinylated 5F2 7 ng/µl; MSD-labeled 5F2 10 ng/µl, labeled by Meso Scale MSD Sulfo-Tag NHS-Ester R91AN-1), α-GA-CT (C-terminal tail) clone 5C3 [22] (rat monoclonal, 1:50), α-p62/SQSTM1 (IF 1:100, IHC 1:1000, MBL, PM045), α-pTDP-43 (Ser409/Ser410) clone 1D3 [20] (purified rat monoclonal, 1:50), α-TDP-43 (1:1000, Cosmo Bio, TIP-TD-P09), α-RanGAP1 (1:100, Abcam, ab92360), α-nucleolin (1:1000, Abcam, ab50729), α-CD68 (1:1000, Abcam, ab125212), α-Iba1 (1:500, Wako, 091-19741), α-GFAP (1:5000, Dako, Z0334), α-NeuN (1:1000, Abcam, ab177487), α-ChAT (IF 1:300, IHC 1:5000, Millipore, AB144P), α-Calnexin (1:3000, Enzo Life Science, SPA-860F), α-Calbindin

(1:300, Abcam, ab49899), α-Calretinin (1:1000, Abcam, ab702) α-Parvalbumin (1:750, Abcam, ab11427), α-Mlf2 #1 (1:1000, Sigma-Aldrich, HPA010811-100UL), α-Mlf2 #2 (1:1000, Santa Cruz, sc-166874), α-Laminin (1:200, Abcam, ab11575), α-goat-IgG (1:400, Dako, E0466), α-mouse Alexa Fluor 488 (1:500, Thermo Fischer Scientific, A11029), α-rabbit Alexa Fluor 488 (1:500, Thermo Fischer Scientific, A11034), α-rat Alexa Fluor 488 (1:500, Thermo Fischer Scientific, A11006), α-mouse Alexa Fluor 555 (1:500, Thermo Fischer Scientific, A21424), α-rabbit Alexa Fluor 555 (1:500, Thermo Fischer Scientific, A21429), α-rat Alexa Fluor 555 (1:500, Thermo Fischer Scientific, A21434), Streptavidin Alexa Fluor 488 (1:500, Thermo Fischer Scientific, S11223), nuclei were stained with DAPI (Roche Applied Science, Penzberg, Germany).

### Immunoassay analysis of poly-GA in tissue homogenates

Mouse brainstem and spinal cord samples and *C9orf72* patient motor cortex samples were sonicated in 500–700 µl of cold RIPA buffer (137 mM NaCl, 20 mM Tris pH 7.5, 10% Glycin, 1% Triton X 100, 0.5% Na-deoxycholate, 0.1% SDS, 2 mM EDTA, protease and phosphatase inhibitors). 100 µl of this homogenized tissue stock solutions were diluted to 300 µl with RIPA and centrifuged at 100,000×g for 30 min at 4 °C. To avoid cross contamination, the RIPA-insoluble pellets were resuspended in 300 µl RIPA, re-sonicated and re-centrifuged. Afterwards the RIPA-insoluble pellets were sonicated in U-RIPA (RIPA buffer containing 3.5 M Urea) and the protein concentration determined by Bradford assay. Streptavidin Gold multi-array 96-well plates (MesoScale, L15SA-1) were blocked for 30 min with block solution (1% BSA, 0.05% Tween20 in PBS) and incubated with biotinylated α-GA clone 5F2 overnight at 4 °C. Equal amounts of protein of all samples were added in duplicate wells for 2 h, followed by 2 h incubation with the secondary MSD-labeled α-GA clone 5F2. Serial dilution of recombinant GST-GA<sub>15</sub> in blocking buffer was used to prepare a standard curve. The wells intensity of emitted light upon electrochemical stimulation was measured using the MSD Quickplex 520 and the background corrected by the average response obtained from blank wells. Sensitivity and specificity of the immunoassay were confirmed using purified 15-mer DPRs fused to GST (Fig. S3a, b).

### Phenotypic analysis of mice

The study was conducted in accordance with European and national guidelines for the use of experimental animals, and the protocols were approved by the governmental committee (Regierungspräsidium Oberbayern, Germany). All experimenters were blind to the genotype.



Barnes maze (Stoelting Europe, Ireland) assay to test spatial, hippocampus-dependent long-term memory in mice was performed on a circular surface (diameter 91 cm) with 20 circular holes (diameter 5 cm) around its circumference [3]. Under one hole was an “escape box” (diameter 4 cm, depth 15 cm). The table surface was brightly lit by overhead lightning (900 lx). For each trial the mice had 3 min to find and hide in the “escape box”. For the statistical analysis failed attempts were set to 3 min.

In the balance beam test, the mice were placed on a wooden beam (round surface, length 58 cm, diameter 8 mm) and had 1 min to cross the beam. The test was finished either when the mice reached the end of the stick, they dropped down or the time ran out. For the statistical analysis failed attempts were set to 1 min. The experimenters were blind to the genotype, and trials were either video documented or recorded by AnyMaze (Stoelting Europe). AnyMaze Software was used to track the mice and to analyze the data.

In the Rotarod test (Ugo Basile), we accelerated the spindle speed from 5 to 50 rpm over 5 min. The test finished either after 5 min or when the mouse dropped down. The average time of two trials with 1 h break in between was used.

Modified SHIRPA analysis and grip strength testing was performed as described [11].

The beam ladder consists of two Plexiglas screens connected with several metal beams of variable distance. The test is used to evaluate skilled walking of the mice. Mice traverse the ladder and foot slips of fore paws and hind paws are counted separately as well as the time to traverse the beam.

The open field test as an assessment of spontaneous exploratory and anxiety-related behavior in a novel environment was carried out as previously described [12, 14, 39]. It consisted of a transparent and infra-red light permeable acrylic test arena with a smooth floor (internal measurements: 45.5 × 45.5 × 39.5 cm). Illumination levels were set at approximately 150 lx in the corners and 200 lx in the middle of the test arena. Each animal was placed individually into the middle of one side of the arena facing the wall and allowed to explore it freely for 20 min. For data analysis, the arena was divided by the computer in two areas, the periphery defined as a corridor of 8 cm width along the walls and the remaining area representing the center of the arena (42% of the total arena). Data were recorded and analyzed using the ActiMot system (TSE, Bad Homburg, Germany).

Acoustic startle and its prepulse inhibition were assessed using a startle apparatus setup (Med Associates Inc., VT, USA) including four identical sound-attenuating cubicles. The protocol is based on the Eumorphia protocol (<http://www.empress.har.mrc.ac.uk>), adapted to

the specifications of our startle equipment, and constantly used in the primary screen of the GMC [30]. Background noise was 65 dB, and startle pulses were bursts of white noise (40 ms). A session was initiated with a 5-min-acclimation period followed by five presentations of leader startle pulses (110 dB) that were excluded from statistical analysis. Trial types included prepulse alone trials at four different sound pressure levels (67, 69, 73, 81 dB), and trials in which each prepulse preceded the startle pulse (110 dB) by a 50 ms inter-stimulus interval. Each trial type was presented ten times in random order, organized in ten blocks, each trial type occurring once per block. Inter-trial intervals varied from 20 to 30 s.

### DNA constructs and lentivirus production

cDNA of rat Mif2 (NCBI Gene ID: 312709) containing an N-terminal HA-tag was expressed from a lentiviral vector driven by human ubiquitin promoter (FUW2-HA). Previously described (GA)<sub>175</sub>-GFP cDNA expressed from a synthetic gene lacking repetitive (ggggcc)<sub>n</sub> sequences with ATG start codon and EGFP was cloned in a lentiviral packaging vector (FhSynW2) containing the human synapsin promoter [21]. Lentivirus was produced in HEK293FT cells (Life Technologies) as described previously [10].

### Cell culture, RNA isolation and immunoprecipitation

Primary hippocampal neurons from embryonic day 19 rats were cultured and transduced with lentivirus as described previously [32]. Immunofluorescence staining was performed on 10 min PFA (4% paraformaldehyde and 4% sucrose) fixed primary neurons. The primary and secondary antibodies were diluted in GDB buffer (0.1% gelatin, 0.3% Triton X-100, 450 mM NaCl, 16 mM sodium phosphate pH 7.4) and incubated over night at 4 °C or 1 h at room temperature. Confocal images were taken using a LSM710 confocal laser scanning system (Carl Zeiss, Jena, Germany) with 40× or 63× oil immersion objectives. RNA isolation and qPCR was performed as described previously [23] using the following primers (CD68 ttctgctgtggaaatgcaag and gagaaacatggcccgaagt; Iba1 acagcaatgatgaggatctgc and ctctaggtgggtcttgggaac; GFAP ttctcgatctggaggttg and agatcgccacctacaggaaa; ACTB atggagggaatacagccc and ttcttgcagctcctctgt; GAPDH caacagcaactcccactcttc and ggtccagggttcttactctt).

### Patient material

Tissue samples of patient autopsy cases were provided by the Neurobiobank Munich, Ludwig-Maximilians-University (LMU) Munich and collected according to the guidelines of the local ethics committee.

## Statistics and analysis

Statistical analysis was performed with GraphPad Prism software (version 7.01). For neuron and motoneuron count, images of the left and right anterior horns of the spinal cord were taken and all positively stained cells were manually counted. The count number represents the neurons/motoneurons averaged on one side. Experiments with two groups were analyzed by *t* test (unpaired, two-sided, *t* = size of the difference relative to the variation; *df* = degrees of freedom). Behavioral data was analyzed by two-way ANOVA with Bonferroni post hoc test (*F* = equality of variances).

## Phospho-TDP-43 immunoassays

For phosphorylated TDP-43 measurements, sarkosyl-soluble and urea-soluble fractions of mouse spinal cord tissues were prepared as previously described [5]. In brief, 25–60 mg of tissue were subjected to a sequential extraction protocol using Tris–EDTA buffer (50 mM Tris pH 7.4, 50 mM NaCl, 1 mM EDTA), high salt Triton X-100 buffer, Triton X-100 buffer + 30% sucrose, and sarkosyl buffer. Sarkosyl-insoluble material was further extracted in urea buffer. The protein concentrations of sarkosyl-soluble fractions were determined using a bicinchoninic acid assay (Thermo Scientific), whereas a Bradford assay was utilized to measure protein concentrations of urea-soluble fractions. Phosphorylated TDP-43 levels in both these fractions were evaluated using a sandwich immunoassay that utilizes MSD electrochemiluminescence detection technology [15]. A mouse monoclonal antibody that detects TDP-43 phosphorylated at serines 409 and 410 (Cosmo Bio, #CAC-TIP-PTD-M01, 1:500) was used as the capture antibody. The detection antibody was a sulfo-tagged rabbit polyclonal C-terminal TDP-43 antibody (Proteintech, 12892-1-AP, 2 µg/ml). Response values corresponding to the intensity of emitted light upon electrochemical stimulation of the assay plate using the MSD QUICK-PLEX SQ120 were acquired and background corrected using the average response from buffer only.

## Results

### *Thy1* (GA)<sub>149</sub>-CFP mice accumulate poly-GA inclusions in the spinal cord and brainstem

We generated a *Thy1*-based vector to express (GA)<sub>149</sub> using a synthetic sequence, which unlike the repeat expansion in patients has no extensive (ggggcc)<sub>n</sub> stretches, fused with a C-terminal fluorescent CFP tag (Figs. 1a, S1a). Since the relevance of the C-terminal tail of endogenous DPR products is unknown, we additionally included 31 amino acids

translated from the endogenous locus in the poly-GA reading frame [22]. Using pronuclear injections into C57BL/6 mice, we generated a founder line (termed GA-CFP) with germline transmission and poly-GA expression. Transgenic mice were born at Mendelian frequency and did not differ in adult viability. Sequencing confirmed transmission of the full length open reading frame in all analyzed animals (*n* = 3, data not shown) and genomic PCR from different tissues further confirmed the somatic stability of the synthetic repeat gene (Fig. S1b). We identified the integration site using whole genome sequencing and validated our findings by PCR and Sanger sequencing (Fig. S2). Several transgene copies integrated on chromosome 14 about 330 kb downstream of the nearest transcript, the long non-coding RNA 4930474H20Rik, strongly suggesting that no endogenous genes are disrupted.

Using immunohistochemistry, we characterized poly-GA protein expression in different brain regions in 4–6-month-old mice. Expression of the aggregated full length product was detected with antibodies targeting CFP, poly-GA or the C-terminal DPR tail (GA-CT) (Fig. S1c). While most of the poly-GA inclusions were cytoplasmic, a few inclusions were observed in the nucleus (Fig. S1d). In GA-CFP mice, poly-GA-inclusion pathology was restricted to neurons of brain stem, cerebellar nuclei and spinal cord. There were numerous poly-GA-immunopositive inclusions in large neurons of the brainstem, the lateral (dentate) and interposed cerebellar nuclei and (most abundantly) the anterior horn of the spinal cord, particularly in the cervical, thoracic and lumbar regions (Fig. 1b). Inclusion pathology was additionally observed in interneurons (Fig. S1e) in the laminae IV, V and VI of the posterior horn. No poly-GA inclusions were detected in the olfactory bulb, the molecular and granular layer of the cerebellum, the hippocampus or the neocortex, including the motor cortex (Fig. 1b).

Next, we analyzed the progression of poly-GA pathology in GA-CFP mice with age. Inclusions were visible by IHC in the spinal cord and brain stem at 1 month of age, and the number and size of inclusions increased with age (Fig. 1c). Consistent with these findings, levels of RIPA-insoluble poly-GA in brain stem and spinal cord lysates increased over time, as assessed using a poly-GA-specific immunoassay (Figs. 1d, e, S3a, S3b), whereas no signal was detected in non-transgenic littermates. No poly-GA was detectable in the RIPA-soluble fraction of the spinal cord and brainstem (Fig. S3c). Fair comparison of poly-GA levels in mice and patients is complicated by the different regional expression pattern in mice and patients and variable poly-GA levels in patients. However, we measured the expression of poly-GA in spinal cord of 4–6-month-old GA-CFP mice and motor cortex of *C9orf72* ALS/FTD patients with abundant poly-GA pathology by immunoassay (Fig. S3d) and additionally counted the frequency of neuronal poly-GA inclusions in the most affected regions of GA-CFP mice

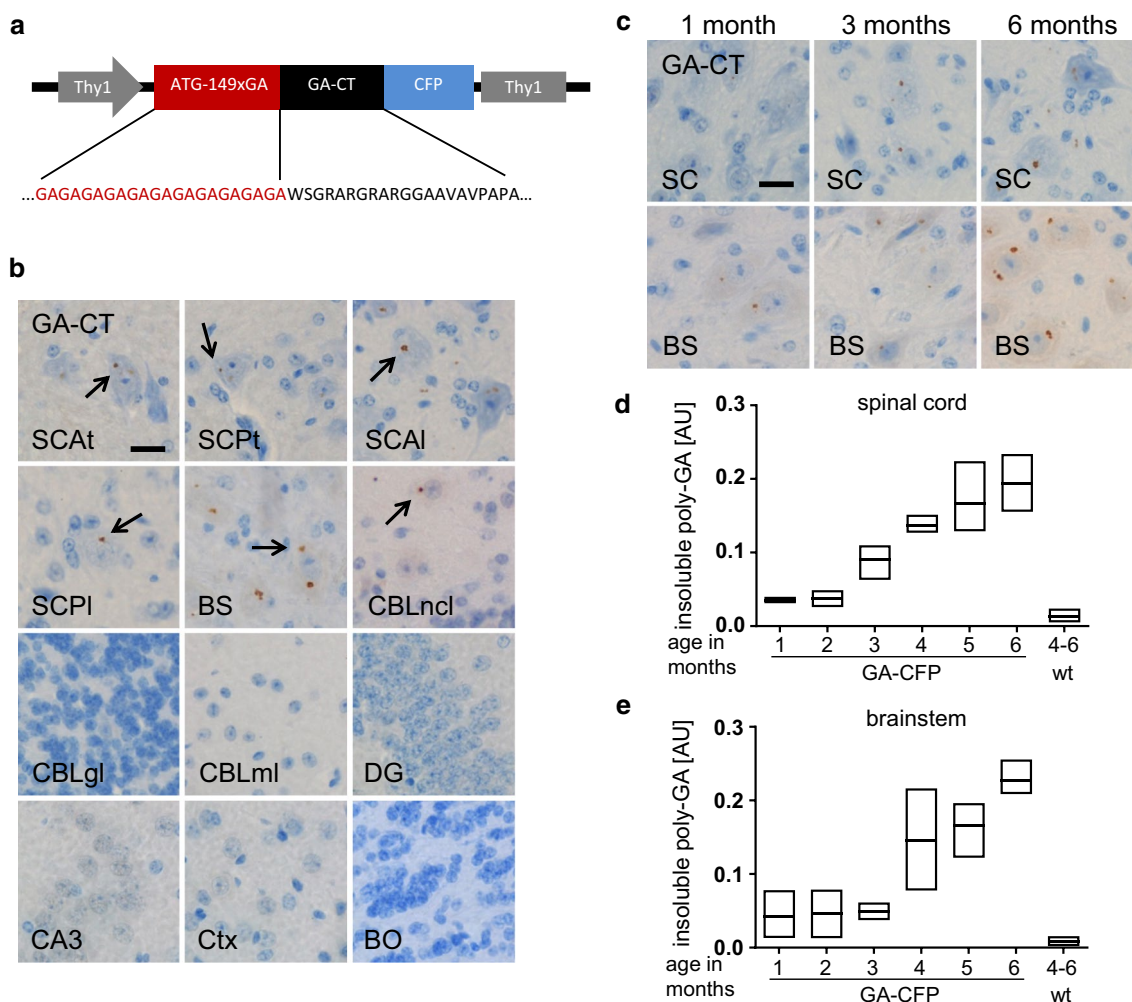


**Fig. 1** Expression and distribution pattern of poly-GA aggregates in GA-CFP mice. **a** Schematic diagram of the construct containing the murine Thy1 promoter driving expression of a synthetic gene encoding (GA)<sub>149</sub> with its endogenous C-terminal tail fused to CFP. (GA)<sub>149</sub>-CFP is replacing the endogenous coding region. **b** Distribution of GA aggregates show many inclusions in the spinal cord and brainstem and no aggregates in cortical regions, hippocampus or molecular and granular layer of the cerebellum. *BO* olfactory bulb, *BS* brainstem, *CA3* cornu ammonis fields 3, *CBLgl* cerebellar granular cell layer, *CBLml* cerebellar molecular cell layer, *CBLncl* lateral cerebellar nuclei, *DG* dentate gyrus, *SCAl* anterior horn of lumbar

spinal cord, *SCAt* anterior horn of thoracic spinal cord, *SCPl* posterior horn of lumbar spinal cord, *SCPt* posterior horn of thoracic spinal cord. *Scale bars* represent 20  $\mu$ m. **c** Increasing number and accumulation of aggregates in spinal cord (SC; *upper row*) and brainstem (BS; *lower row*) of 1-, 3- and 6-month-old GA-CFP mice detected by immunohistochemical staining using GA-CT antibody. *Scale bar* represents 20  $\mu$ m. Quantitative immunoassay of RIPA-insoluble poly-GA in the spinal cord (**d**) and brainstem (**e**) of 1–6-month-old GA-CFP mice ( $n = 3$  mice per time-point; measured in duplicates) shows increasing amounts of poly-GA in a time dependent manner. *AU* arbitrary unit, data are shown as mean, minimum and maximum

and the neocortex of *C9orf72* patients (Fig. S3e, f). Both assays show that poly-GA expression is not grossly exaggerated in GA-CFP mice. Thus, GA-CFP mice are a suitable model to address the pathomechanisms of poly-GA in the motor system.

### Poly-GA co-aggregates with p62, Rad23b and the chaperone-associated protein Mif2

To investigate potential downstream effects of poly-GA expression, we analyzed whether poly-GA co-aggregates

with other proteins. Similar to findings in *C9orf72* ALS/FTD patients [23], the vast majority of poly-GA inclusions co-localized with p62 (Fig. 2a, b, first row and Table S1). Rad23b, a known poly-GA-interacting protein involved in the ubiquitin proteasome pathway, also aggregated in GA-CFP mice (Fig. 2a, b, second row) similar to previous reports [21, 37]. In contrast to overexpression of poly-GA in rat primary neurons [21], GA-CFP mice showed no sequestration of Unc119 (Fig. S4a) and no mislocalization or co-localization of RanGAP1 with poly-GA (Fig. S4b first row, and Table S1), which is consistent with our cell

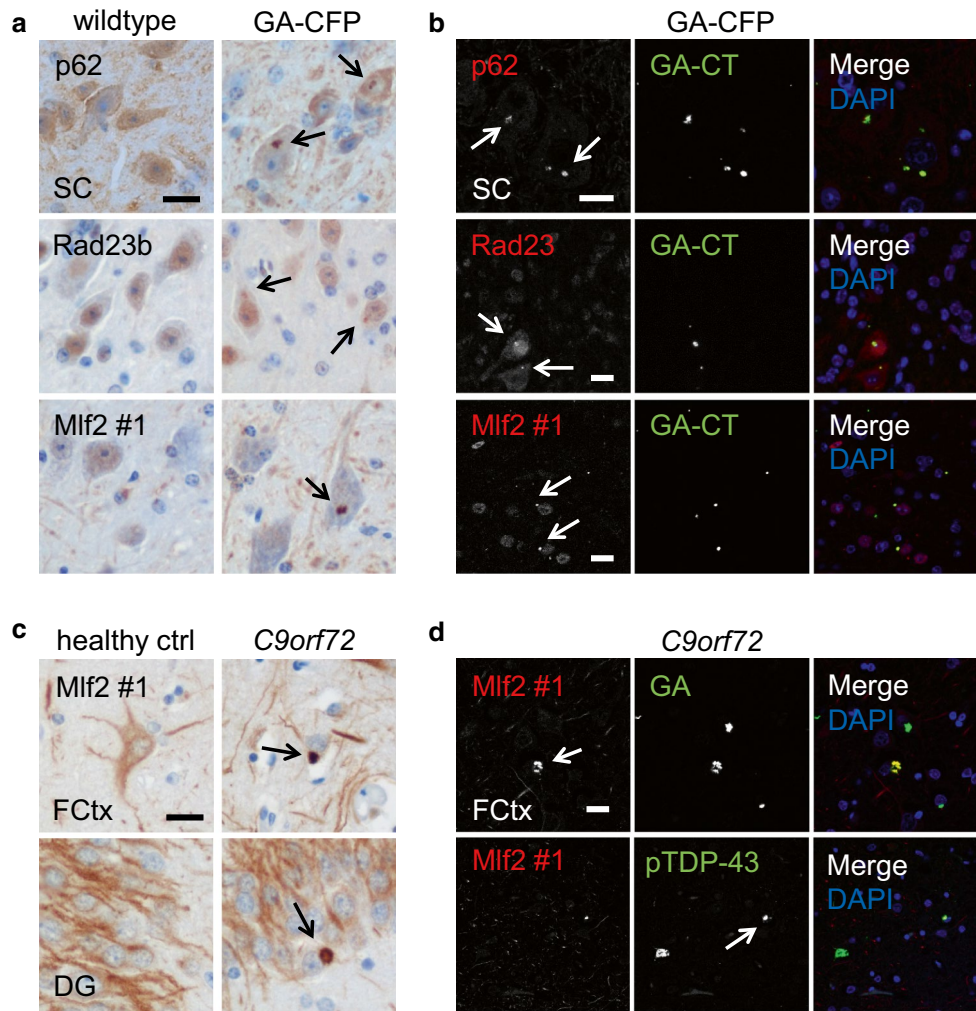


**Fig. 2** GA-CFP mice develop p62, Rad23b and Mlf2 pathology similar to human *C9orf72* mutation carriers. **a** Immunohistochemistry shows p62, Rad23b and Mlf2 aggregates in the spinal cord (SC) of 6-month-old GA-CFP mice but not of wildtype mice. **b** Immunofluorescence stainings show p62, Rad23b and Mlf2 positive inclusions that co-localize with poly-GA in the spinal cord of 6-month-old GA-

CFP mice. **c** Immunohistochemistry detects specific Mlf2 aggregates in the frontal cortex (FCtx) and dentate gyrus (DG) of *C9orf72* ALS/FTLD patients. **d** Double immunofluorescence reveals colocalization of Mlf2 aggregates with poly-GA and phosphorylated TDP-43 inclusions in *C9orf72* patients. Scale bars represent 20  $\mu$ m

culture data [17]. We also found no evidence of nucleolar pathology using nucleolin immunostaining (Fig. S4b second row).

Additionally, we analyzed whether poly-GA co-aggregates with proteins identified in poly-GA immunoprecipitates in primary hippocampal neurons in our recent mass spectrometry screen [21]. Among such proteins that had not been previously validated, the Hsp70-associated protein, Mlf2, showed the strongest co-aggregation with poly-GA in the spinal cord of GA-CFP mice, whereas no Mlf2 aggregates were detected in wildtype mice (Fig. 2a, b, third row). Co-transduction of HA-Mlf2 and (GA)<sub>175</sub>-GFP in primary hippocampal neurons of wildtype rats corroborated the sequestration of Mlf2 into poly-GA inclusions (Fig. S4c). Moreover, endogenous Mlf2 was sequestered into

poly-GA inclusions in primary neurons transduced with (GA)<sub>175</sub>-GFP (Fig. S4d). These data led us to examine Mlf2 aggregation in *C9orf72* ALS/FTD patients. We detected Mlf2 pathology in the frontal cortex and hippocampus of *C9orf72* ALS/FTD patients but not healthy controls using two independent Mlf2 antibodies (Figs. 2c, S4e). In addition, double immunofluorescence staining confirmed the co-aggregation of Mlf2 with poly-GA in *C9orf72* patients (Fig. 2d, first row). While in GA-CFP mice Mlf2 was co-aggregating in ~55% of the poly-GA inclusions, in *C9orf72* patients only 0.3–2.7% of the poly-GA aggregates showed Mlf2 sequestration, depending on the brain region (Table S2). However, we detected Mlf2 also occasionally in cytoplasmic phospho-TDP-43 inclusions in *C9orf72* patients (Fig. 2d, second row). Thus, our GA-CFP mice recapitulate

the poly-GA component of pathology in *C9orf72* ALS/FTD patients, including the co-aggregation of poly-GA with p62, Rad23b and Mif2.

### Poly-GA triggers mild TDP-43 phosphorylation but no overt neuron loss

We next analyzed whether poly-GA expression drives neurodegeneration. Consistent with the expression pattern

of the *Thy1* promoter, poly-GA was exclusively found in NeuN-positive neurons (Fig. 3a) and no expression was detectable in microglia or muscle fibers (Fig. S4f). However, Nissl staining and NeuN immunostaining revealed no overt neuron loss in the spinal cord (Fig. 3b, c). Poly-GA was found in most choline acetyltransferase (ChAT) positive motoneurons in the anterior horn of the spinal cord (Fig. 3d), but ChAT immunostaining revealed no statistically significant loss of motoneurons at 6 months

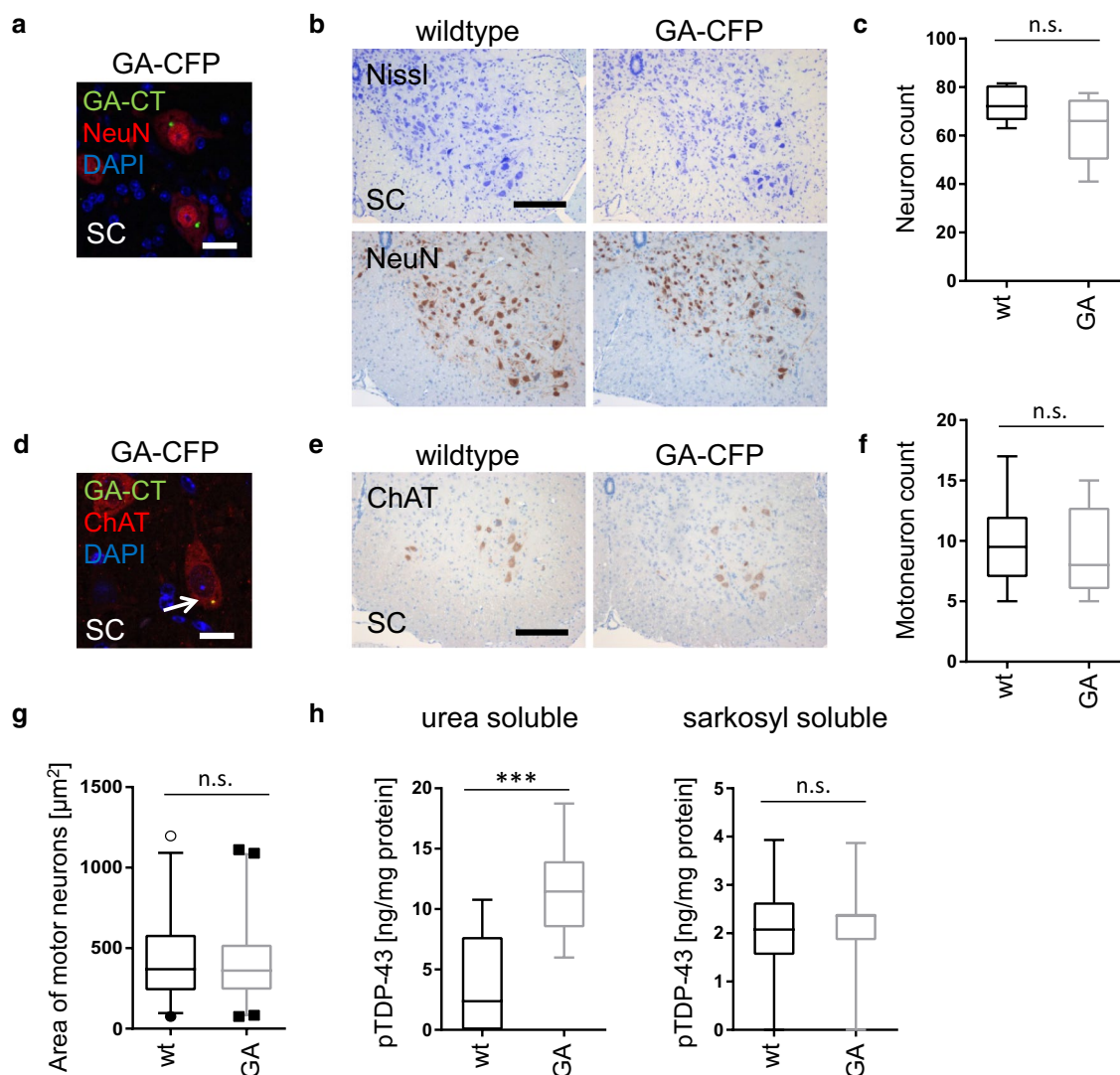


**Fig. 3** GA-CFP mice show no evidence for neuronal loss but increased TDP-43 phosphorylation. **a** Double immunofluorescence of 6-month-old GA-CFP spinal cord tissue (SC) shows poly-GA inclusions exclusively in NeuN-positive cells. *Scale bar* represents 20  $\mu\text{m}$ . **b, c** Nissl staining and NeuN immunohistochemistry of 6-month-old GA-CFP and wildtype spinal cords. *Scale bar* represents 100  $\mu\text{m}$ . Quantitative analysis of NeuN-positive neurons shows no significant difference between wildtype and GA-CFP mice ( $n_{\text{GA-CFP/wt}} = 3$ ). **d** Immunostaining of poly-GA aggregates in choline acetyltransferase (ChAT)-positive motoneurons. *Scale bar* represents 20  $\mu\text{m}$ . **e–g** Immunohistochemistry and quantitative analysis of ChAT-positive

motoneurons of 6-month-old mice in the anterior horn of the spinal cord revealed no statistically significant differences in neuron count ( $n_{\text{GA-CFP/wt mice}} = 4$ ) and size ( $n_{\text{GA-CFP motoneurons}} = 228$ ;  $n_{\text{wt motoneurons}} = 195$ ). Neurons were counted as described in the “Statistics” section. *Scale bar* represents 100  $\mu\text{m}$ . **h** Immunoassay for phosphorylated TDP-43 in sarkosyl (1%)-soluble or urea (7M)-soluble spinal cord fractions from 6-month-old GA-CFP or wildtype (wt) mice.  $n_{\text{(wt)}} = 12$ ;  $n_{\text{(GA-CFP)}} = 8$ . Unpaired *t* test (two-tailed; sarkosyl  $t = 0.3034$ ,  $df = 18$ ; urea  $t = 4.172$ ,  $df = 18$ ). Data are shown as box plot with whiskers at the 1st and 99th percentile. \*\*\* $p < 0.001$ , *ns* not significant

(Fig. 3e–g). Furthermore, the size and shape of motoneurons in GA-CFP mice did not show signs of degeneration and were not discernible from the corresponding neurons in wildtype mice.

Next, we analyzed another neuropathological hallmark of ALS, namely TDP-43 phosphorylation, in aged GA-CFP mice. We quantified levels of phosphorylated TDP-43 (at serines 409 and 410) in the spinal cord of mice at 6 months of age by ELISA. Phosphorylated TDP-43 levels were approximately threefold higher in the urea-soluble (but sarkosyl-insoluble) fraction of GA-CFP mice compared to wildtype mice, but no difference was detected in the sarkosyl-soluble fraction (Fig. 3h). While mature TDP-43 inclusions and cytoplasmic TDP-43 mislocalization were not observed in GA-CFP mice, even at 12 months of age (Fig. S4g, h; Table S1), these data may nonetheless indicate that poly-GA contributes to the onset of TDP-43 pathology.

### Poly-GA induces microglia activation without astrogliosis

Next, we analyzed the GA-CFP mice for signs of neuroinflammation. Immunohistochemistry for CD68 and Iba1 in 1- and 6-month-old mice revealed strong upregulation of these markers of phagocytic microglia in the spinal cord of 6-month-old GA-CFP mice (Fig. 4a, b) while little microglia activation was detectable at 1 month of age. Quantitative RT-PCR further confirmed enhanced mRNA expression of CD68 and Iba1 (Fig. 4c, d). In contrast, GFAP immunostaining and mRNA expression analysis revealed no signs of poly-GA-induced astrogliosis (Fig. 4e, f). Furthermore, in the neocortex of GA-CFP mice, a region lacking poly-GA pathology, no activation of CD68, Iba1 or GFAP was detected (Fig. S5a). Thus, neuronal poly-GA expression induces regional microglia activation in the absence of overt neuron loss in GA-CFP mice.

### GA-CFP mice develop progressive motor deficits

To analyze the functional consequences of poly-GA pathology and its downstream effects, we performed in depth phenotyping of mice at 3–4 months of age when poly-GA pathology starts building up. Open field testing revealed no signs of anxiety as GA-CFP and wildtype mice spent a similar time in the center of the arena, but the decreased rearing activity of GA-CFP mice may indicate decreased motor performance or alterations in the relevant brain circuits (Fig. 5a). The overall distance traveled was not significantly reduced in GA-CFP mice. However, when walking across a beam ladder with irregular step distance, male GA-CFP mice showed significantly more hind paw slips, without a difference in total traversing time (Fig. 5b). In the SHIRPA analysis, the majority of GA-CFP mice showed hind paw clenching

(84% compared to 35% of controls; Fig. 5c) and a broad, wagging gait (77% compared to 24% of controls). Grip strength of fore and hind limbs measured individually or combined was normal (data not shown). Decreased acoustic startle response and prepulse inhibition in GA-CFP mice suggest impaired sensorimotor gaiting and recruitment ability (Figs. S5b/c).

We repeated a subset of tests in 13–14-month-old mice. At this age, both male and female mice took significantly longer to cross the beam ladder and slipped more often with their hind paws (Fig. 5d). In the SHIRPA analysis, 87% of GA-CFP mice showed hind paw clenching compared to 8% of controls and abnormal gait (93% compared to 38% of controls) (Fig. 5e). However, out of the sixty mice used for this study, only three control mice and one GA-CFP mouse had died unexpectedly until the age of 16 months.

We additionally used an independent, smaller cohort of mice from 2–6 months of age for a longitudinal study focusing on memory function and motor coordination. While GA-CFP and wildtype mice initially gained weight normally for the first 6 months (Fig. S5d), transgenic mice showed reduced body weight compared to wildtype littermates after 15 months (male wildtype  $38.6 \text{ g} \pm 3.1$ , male GA-CFP  $32.1 \text{ g} \pm 1.7$ , female wildtype  $31.1 \text{ g} \pm 4.0$ , female GA-CFP  $26.4 \text{ g} \pm 2.3$ ; ANOVA genotype effect  $p < 0.001$ ). Hippocampus-dependent spatial memory of all mice was tested weekly using the Barnes maze; at all time-points, GA-CFP mice performed like their wildtype littermates, indicating that their spatial memory was not impaired (Fig. S5e). Moreover, we used the accelerated rotarod as a test for overall motor performance. Within 6 months, no difference in the performance of motor planning and physical condition was observed between GA-CFP mice and wildtype littermates (Fig. S5f). To measure balance and coordination more directly, mice were made to walk across a balance beam every week. The beam walk revealed progressive deficits in male and female transgenic mice (Fig. 5f, g). GA-CFP mice and their wildtype littermates showed similar performance from week 8 to 17, but from week 20 onward GA-CFP mice took a significantly longer time to cross the beam (Fig. 5f) or failed the test entirely by dropping down (Fig. 5g).

Taken together, GA-CFP mice develop progressive gait and balance impairments, while muscle strength and spatial memory are spared. These findings are consistent with the poly-GA pathology found exclusively in spinal cord, brainstem and cerebellum.

## Discussion

We generated the first germline transgenic mouse model of pure DPR pathology without  $(\text{ggggcc})_n$  repeat RNA

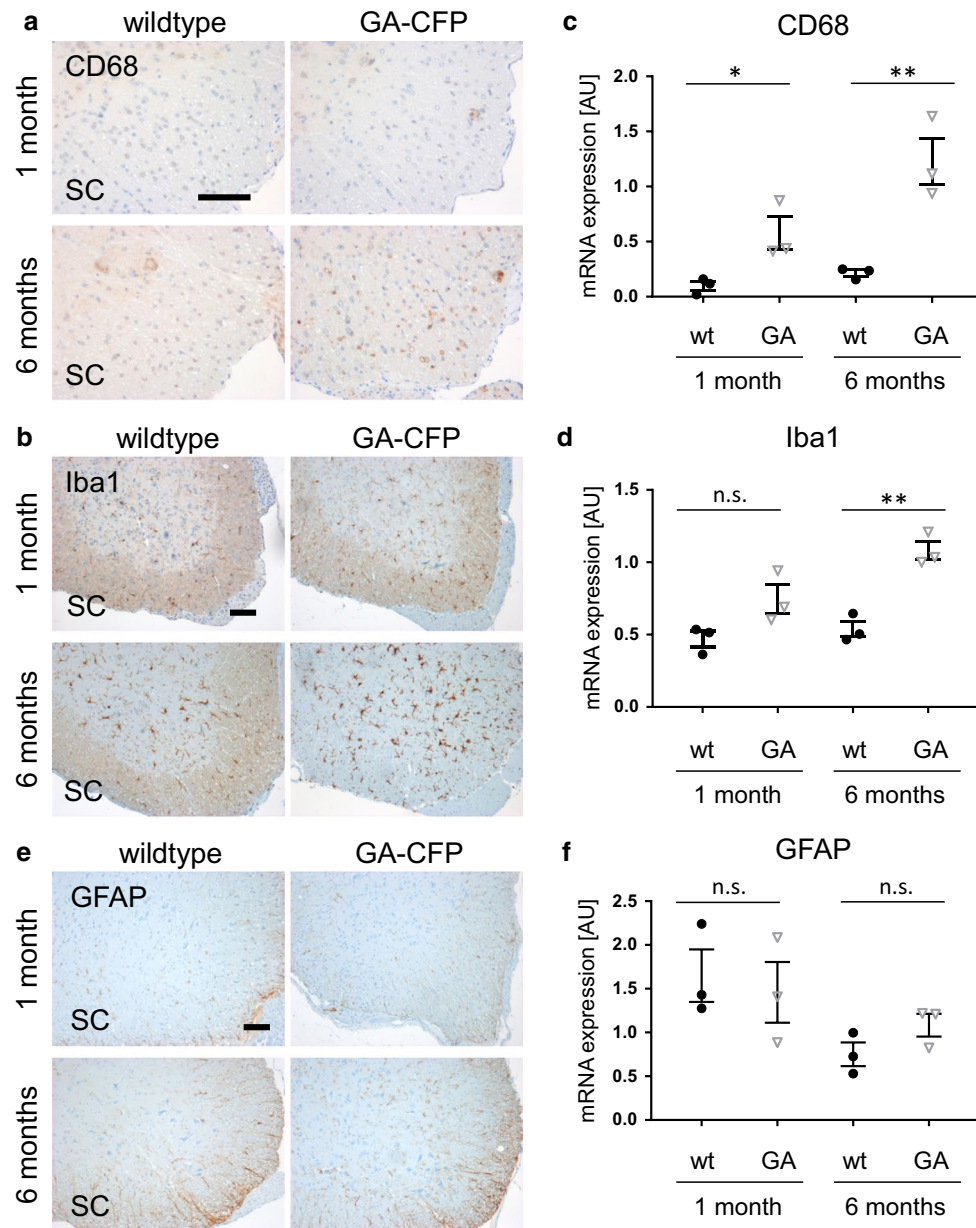


**Fig. 4** Activation of phagocytic microglia in GA-CFP mice. **a, b, e** Immunohistochemistry of 1- and 6-month-old mice shows microglia activation detected by the markers CD68 and Iba1 in the spinal cord (SC) of 6-month-old GA-CFP mice compared to wildtype mice in the anterior horn of the spinal cord. No clear difference was observed for the astrocyte marker GFAP. Scale bars represent 100  $\mu\text{m}$ . **c, d, f** Quantitative RT-PCR shows increased mRNA expression of CD68 and Iba1 but not GFAP in 6-month-old GA-CFP mice compared to

1-month-old GA-CFP mice and controls. Expression was normalized to GAPDH and  $\beta$ -actin using the  $\Delta\Delta Ct$  method.  $n_{(\text{wt})} = 3$ ;  $n_{(\text{GA-CFP})} = 3$ ; Statistical analyses were performed by an unpaired  $t$  test (two-tailed;  $\text{CD68}_{1\text{-month}} t = 3.079$ ,  $df = 4$ ;  $\text{Iba1}_{1\text{-month}} t = 2.385$ ,  $df = 4$ ;  $\text{GFAP}_{1\text{-month}} t = 0.4147$ ,  $df = 4$ ;  $\text{CD68}_{6\text{-months}} t = 4.805$ ,  $df = 4$ ;  $\text{Iba1}_{6\text{-months}} t = 6.399$ ,  $df = 4$ ;  $\text{GFAP}_{6\text{-months}} t = 1.771$ ,  $df = 4$ ) and data are shown as mean  $\pm$  SEM; \* $p < 0.05$ ; \*\* $p < 0.01$ , *ns* not significant

and analyzed the contribution of poly-GA to *C9orf72* ALS/FTD pathophysiology. We show that chronic accumulation of poly-GA proteins in the spinal cord, brain stem and deep cerebellar nuclei in GA-CFP mice results in progressive gait and balance impairment. These deficits

are associated with the sequestration of p62, Rad23b and the chaperone-associated protein Mif2. Accompanying regional microglia activation and modest TDP-43 phosphorylation suggest that poly-GA inclusions impair neuronal function prior to neuron loss in *C9orf72* ALS/FTD.

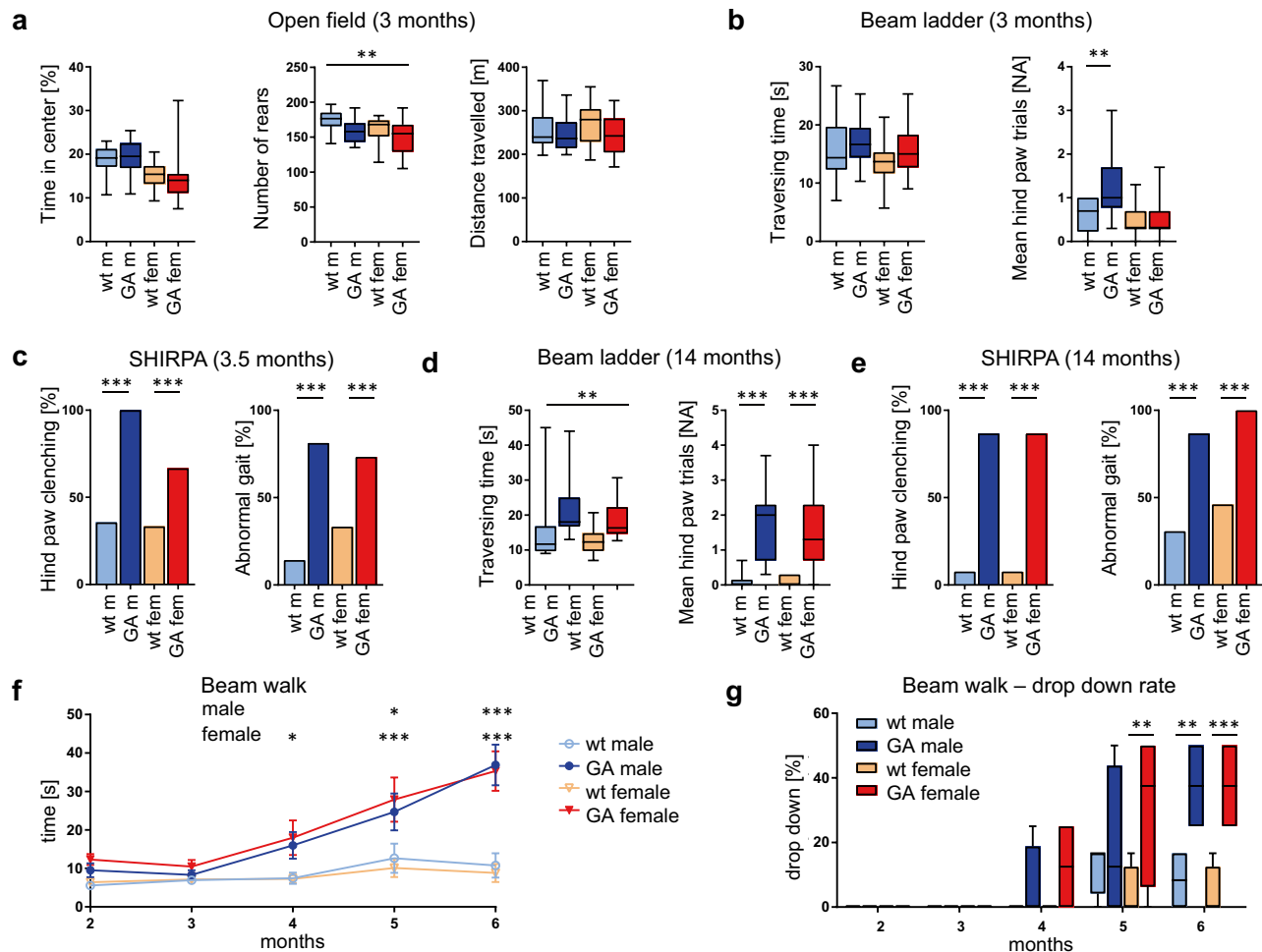


**Fig. 5** GA-CFP mice are less active and develop balancing deficits. **a–e** Neurological and behavioral analysis of GA-CFP and wildtype (wt) littermates at 3–4 months (**a–c**) and 14 months of age (**d, e**). **a** Open field analysis at 3 months. Automated analysis of the time spent in the center, the rearing activity (total count) and the total distance traveled within 20 min for the different genotypes and genders. **b** Beam ladder with irregular step distance. Automated analysis of average time needed to cross the ladder and the number of hind paw slips at the age of 4 months. **c** Gait analysis according to the SHIRPA protocol. Fraction of mice showing hindlimb clenching and abnormal gait is shown (at the age of 3.5 months).  $n_{(GA-CFP\ male)} = 16$ ;  $n_{(GA-CFP\ female)} = 15$ ;  $n_{(wt\ male)} = 14$ ;  $n_{(wt\ female)} = 15$  for all tests at 3 months of age. **d, e** Repetition of the beam ladder and SHIRPA analysis of GA-CFP and wildtype (wt) littermates at 14 months of age.  $n_{(GA-CFP\ male)} = 15$ ;  $n_{(GA-CFP\ female)} = 15$ ;  $n_{(wt\ male)} = 13$ ;  $n_{(wt\ female)} = 13$ . **f, g** Longitudinal analysis using a balance beam. GA-CFP males

and females take more time to cross the beam and fall more often than wildtype mice starting at 4 months.  $n_{(GA-CFP\ male)} = 4$ ;  $n_{(GA-CFP\ female)} = 4$ ;  $n_{(wt\ male)} = 6$ ;  $n_{(wt\ female)} = 6$ . Statistical analysis of open field and beam ladder assay was performed by a two-way ANOVA between sex and genotype followed by Bonferroni post hoc test. Statistical analysis of the beam walk was performed by a two-way ANOVA between time and genotype for each sex followed by Bonferroni post hoc test. Asterisks for open field analysis and beam ladder traversing time depict significance of genotype effects [open field  $F(1, 56) = 7.579$ ; beam ladder traversing time  $F(1, 52) = 10.2$ ]. Asterisks for beam ladder hind paw trials, SHIRPA and beam walk depict significance of genotype and sex-dependent effects (Bonferroni). Statistical analysis of hind paw clenching and gait was performed by a Chi-square test. Data are shown as box plot with whiskers at the 1st and 99th percentile (**a–e, g**) or as mean  $\pm$  SEM (**f**); \* $p < 0.05$ ; \*\* $p < 0.01$ ; \*\*\* $p < 0.001$

### GA-CFP mice model pure poly-GA pathology

The *Thy1*-driven GA-CFP mice express poly-GA proteins at levels roughly similar to human *C9orf72* ALS/FTD patients although with a different regional expression pattern. GA-CFP mice develop poly-GA pathology in motoneurons and other neurons of the spinal cord and brain stem

and in deep cerebellar nuclei. In patients, poly-GA inclusions are found in the spinal cord, including motoneurons, but they are much more frequent in the neocortex, hippocampus, thalamus and cerebellum [20, 23, 31]. This has led to speculations that spinal cord motoneurons in patients may be particularly vulnerable to DPR protein expression. However, expression of poly-GA in GA-CFP mice does not



cause a rapid loss of motoneurons. Our data indicate that poly-GA aggregates in neurons of the motor system disturb normal neuronal function in the absence of overt neuron loss, for example, by sequestration of cellular proteins.

We observed co-aggregation of poly-GA with p62 and Rad23 as reported previously [21, 23, 37]. For unknown reasons we did not detect sequestration of Unc119 into poly-GA inclusions in GA-CFP mice, which we had initially discovered in rat primary neurons and confirmed in *C9orf72* patients [21, 31]. Furthermore, we discovered that the chaperone-associated protein Mif2 co-aggregates with half of the poly-GA inclusions in the spinal cord of GA-CFP mice, but only in 0.3–2.7% of the poly-GA inclusions in the cortex of *C9orf72* ALS/FTD patients. The differential co-aggregation of Mif2 and Unc119 in GA-CFP mice and *C9orf72* cases highlights the importance of validating data from all model systems in patient tissue. The unexpected co-aggregation of Mif2 and phospho-TDP-43 in *C9orf72* patients needs to be investigated further. While the drosophila homolog of Mif2 has been shown to co-aggregate with poly-Q and modulate its toxicity in a Huntington's disease model [16, 18], preliminary experiments in rat primary neuron culture did not show clear effects of Mif2 on poly-GA toxicity (data not shown).

Consistent with cellular models [21, 38], poly-GA expression by itself did not induce visible TDP-43 inclusions. However, we did notice increased levels of phosphorylated TDP-43 in the urea-soluble fraction, indicating that poly-GA may contribute to the onset of TDP-43 pathology. Similarly, in an AAV-based model with much higher GFP-(GA)<sub>50</sub> expression, only very few TDP-43 aggregates were detected [37]. While *C9orf72* patients show robust astrogliosis and microgliosis, the BAC transgenic and poly-GA expressing mice showed variable extent of astrocyte and microglia activation [15, 19, 26, 37]. The strong activation of microglia in the spinal cord of our GA-CFP mice may be due to neuronal dysfunction alarming microglia, extracellular release of poly-GA aggregates [35] or low levels of neurodegeneration not detected by our quantitative analysis. In ALS patients, microglia activation correlates with disease progression, and *C9orf72* carriers show higher microglia activation than non-carriers [4].

### Motor deficits in GA-CFP mice

So far, no transgenic *C9orf72* model has robustly replicated the full complement of ALS and/or FTD phenotypes in animals. BAC transgenic mice with human-like *C9orf72* expression levels show variable phenotypes and cannot differentiate between RNA and DPR toxicity [13]. Mice overexpressing poly-GA using AAV show signs of impaired nucleocytoplasmic transport and sequestration of Rad23b by poly-GA inclusions in the cortex [37]. Motor

and balance deficits in these mice were attributed to the cerebellar poly-GA aggregation and neuron loss, because these mice rarely showed poly-GA inclusions in the spinal cord. In contrast, the motor system is directly affected in our transgenic GA-CFP mice. The motor phenotype of GA-CFP mice is consistent with the predominant expression of poly-GA in spinal cord and brain stem. Poly-GA inclusions in the deep cerebellar nuclei may further contribute to this phenotype. The impaired acoustic startle response and its prepulse inhibition, together with the distribution of poly-GA inclusions in the brainstem, suggest that poly-GA inhibits activity of this complex circuit involving the brain stem [8, 36]. However, we cannot retrospectively exclude that early deafness may have affected these measurement in GA-CFP mice, because C57BL/6 mice commonly develop hearing loss at 3–6 months. By 14 months all female mice were deaf, while male GA-CFP mice were more severely affected than controls (data not shown).

The most prominent phenotype of GA-CFP mice, however, is their impaired balance and gait, which particularly affected the hind limbs. This is consistent with the widespread poly-GA pathology in the lumbar segments both in motoneurons and laminae IV, V and VI neurons implicated in proprioception. At 4 months of age, male mice slip more often with their hind paws on the beam ladder and show decreased rearing activity in the open field arena indicating deficits in motor control, which requires cortical input and proper function of the spinal cord circuits. Both male and female GA-CFP mice show enhanced hind limb clenching and an abnormal gait as well as progressive impairment on the balance beam starting at 3–4 months of age. Normal grip strength and endurance in the rotarod corroborates the absence of overt motoneuron loss and suggests poly-GA disturbs proper neuronal function and thus impairs coordination and motor control.

### Summary

In patients, expression of poly-GA and the other DPR species correlates poorly with regional neuron loss [20, 31] and DPR pathology precedes overt ALS/FTD symptoms by many years [2, 27]. Our findings suggest that poly-GA-induced protein sequestration and regional microglia activation may be responsible for the prodromal cognitive deficits observed prior to complete ALS/FTD symptoms in *C9orf72* mutation carriers [29]. Combined chronic DPR and RNA toxicity likely trigger the second disease stage with TDP-43 pathology and overt neuron loss [7]. Finally, GA-CFP mice are a good model to test poly-GA-based therapeutic approaches, because motor deficits appear early and homogeneously in all animals.

**Acknowledgements** We thank M. K. Schmidt, B. Kraft, I. Pigur, I. Brandstetter and E. Graf for excellent technical assistance and A. Flately and R. Feederle for purified poly-GA antibodies. We thank G. Kleinberger, K. LaClair and B. Schmid for critical comments to the manuscript. We thank F. Bareyre for providing the Thy1.2 empty vector. This work was supported by NOMIS foundation and the Hans und Ilse Breuer Foundation (D.E.), the Munich Cluster of Systems Neurology (SyNergy) (M.H.S., L.D., Q.Z., J.W., W.W., T.K. and D.E.), the European Community's Health Seventh Framework Programme under Grant Agreement 617198 [DPR-MODELS] (D.E.), the National Institutes of Health (NIH)/National Institute of Neurological Disorders and Stroke [P01NS084974 (L.P.); R01 NS093865-01 (L.P.)]; the ALS Association (T.F.G., L.P.), and the Muscular Dystrophy Association (T.F.G., L.P.) and by the German Federal Ministry of Education and Research (Infrafrontier Grant 01KX1012) (M.HdA.).

**Author contributions** MHS performed biochemical, pathological and neurological analysis. FS, BP, LD, AvT, JT, BS and MD contributed to the mouse phenotyping and study design. LB, LG, SMH, WW, VG-D, HF, MHDa designed, performed and supervised neurological and behavioral experiments at the German Mouse Clinic. TG and LP performed ELISA analysis of mouse tissue. BMS, QZ, KR, SM, MM and DE contributed to cell biological experiments and mouse generation. TMS, JW and DE analyzed the transgene integration site. TA supervised neuropathological analysis and provided human tissue. MHS, TK, TA and DE designed the project. DE and MHS wrote the manuscript with input from all coauthors.

**Open Access** This article is distributed under the terms of the Creative Commons Attribution 4.0 International License (<http://creativecommons.org/licenses/by/4.0/>), which permits unrestricted use, distribution, and reproduction in any medium, provided you give appropriate credit to the original author(s) and the source, provide a link to the Creative Commons license, and indicate if changes were made.

## References

- Ash PE, Bieniek KF, Gendron TF, Caulfield T, Lin WL, DeJesus-Hernandez M, van Blitterswijk MM, Jansen-West K, Paul JW 3rd, Rademakers R et al (2013) Unconventional translation of C9ORF72 GGGGCC expansion generates insoluble polypeptides specific to c9FTD/ALS. *Neuron* 77:639–646. doi:10.1016/j.neuron.2013.02.004
- Baborie A, Griffiths TD, Jaros E, Perry R, McKeith IG, Burn DJ, Masuda-Suzukake M, Hasegawa M, Rollinson S, Pickering-Brown S et al (2014) Accumulation of dipeptide repeat proteins predates that of TDP-43 in frontotemporal lobar degeneration associated with hexanucleotide repeat expansions in C9ORF72 gene. *Neuropathol Appl Neurobiol*. doi:10.1111/nan.12178
- Barnes CA (1979) Memory deficits associated with senescence: a neurophysiological and behavioral study in the rat. *J Comp Physiol Psychol* 93:74–104
- Brettschneider J, Toledo JB, Van Deerlin VM, Elman L, McCluskey L, Lee VM, Trojanowski JQ (2012) Microglial activation correlates with disease progression and upper motor neuron clinical symptoms in amyotrophic lateral sclerosis. *PLoS One* 7:e39216. doi:10.1371/journal.pone.0039216
- Chew J, Gendron TF, Prudencio M, Sasaguri H, Zhang YJ, Castanedes-Casey M, Lee CW, Jansen-West K, Kurti A, Murray ME et al (2015) Neurodegeneration. C9ORF72 repeat expansions in mice cause TDP-43 pathology, neuronal loss, and behavioral deficits. *Science* 348:1151–1154. doi:10.1126/science.1229344
- DeJesus-Hernandez M, Mackenzie IR, Boeve BF, Boxer AL, Baker M, Rutherford NJ, Nicholson AM, Finch NA, Flynn H, Adamson J et al (2011) Expanded GGGGCC hexanucleotide repeat in noncoding region of C9ORF72 causes chromosome 9p-linked FTD and ALS. *Neuron* 72:245–256. doi:10.1016/j.neuron.2011.09.011
- Edbauer D, Haass C (2016) An amyloid-like cascade hypothesis for C9orf72 ALS/FTD. *Curr Opin Neurobiol* 36:99–106. doi:10.1016/j.conb.2015.10.009
- Fendt M, Li L, Yeomans JS (2001) Brain stem circuits mediating prepulse inhibition of the startle reflex. *Psychopharmacology* 156:216–224
- Feng G, Mellor RH, Bernstein M, Keller-Peck C, Nguyen QT, Wallace M, Nerbonne JM, Lichtman JW, Sanes JR (2000) Imaging neuronal subsets in transgenic mice expressing multiple spectral variants of GFP. *Neuron* 28:41–51
- Fleck D, van Bebber F, Colombo A, Galante C, Schwenk BM, Rabe L, Hampel H, Novak B, Kremmer E, Tahirovic S et al (2013) Dual cleavage of neuregulin 1 type III by BACE1 and ADAM17 liberates its EGF-like domain and allows paracrine signaling. *J Neurosci* 33:7856–7869. doi:10.1523/JNEUROSCI.3372-12.2013
- Fuchs H, Gailus-Durner V, Adler T, Aguilar-Pimentel JA, Becker L, Calzada-Wack J, Da Silva-Buttkus P, Neff F, Gotz A, Hans W et al (2011) Mouse phenotyping. *Methods* 53:120–135. doi:10.1016/j.ymeth.2010.08.006
- Garrett L, Lie DC, Hrabe de Angelis M, Wurst W, Holter SM (2012) Voluntary wheel running in mice increases the rate of neurogenesis without affecting anxiety-related behaviour in single tests. *BMC neuroscience* 13:61. doi:10.1186/1471-2202-13-61
- Hayes LR, Rothstein JD (2016) C9ORF72-ALS/FTD: transgenic mice make a come-BAC. *Neuron* 90:427–431. doi:10.1016/j.neuron.2016.04.026
- Holter SM, Stromberg M, Kovalenko M, Garrett L, Glasl L, Lopez E, Guide J, Gotz A, Hans W, Becker L et al (2013) A broad phenotypic screen identifies novel phenotypes driven by a single mutant allele in Huntington's disease CAG knock-in mice. *PLoS One* 8:e80923. doi:10.1371/journal.pone.0080923
- Jiang J, Zhu Q, Gendron TF, Saberi S, McAlonis-Downes M, Seelman A, Stauffer JE, Jafar-Nejad P, Drenner K, Schulte D et al (2016) Gain of toxicity from ALS/FTD-linked repeat expansions in C9ORF72 is alleviated by antisense oligonucleotides targeting GGGGCC-containing RNAs. *Neuron* 90:535–550. doi:10.1016/j.neuron.2016.04.006
- Kazemi-Esfarjani P, Benzer S (2002) Suppression of polyglutamine toxicity by a Drosophila homolog of myeloid leukemia factor 1. *Hum Mol Genet* 11:2657–2672
- Khosravi B, Hartmann H, May S, Mohl C, Ederle H, Michaelson M, Schludi MH, Dormann D, Edbauer D (2016) Cytoplasmic poly-GA aggregates impair nuclear import of TDP-43 in C9orf72 ALS/FTD. *Hum Mol Genet*. doi:10.1093/hmg/ddw432
- Kim WY, Fayazi Z, Bao X, Higgins D, Kazemi-Esfarjani P (2005) Evidence for sequestration of polyglutamine inclusions by Drosophila myeloid leukemia factor. *Mol Cell Neurosci* 29:536–544. doi:10.1016/j.mcn.2005.04.005
- Liu Y, Pattamatta A, Zu T, Reid T, Bardhi O, Borchelt DR, Yachnis AT, Ranum LP (2016) C9orf72 BAC mouse model with motor deficits and neurodegenerative features of ALS/FTD. *Neuron* 90:521–534. doi:10.1016/j.neuron.2016.04.005
- Mackenzie IR, Arzberger T, Kremmer E, Troost D, Lorenzl S, Mori K, Weng SM, Haass C, Kretschmar HA, Edbauer D et al (2013) Dipeptide repeat protein pathology in C9ORF72 mutation

- cases: clinico-pathological correlations. *Acta Neuropathol* 126:859–879. doi:[10.1007/s00401-013-1181-y](https://doi.org/10.1007/s00401-013-1181-y)
21. May S, Hornburg D, Schludi MH, Arzberger T, Rentzsch K, Schwenk BM, Grasser FA, Mori K, Kremmer E, Banzhaf-Strathmann J et al (2014) C9orf72 FTL/ALS-associated Gly-Ala dipeptide repeat proteins cause neuronal toxicity and Unc119 sequestration. *Acta Neuropathol* 128:485–503. doi:[10.1007/s00401-014-1329-4](https://doi.org/10.1007/s00401-014-1329-4)
  22. Mori K, Arzberger T, Grasser FA, Gijssels I, May S, Rentzsch K, Weng SM, Schludi MH, van der Zee J, Cruts M et al (2013) Bidirectional transcripts of the expanded C9orf72 hexanucleotide repeat are translated into aggregating dipeptide repeat proteins. *Acta Neuropathol* 126:881–893. doi:[10.1007/s00401-013-1189-3](https://doi.org/10.1007/s00401-013-1189-3)
  23. Mori K, Weng SM, Arzberger T, May S, Rentzsch K, Kremmer E, Schmid B, Kretschmar HA, Cruts M, Van Broeckhoven C et al (2013) The C9orf72 GGGGCC repeat is translated into aggregating dipeptide-repeat proteins in FTL/ALS. *Science* 339:1335–1338. doi:[10.1126/science.1232927](https://doi.org/10.1126/science.1232927)
  24. O'Rourke JG, Bogdanik L, Muhammad AK, Gendron TF, Kim KJ, Austin A, Cady J, Liu EY, Zarrow J, Grant S et al (2015) C9orf72 BAC transgenic mice display typical pathologic features of ALS/FTD. *Neuron* 88:892–901. doi:[10.1016/j.neuron.2015.10.027](https://doi.org/10.1016/j.neuron.2015.10.027)
  25. O'Rourke JG, Bogdanik L, Yanez A, Lall D, Wolf AJ, Muhammad AK, Ho R, Carmona S, Vit JP, Zarrow J et al (2016) C9orf72 is required for proper macrophage and microglial function in mice. *Science* 351:1324–1329. doi:[10.1126/science.aaf1064](https://doi.org/10.1126/science.aaf1064)
  26. Peters OM, Cabrera GT, Tran H, Gendron TF, McKeon JE, Metterville J, Weiss A, Wightman N, Salameh J, Kim J et al (2015) Human C9ORF72 hexanucleotide expansion reproduces RNA foci and dipeptide repeat proteins but not neurodegeneration in BAC transgenic mice. *Neuron* 88:902–909. doi:[10.1016/j.neuron.2015.11.018](https://doi.org/10.1016/j.neuron.2015.11.018)
  27. Proudfoot M, Gutowski NJ, Edbauer D, Hilton DA, Stephens M, Rankin J, Mackenzie IR (2014) Early dipeptide repeat pathology in a frontotemporal dementia kindred with C9ORF72 mutation and intellectual disability. *Acta Neuropathol* 127:451–458. doi:[10.1007/s00401-014-1245-7](https://doi.org/10.1007/s00401-014-1245-7)
  28. Renton AE, Majounie E, Waite A, Simon-Sanchez J, Rollinson S, Gibbs JR, Schymick JC, Laaksovirta H, van Swieten JC, Myllykangas L et al (2011) A hexanucleotide repeat expansion in C9ORF72 is the cause of chromosome 9p21-linked ALS-FTD. *Neuron* 72:257–268. doi:[10.1016/j.neuron.2011.09.010](https://doi.org/10.1016/j.neuron.2011.09.010)
  29. Rohrer JD, Nicholas JM, Cash DM, van Swieten J, Dopper E, Jiskoot L, van Minkelen R, Rombouts SA, Cardoso MJ, Clegg S et al (2015) Presymptomatic cognitive and neuroanatomical changes in genetic frontotemporal dementia in the Genetic Frontotemporal dementia Initiative (GENFI) study: a cross-sectional analysis. *Lancet Neurol* 14:253–262. doi:[10.1016/S1474-4422\(14\)70324-2](https://doi.org/10.1016/S1474-4422(14)70324-2)
  30. Saarikangas J, Kourdougli N, Senju Y, Chazal G, Segerstrale M, Minkevičienė R, Kuurne J, Mattila PK, Garrett L, Holter SM et al (2015) MIM-induced membrane bending promotes dendritic spine initiation. *Dev Cell* 33:644–659. doi:[10.1016/j.devcel.2015.04.014](https://doi.org/10.1016/j.devcel.2015.04.014)
  31. Schludi MH, May S, Grasser FA, Rentzsch K, Kremmer E, Kupper C, T. K, Degeneration GCfFL, Alliance BBB, Arzberger T et al (2015) Distribution of dipeptide repeat proteins in cellular models and C9orf72 mutation cases suggests link to transcriptional silencing. *Acta Neuropathol* 130:537–555. doi:[10.1007/s00401-015-1450-z](https://doi.org/10.1007/s00401-015-1450-z)
  32. Schwenk BM, Lang CM, Hög S, Tahirovic S, Orozco D, Rentzsch K, Lichtenthaler SF, Hoogenraad CC, Capell A, Haass C et al (2014) The FTL risk factor TMEM106B and MAP6 control dendritic trafficking of lysosomes. *EMBO J* 33:450–467. doi:[10.1002/embj.201385857](https://doi.org/10.1002/embj.201385857)
  33. Thorvaldsdóttir H, Robinson JT, Mesirov JP (2013) Integrative Genomics Viewer (IGV): high-performance genomics data visualization and exploration. *Brief Bioinform* 14:178–192. doi:[10.1093/bib/bbs017](https://doi.org/10.1093/bib/bbs017)
  34. Tran H, Almeida S, Moore J, Gendron TF, Chalasani U, Lu Y, Du X, Nickerson JA, Petrucelli L, Weng Z et al (2015) Differential toxicity of nuclear RNA foci versus dipeptide repeat proteins in a Drosophila model of C9ORF72 FTD/ALS. *Neuron* 87:1207–1214. doi:[10.1016/j.neuron.2015.09.015](https://doi.org/10.1016/j.neuron.2015.09.015)
  35. Westergard T, Jensen BK, Wen X, Cai J, Kropf E, Iacovitti L, Pasinelli P, Trotti D (2016) Cell-to-cell transmission of dipeptide repeat proteins linked to C9orf72-ALS/FTD. *Cell Rep* 17:645–652. doi:[10.1016/j.celrep.2016.09.032](https://doi.org/10.1016/j.celrep.2016.09.032)
  36. Yeomans JS, Frankland PW (1995) The acoustic startle reflex: neurons and connections. *Brain Res Brain Res Rev* 21:301–314
  37. Zhang YJ, Gendron TF, Grima JC, Sasaguri H, Jansen-West K, Xu YF, Katzman RB, Gass J, Murray ME, Shinohara M et al (2016) C9ORF72 poly(GA) aggregates sequester and impair HR23 and nucleocytoplasmic transport proteins. *Nat Neurosci* 19:668–677. doi:[10.1038/nn.4272](https://doi.org/10.1038/nn.4272)
  38. Zhang YJ, Jansen-West K, Xu YF, Gendron TF, Bieniek KF, Lin WL, Sasaguri H, Caulfield T, Hubbard J, Daugherty L et al (2014) Aggregation-prone c9FTD/ALS poly(GA) RAN-translated proteins cause neurotoxicity by inducing ER stress. *Acta Neuropathol* 128:505–524. doi:[10.1007/s00401-014-1336-5](https://doi.org/10.1007/s00401-014-1336-5)
  39. Zimprich A, Garrett L, Deussing JM, Wotjak CT, Fuchs H, Gailus-Durner V, de Angelis MH, Wurst W, Holter SM (2014) A robust and reliable non-invasive test for stress responsiveness in mice. *Front Behav Neurosci* 8:125. doi:[10.3389/fnbeh.2014.00125](https://doi.org/10.3389/fnbeh.2014.00125)
  40. Zu T, Liu Y, Banez-Coronel M, Reid T, Pletnikova O, Lewis J, Miller TM, Harms MB, Falchook AE, Subramony SH et al (2013) RAN proteins and RNA foci from antisense transcripts in C9ORF72 ALS and frontotemporal dementia. *Proc Natl Acad Sci USA* 110:E4968–E4977. doi:[10.1073/pnas.1315438110](https://doi.org/10.1073/pnas.1315438110)

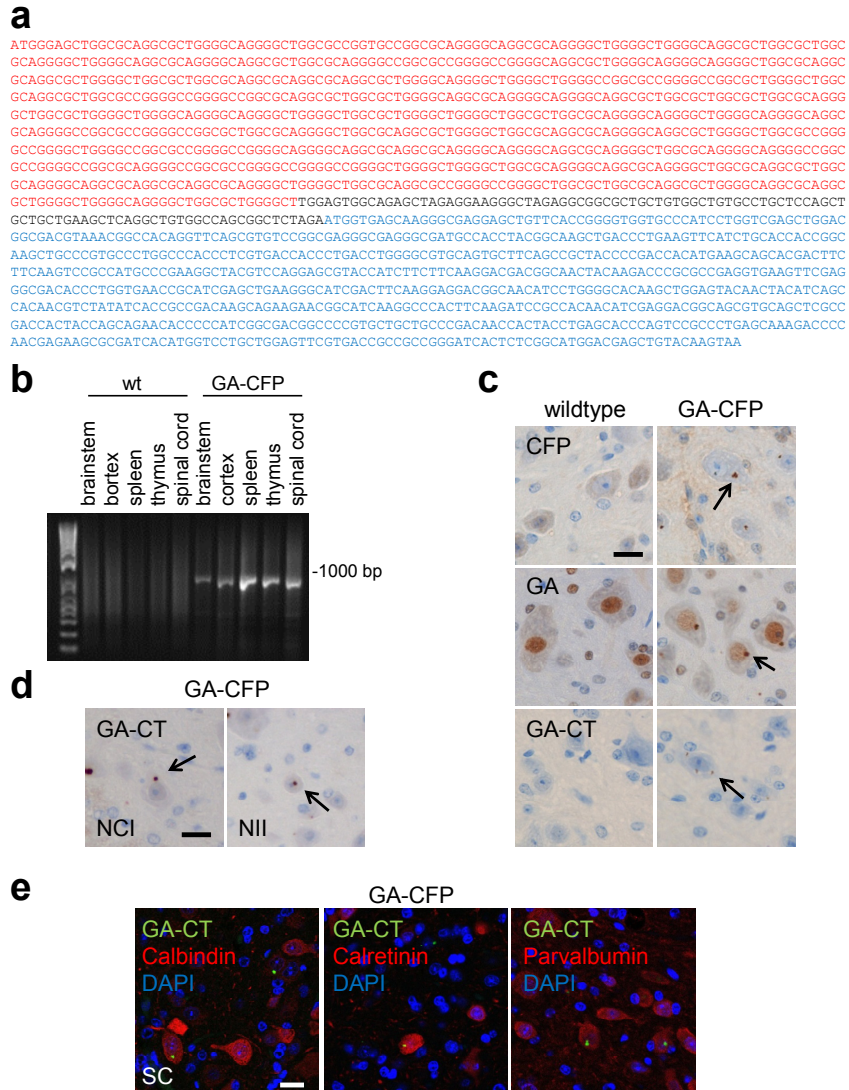


**Figure S1: Transgenic mice show germline transmission of a GA-CFP construct**

**(a)** Coding sequence of the transgene expressing (GA)<sub>149</sub>-CFP. The poly-GA sequence with strongly reduced ggggcc content (red), the C-terminal tail (CT) expressed from the endogenous *C9orf72* repeat locus in the poly-GA reading frame (black) and CFP (blue). **(b)** In GA-CFP transgenic mice the full length poly-GA sequence is detectable in genomic DNA extracted from brainstem, cortex, spleen, thymus and spinal cord. **(c)** Immunohistochemical staining of the spinal cord for CFP, GA (5F2-HRP) and the C-terminal tail GA-CT (5C3) in GA-CFP mice (right column) and wildtype mice (left column) at 6 months of age. **(d)** Poly-GA forms predominantly neuronal cytoplasmic inclusions (NCI) and rarely neuronal intranuclear inclusions (NII). **(e)** Double immunofluorescence staining shows poly-GA inclusions in calbindin, calretinin and parvalbumin positive neurons in the spinal cord (SC). Scale bars represent 20  $\mu\text{m}$ .

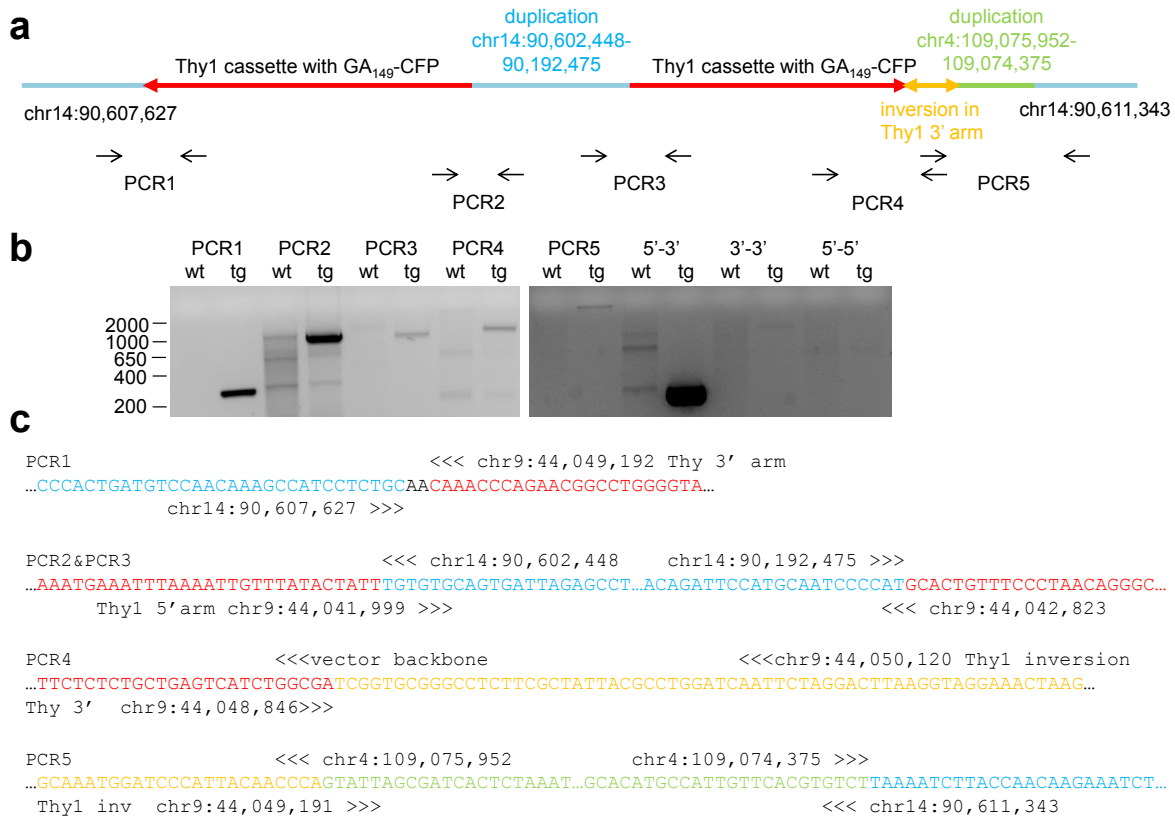


**Figure S2: Thy1 cassette is integrated at an intergenic site on chromosome 14**

**(A)** Schema of the transgene integration on chromosome 14. Whole genome sequencing at ~100x coverage revealed integration of two blocks of tandem repeats of the transgene integrated in chromosome 14 at position 90,607,627-90,611,343 leading to a 3716bp intergenic deletion about 330 kb downstream of the nearest transcript a long non-coding RNA (4930474H2ORik). The integration involves duplication of a 410kb stretch of chromosome 14 (including the 3' part of 4930474H2ORik without the promoter region) and a 1577 nucleotide stretch from chromosome 4 (intronic region of *Ospbl9*). All genome coordinates are based on the GRC38/mm10 mouse genome assembly. Coordinates for the Thy1 cassette correspond to the genomic numbering of the endogenous mouse Thy1 locus on chromosome 9, spanning chr9:44,041,811-44,045,981 (5' arm) and chr9:44,047,482-44,050,120 (3' arm) in the transgene vector. The increased sequence coverage in that region suggests that at least 10 copies of the transgene are integrated in the block. The 3' arm of the distal Thy1 cassette fused to the chromosome 4 duplication contains a 969 nucleotide inversion. Arrows indicate primers used for PCR validation. Primer sequences PCR1 (cctcccaccactcaatgag, tgggctggagtacgaaacat), PCR2 (aggctctaatacactgcacaca, cctggctgtttctgcttcc), PCR3 (acctatgatatttctagatgca, cctggctgtttctgcttcc), PCR4 (aattaccaccactcgctccc, attccttgcctcctgtctc),

PCR5 (tcatctgttgtaaaaggcca, gggagcgagtgggtgtaatt). Not drawn to scale. **(B)** Genomic PCR from wildtype and transgenic littermates confirms integration and chromosomal rearrangement. Bands specific to GA-CFP mice were excised and sequenced. To analyze tandem inserts we additionally used primers facing outside of the Thy1 cassette (5'-3' tcgttcactgtccttattctctc, gtcaggcttgctgtagg; 3'-3' tcgttcactgtccttattctctc; 5'-5' gtcaggcttgctgtagg) confirming the presence of head to tail tandem repeats. Other tandem orientations containing larger 5' or 3' deletions of the transgene cassette may exist. **(C)** Sequence at the chromosomal rearrangements involving the Thy1 cassette based on Sanger sequencing of the PCR products from (B).

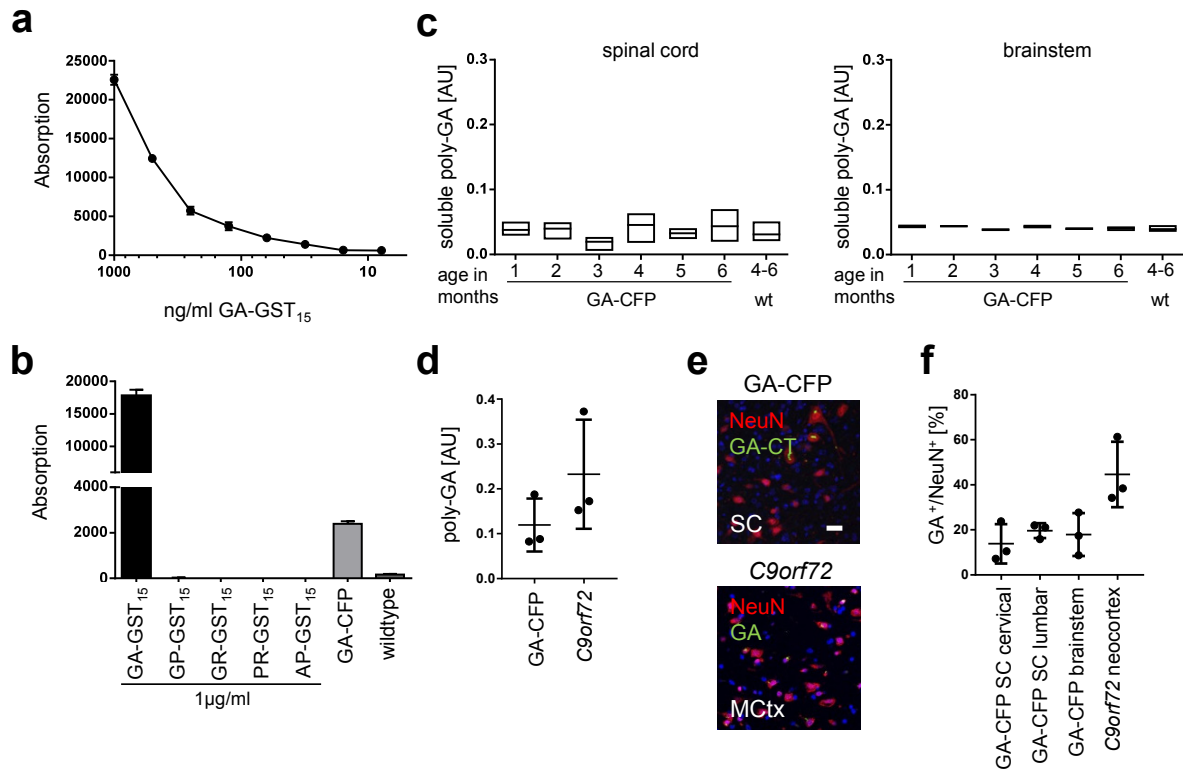


**Figure S3: Comparison of poly-GA in GA-CFP spinal cord and *C9orf72* ALS/FTD patient neocortex**

**(a)** Poly-GA sandwich immunoassay using biotinylated and sulfo-tagged  $\alpha$ -GA 5F2 antibody shows the detection limit on recombinant GST-GA<sub>15</sub>. **(b)** Anti-GA immunoassay specifically detects GST-GA<sub>15</sub> and RIPA-insoluble poly-GA in the spinal cord of a GA-CFP mouse. No signal was detected for other DPR antigens or in wildtype mice. Mean + SEM. **(c)** poly-GA immunoassay from the RIPA-soluble fraction of spinal cord (SC) and brainstem (BS) of 1 to 6 months old GA-CFP mice ( $n = 3$  mice per time-point; measured in duplicates, box plot shows minimum, mean and maximum) detects no poly-GA signal above background. Compare data from RIPA-insoluble fraction in Figs. 2d/e. AU = arbitrary unit. **(d)** Poly-GA protein levels in the RIPA-insoluble fraction of the spinal cord of 4-6 months-old GA-CFP mice are not grossly higher than in the motor cortex of *C9orf72* mutation carriers. All tissues were analyzed in parallel following the same extraction protocol. Mean, minimum and maximum are shown. Due to the high variability of poly-GA pathology in *C9orf72* patients and the small cohort size we did not perform statistical analysis. Mean  $\pm$  SD. **(e, f)** Double immunofluorescence with the neuronal marker NeuN shows that neuronal poly-GA inclusions are less common in the spinal cord and brainstem of 6-months-old GA-CFP mice than in the motor cortex of *C9orf72* patients.  $n_{\text{GA-CFP}} = 3$ ;  $n_{\text{C9orf72}} = 3$ ; For quantification 3-4 images ( $424.7 \times 424.7 \mu\text{m}^2$ ) were taken and the fraction of poly-GA inclusion bearing NeuN positive neurons were counted. Mean  $\pm$  SD. AU=arbitrary unit. Scale bar represents 20  $\mu\text{m}$ .

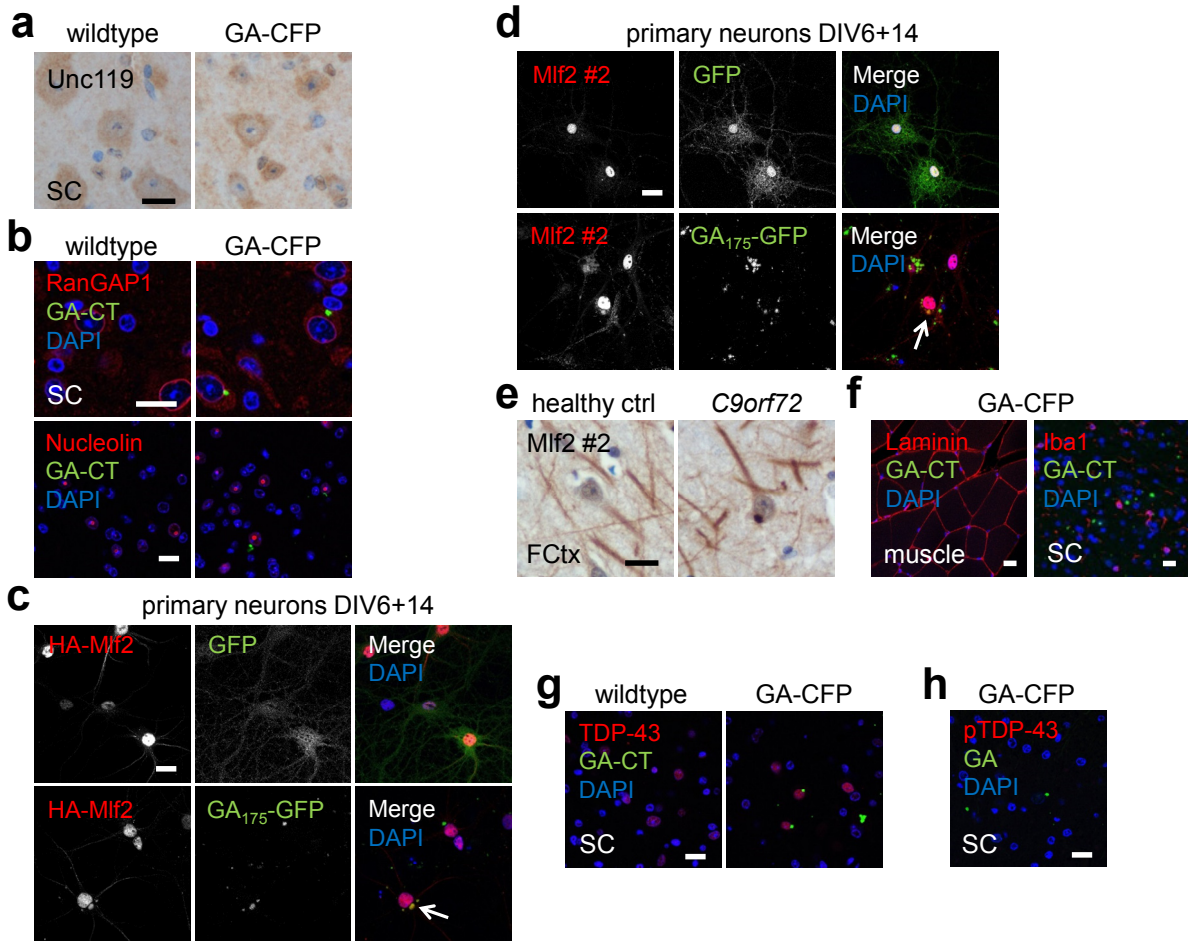


**Figure S4: poly-GA does not affect TDP-43, RanGAP1 and nucleolin but is co-localized with Mlf2**

(a) Immunohistochemistry did not reveal Unc119 aggregates in the spinal cord (SC) of GA-CFP mice. (b) Immunofluorescence in 12 month-old GA-CFP mice shows similar RanGAP1 and nucleolin localization in GA-CFP mice and wildtype littermates. (c) Lentiviral co-transduction of HA-Mlf2 with either GA<sub>175</sub>-GFP or GFP control in primary hippocampal neurons of wildtype rats at 6 days *in vitro*. Immunofluorescence 14 days later (DIV6+14) detects specific co-localization of HA-Mlf2 with GA<sub>175</sub>-GFP. (d) Mlf2 immunostaining in rat primary hippocampal transduced with GA<sub>175</sub>-GFP or GFP detects specific co-localization of endogenous Mlf2 with GA<sub>175</sub>-GFP (arrow). (e) Immunohistochemistry using a second Mlf2 antibody (compare Figs. 2c,d) detects specific Mlf2 aggregates in the frontal cortex (FCtx) of C9orf72 ALS/FTLD patients. No inclusions were detectable in healthy controls. Scale bar represents 20 μm. (f) Immunofluorescence staining showed no poly-GA aggregates in laminin-labeled muscle fibers (quadriceps femoris, left) or Iba1-positive microglial cells (spinal cord, right). (g, h) Immunofluorescence analysis did not reveal cytoplasmic mislocalisation of TDP-43 or phosphorylation at serine 409/410 in GA-CFP mice. Scale bars represent 20 μm.



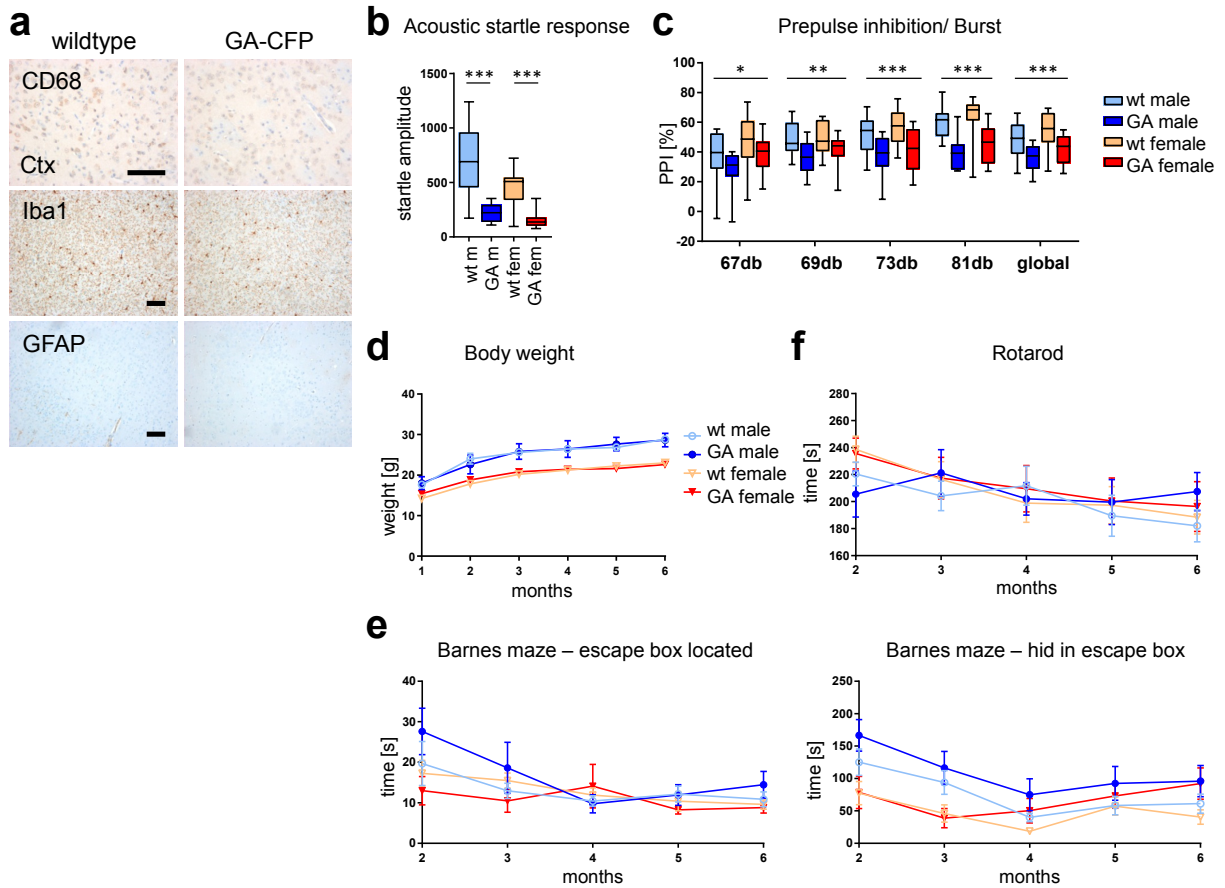


**Figure S5: GA-CFP mice show no microglia activation in the neocortex, normal spatial memory, but impaired prepulse inhibition**

**(a)** Immunohistochemistry of neocortex shows comparable levels of CD68, Iba1 and GFAP in GA-CFP and control mice at 6 months of age. Scale bars represent 100 $\mu$ m. **(b, c)** Neurological analysis of GA-CFP and wildtype littermates at 3-4 months of age. Box plot with whiskers at 1<sup>st</sup> and 99<sup>th</sup> percentile.  $n_{(GA-CFP\ male)} = 16$ ;  $n_{(GA-CFP\ female)} = 15$ ;  $n_{(wt\ male)} = 14$ ;  $n_{(wt\ female)} = 15$ . Acoustic startle response **(b)** and its prepulse inhibition **(c)** are decreased in GA-CFP male and female mice at 13 weeks. Prepulse inhibition 67db F (1, 56) = 4.588; 69db F (1, 56) = 10.52; 73db F (1, 56) = 18.35; 81db F (1, 56) = 40.56; global db F (1, 56) = 21.39). Asterisks for prepulse inhibition depict significance of genotype, asterisks for acoustic startle depict significance of genotype and sex-dependent effects (Bonferroni). **(d-f)** Longitudinal analysis of body weight **(d)**, spatial memory **(e)** and motor performance **(f)** of GA-CFP mice and wildtype littermates. **(d)** No differences in the body weight were observed between transgenic and wildtype male and female mice from birth until the age of 6 months. **(e)** Spatial learning and long-term memory was normal in 2-6 months old transgenic or wildtype mice. Left panel shows the time needed to locate the escape box, the

right panel shows the time until the mice crawl into the escape box. **(f)** No differences in the rotarod performance of GA-CFP mice up to 6 month compared to wildtype mice. Statistical analysis of the body weight and Barnes maze was performed by a 2-way ANOVA between time and genotype for each sex followed by Bonferroni post hoc test.  $n_{(\text{GA-CFP male})} = 4$ ;  $n_{(\text{GA-CFP female})} = 4$ ;  $n_{(\text{wt male})} = 6$ ;  $n_{(\text{wt female})} = 6$ . Data are shown as mean  $\pm$  SEM; \* $p < 0.05$ ; \*\* $p < 0.01$ ; \*\*\* $p < 0.001$ .

**Table S1: Colocalization of poly-GA inclusions in GA-CFP mice**

Quantitative analysis of double immunofluorescence stainings from GA-CFP mice to address colocalization of poly-GA with p62 and RanGAP1 and mislocalization of total TDP-43 and TDP-43 phosphorylated at Ser409/410. Stainings were performed on spinal cord slices from three 12-month-old mice. Mean percentages  $\pm$  SD are shown.

Protein	counted GA aggregates	Mean $\pm$ SD
p62	110	94.55 $\pm$ 5.13 % colocalization
RanGAP1	112	0.00 % colocalization or mislocalization
TDP-43	123	0.00 % mislocalization
pTDP-43	117	0.00 % mislocalization

**Table S2: Colocalization of Mlf2 and poly-GA in *C9orf72* patients and GA-CFP mice**

Double immunostainings of Mlf2 and poly-GA in *C9orf72* patients and GA-CFP mice. The fraction of poly-GA inclusions containing Mlf2 was manually quantified in the indicated regions. Three *C9orf72* patients and three GA-CFP mice (12-month-old) were analyzed. Mean percentages  $\pm$  SD are shown.

Region	counted GA aggregates	% Mlf2
<i>C9orf72</i> FCtx	283	1.06 $\pm$ 1.08 %
<i>C9orf72</i> MCtx	162	0.62 $\pm$ 0.80 %
<i>C9orf72</i> OCtx	338	0.30 $\pm$ 0.35 %
<i>C9orf72</i> DG	677	2.66 $\pm$ 1.45 %
GA-CFP SC	116	55.17 $\pm$ 5.32 %

## **2.2 Contribution to the publication**

As first author of this publication, I had major contributions to the experimental work and study design. In detail, I performed all experiments shown in this publication except of the phospho-TDP-43 immunoassay in figure 3h, behavioral tests in figures 5a-e and S5b/c, genotyping in figure S1b, and the determination of the integration locus in figure S2.

## V. Acknowledgements

After 1511 days in the Eddie Lab, today is the day: writing this note of thanks to the people, who have helped and supported me in this period of my life, is the finishing touch on my dissertation. It was an intense period of learning in the scientific area, but also on a personal level.

*Prof. Dr. Dieter Edbauer (alias Eddie):* You are an excellent supervisor and supported me greatly in my work with much help and advice. Thank you very much for the opportunity to do my PhD thesis in your lab. I had a wonderful time in your lab, inclusive many interesting experiences and stories. “Everything is awesome!”

*Prof. Dr. Dr. h.c. Christian Haass:* Thank you very much for your scientific input and to be my official doctorate supervisor and chairman of my doctoral committee. You have a contagious scientific enthusiasm and always had a sympathetic ear for me.

*Dr. Thomas Arzberger:* Thank you very much, for being my neuropathology supervisor and that you always supported me patiently with your priceless knowledge of histology. Looking with you through the microscope was a great and instructive experience and you always gave me wise advices and helped my anytime.

Thanks to the members of my doctoral committee: The second reviewer of my thesis *Dr. Dorothee Dormann* and the other reviewers *Prof. Dr. Christian Behrends* and *PD. Dr. Florence Bareyre* for your time spent reading my thesis and your lively scientific discussion at my thesis defense.

*Johannes Trambauer:* You are a great sports and party buddy, although sometimes you prefer travelling by train.

*Dr. Stephanie May:* You were my partner in crime. I enjoyed working with you, not only because we worked as a team very successfully.

*Dr. Benjamin Schwenk:* Our hiking tours were always fun, and thank you that your bench always was as chaotic as my bench.

I would like to thank my current and former Eddie Lab colleagues *Bahram Khosravi* (yes, we will go rafting again), *Henrick Riemschneider*, *Linnea Ransom*, *Qihui Zhou*, *Franziska Schreiber*, *Kristin Rentzsch*, *Hannelore Hartmann*, *Mareike Czuppa*, *Daniel Farny*, *Meike Michaelsen*, *Katherine LaClair*, and *Denise Orozco*, that you were always willing to help me, and the good atmosphere in the Eddie Lab. It really was a great time to work with you.

I would like to thank my collaboration partners and colleagues *Prof. Dr. Leonard Petrucelli* (thank you very much for offering me a postdoc position, it was an

awesome experience to visit you at Mayo Clinic), *Dr. Tania Gendron, Dr. Lore Becker, Dr. Anne von Thaden, Dr. Lillian Garrett, Dr. Leda Dimou, Dr. Tim Strom, Dr. Bastian Popper, Prof. Dr. Juliane Winkelmann, Dr. Elisabeth Kremmer, Prof. Dr. Friedrich Grässer, Jing Tan, Prof. Dr. Benedikt Schoser, Prof. Dr. Marianne Dieterich, Dr. Sabine Hölter, Prof. Dr. Wolfgang Wurst, Prof. Dr. Helmut Fuchs, Dr. Valerie Gailus-Durner, Prof. Dr. Martin Hrabe de Angelis, Prof. Dr. Thomas Klopstock*, the members of the German Consortium for Frontotemporal Lobar Degeneration and the members of the Bavarian Brain Banking Alliance for your scientific input and support.

*Sabine Odoy and Marcel Matt*: Without your maintenance nothing would work in the lab. Thank you for your calmness and helping hands even if I ordered countless antibodies.

I would also like to thank to my best friends and Schafkopf dudes *Daniel Melzer, Andreas Freuer, Leonhard Wörle* and *Harald Johann Schiwall* for the many magic moments we have experienced.

There is one special person: *Carina*, since we met I even eat vegetables and salad. You make me smile every day ♥

Finally, there is my family, my *parents*, and *grandma*: You always supported me with your wise counsel and with help in any situation. And of course, my little sister *Verena*: many thanks for all the years we laughed together, even if I sometimes got on your nerves ☺

## **VI. Curriculum Vitae**

For data protection reasons are no private information available

## VII. List of Publications

- Schludi MH**, Becker L, Garrett L, Gendron TF, Zhou Q, Schreiber F, Popper B, Dimou L, Strom TM, Winkelmann J, von Thaden A, Rentzsch K, May S, Michaelsen M, Schwenk BM, Tan J, Schoser B, Dieterich M, Petrucelli L, Höfler SM, Wurst W, Fuchs H, Gailus-Durner V, Hrabe de Angelis M, Klopstock T, Arzberger T, Edbauer D. Spinal poly-GA inclusions in a *C9orf72* mouse model trigger motor deficits and inflammation without neuron loss. *Acta Neuropathol.* 2017. doi: 10.1007/s00401-017-1711-0
- Lehmer C, Oeckl P, Weishaupt JH, Volk AE, Diehl-Schmid J, Schroeter ML, Lauer M, Kornhuber J, Levin J, Fassbender K, Landwehrmeyer B, German Consortium for Frontotemporal Lobar Degeneration, **Schludi MH**, Arzberger T, Kremmer E, Flatley A, Feederle R, Steinacker P, Weydt P, Ludolph AC, Edbauer D, Otto M. Poly-GP in cerebrospinal fluid links *C9orf72*-associated dipeptide repeat expression to the asymptomatic phase of ALS/FTD. *EMBO Mol Med.* 2017. doi: 10.15252/emmm.201607486
- Zhou Q, Lehmer C, Michaelsen M, Mori K, Alterauge D, Baumjohann D, **Schludi MH**, Greiling J, Farny D, Flatley A, Feederle R, May S, Schreiber F, Arzberger T, Kuhm C, Klopstock T, Hermann A, Haass C, Edbauer D. Antibodies inhibit transmission and aggregation of *C9orf72* poly-GA dipeptide repeat proteins. *EMBO Mol Med.* 2017. doi: 10.15252/emmm.201607054
- Khosravi B, Hartmann H, May S, Möhl C, Ederle H, Michaelsen M, **Schludi MH**, Dormann D, Edbauer D. Cytoplasmic poly-GA aggregates impair nuclear import of TDP-43 in *C9orf72* ALS/FTLD. *Hum Mol Genet.* 2016. doi: 10.1093/hmg/ddw432
- Schwenk BM, Hartmann H, Serdaroglu A, **Schludi MH**, Hornburg D, Meissner F, Orozco D, Colombo A, Tahirovic S, Michaelsen M, Schreiber F, Haupt S, Peitz M, Brüstle O, Küpper C, Klopstock T, Otto M, Ludolph AC, Arzberger T, Kuhn PH, Edbauer D. TDP-43 loss of function inhibits endosomal trafficking and alters trophic signaling in neurons. *EMBO J.* 2016. doi: 10.15252/emj.201694221
- Schludi MH**, May S, Grässer FA, Rentzsch K, Kremmer E, Küpper C, Klopstock T, German Consortium for Frontotemporal Lobar Degeneration, Bavarian Brain Banking Alliance, Arzberger T, Edbauer D. Distribution of dipeptide repeat proteins in cellular models and *C9orf72* mutation cases suggests link to transcriptional silencing. *Acta Neuropathol.* 2015. doi: 10.1007/s00401-015-1450-z
- May S\*, Hornburg D\*, **Schludi MH\***, Arzberger T, Rentzsch K, Schwenk BM, Grässer FA, Mori K, Kremmer E, Banzhaf-Strathmann J, Mann M, Meissner F, Edbauer D. *C9orf72* FTLD/ALS-associated Gly-Ala dipeptide repeat proteins cause neuronal toxicity and Unc119 sequestration. *Acta Neuropathol.* 2014. doi: 10.1007/s00401-014-1329-4. \*authors are contributed equally
- Mori K, Arzberger T, Grässer FA, Gijssels I, May S, Rentzsch K, Weng SM, **Schludi MH**, van der Zee J, Cruts M, Van Broeckhoven C, Kremmer E, Kretschmar HA, Haass C, Edbauer D. Bidirectional transcripts of the expanded *C9orf72* hexanucleotide repeat are translated into aggregating dipeptide repeat proteins. *Acta Neuropathol.* 2013. doi: 10.1007/s00401-013-1189-3

Munich, 19/09/2017

Martin Haribert Schludi